Coagulation and Treatment of Drinking Water in Cold Conditions Using Alum and Dissolved Air Flotation

by:

Richard Hérard

A thesis submitted under the supervision of:

Dr. Roberto M. Narbaitz

Master of Applied Science

in

Civil Engineering*

*The Master in Applied Science in Civil Engineering is a Joint Program with Carleton University, administered by the Ottawa-Carleton Institute of Civil Engineering

Department of Civil Engineering

University of Ottawa

Ottawa, Ontario, Canada

Abstract

Conventional drinking water treatment consists of a coagulation, flocculation, gravity separation, filtration and disinfection processes each working individually but also as an interdependent system. One of the main reagents used for drinking water treatment are coagulants that destabilise the suspended particles which results in the formation of flocs. For many years, the coagulant of choice was aluminum sulphate, also know as alum. Alum has slowly been replaced by new coagulants, such as polyalumium sulphates and polyaluminum chlorides, because they yield more consistent plant performance than with alum over the wide temperature range experienced by Canadian treatment plants. Recent research has determined that the alum solubility envelop varied significantly in terms of pH range with temperature, thus cold temperature performance may be improved by adjusting the coagulation pH. Dissolved air flotation (DAF) is now used at some water treatment plants to replace sedimentation because it is much more compact than gravity settling, and it is somewhat better than sedimentation for the removal of algae, organics and operation in cold temperatures.

The objective of this thesis is to help operators and managers of drinking water treatment plants incorporating DAF by: a) investigating the cold water turbidity removals of DAF systems using alum, the most economical coagulant; and b) investigating the impact of DAF saturator pressure on the bubble sizes produced and floc removal. This first initiative is based on fairly recent research on the impact of pH on the cold-temperature aluminum solubility. It uses this knowledge about the impact of pH to evaluate DAF treatment of Ottawa River water in cold-water conditions using DAF batch tests. The effect of pH against final turbidity at cold temperatures was first evaluated by increasing the pH of the coagulated water, the higher pH helped attain good turbidity removals. For the coagulant dose tested, good turbidity removals were observed for both warm and cold waters at nearly the same pOH conditions. At room temperature the turbidity removals increase with both increasing flocculation G and flocculation time. While at cold

temperatures, when aluminum flocs are known to be much more fragile, the turbidity removals appear to be independent of G and GT.

The second initiative studied the relationship between floc size and bubble size in DAF systems by changing the DAF saturator pressure. Increasing the saturator pressure did not significantly decrease the mean bubble size. The flocs attach to bubbles that were significantly larger than the bubbles. The assessment of DAF efficiency based on the unitized effluent floc distribution proved inconclusive, it may be possible that the conditions resulting with the larger mean effluent floc size has a greater removal efficiency since it began with a smaller fraction of small flocs entering the flotation stage.

Résumé

Le traitement conventionnel de l'eau potable consiste en des processus de coagulation, de floculation, de séparation par gravité, de filtration et de désinfection, chacun fonctionnant individuellement mais aussi comme un système interdépendant. L'un des principaux réactifs utilisés pour le traitement de l'eau potable est le coagulant, qui déstabilise les particules en suspension et entraîne la formation de flocs. Pendant de nombreuses années, le coagulant de choix était le sulfate d'aluminium, également connu sous le nom d'alun. L'alun a été lentement remplacé par de nouveaux coagulants, tels que les sulfates de polyalumium et les chlorures de polyaluminium, parce qu'ils permettent d'obtenir des performances plus constantes qu'avec l'alun dans la large gamme de températures que connaissent les stations d'épuration canadiennes. Des recherches récentes ont permis de déterminer que l'enveloppe de solubilité de l'alun variait considérablement en termes de gamme de pH en fonction de la température, de sorte que les performances à froid peuvent être améliorées en ajustant le pH de coagulation. La flottation à l'air dissous (FAD) est maintenant utilisée dans certaines stations d'épuration pour remplacer la sédimentation parce qu'elle est beaucoup plus compacte que la décantation par gravité et qu'elle est un peu meilleure que la sédimentation pour l'élimination des algues, des matières organiques et des opérations à des températures froides.

L'objectif de cette thèse est d'aider les opérateurs et les gestionnaires d'usines de traitement d'eau potable incorporant la FAD en : a) étudiant l'élimination de la turbidité de l'eau froide des systèmes FAD utilisant de l'alun, le coagulant le plus économique ; et b) étudiant l'impact de la pression du saturateur FAD sur la taille des bulles produites et l'élimination des flocs. Cette première initiative est basée sur des recherches assez récentes concernant l'impact du pH sur la solubilité de l'aluminium à froid. Elle utilise ces connaissances sur l'impact du pH pour évaluer le traitement par FAD de l'eau de la rivière des Outaouais dans des conditions d'eau froide à l'aide d'essais par lots de FAD. L'effet du pH sur la turbidité finale à des températures froides a d'abord été évalué en augmentant le pH de l'eau coagulée, un pH plus élevé permettant d'obtenir une bonne élimination de la turbidité. Pour la dose de coagulant testée, de bonnes réductions de turbidité ont été observées pour les eaux chaudes et froides dans des conditions de pOH

presque identiques. A température ambiante, l'élimination de la turbidité augmente avec l'augmentation de la floculation G et du temps de floculation. Par contre, à des températures froides, lorsque les flocs d'aluminium sont connus pour être beaucoup plus fragiles, l'élimination de la turbidité semble être indépendante de G et GT.

La deuxième initiative a étudié la relation entre la taille des flocs et la taille des bulles dans les systèmes FAD en modifiant la pression du saturateur FAD. L'augmentation de la pression du saturateur n'a pas diminué de manière significative la taille moyenne des bulles. Les flocs s'attachent aux bulles qui sont significativement plus grandes que les bulles. L'évaluation de l'efficacité de la FAD basée sur la distribution unitaire du floc de l'effluent ne s'est pas avérée concluante, il est possible que les conditions résultant de la taille moyenne plus importante du floc de l'effluent aient une plus grande efficacité d'élimination puisqu'elles ont commencé avec une fraction plus petite de petits flocs entrant dans l'étape de flottation.

Acknowledgments

The author would like to thank Dr. Roberto M. Narbaitz for his support, advice, patience and critical review and evaluation of the research. His ideas and help significantly contributed to the research.

I would also like to thank the technical and administrative staff of the University of Ottawa. In particular, Patrick D'aoust the technical technician of the Environmental Engineering department. I would also like to thanks Muguette Allègre, an internship student from the École Nationale Supérieur de Chimie de Rennes, Rennes, France. In addition, I would like to thank the Aylmer drinking water plant for accessing their laboratory to collect water and for providing the alum.

I would like to thank my friends and family for all the support and encouragement during my studies.

I would like to thank NSERC for providing support provided through graduate assistance funded through Dr. Narbaitz's NSERC Discovery Grant

I would also like to thank the following persons who responded to our survey of chemical usage for DAF treatment at Canadian water treatment plants: Alistair Wardlaw, Penticton, BC; Adrien Remillard of the Powers Creek Water Treatment Plant, City of West Kelowna, BC; Fred Wiebe of Aquatera, Inc. and Wetaskiwin, AB; Claresholm, AB; Heather Buhler, City of Winnipeg, MB; Frederick Dubeau, City of Deseronto, ON; Sandra Cooke, City of Smiths Falls, ON; Mario, Aylmer Water Treatment Plant, Ville de Gatineau, QC; Debbie Smith, City of St. Johns, NF; Ryan Gould, City of Corner Brooke, NF.

Table of Content

Table of Figures

List of Tables

List of Abbreviations:

Al_{13}	$AlO_4Al_{12}(OH)_{24}(H_2O)_{12}^{7+}$,
DAF	Dissolved Air Flotation
DLVO	Derjaguin, Landau, Verwey, Overbee
DOC	Dissolved Organic Carbon
HDPE	High Density Polyethylene
LB-DAF	Large Batch Dissolved Air Flotation Tester
NOM	Natural Organic Matter
SUVA	Specific Ultra-Violet Absorption
TOC	Total Organic Carbon

List of Variables

A	Hamaker constant
d_i	Particle diameter of the i^{th} size group
d_j	Particle diameter of the j^{th} size group
d_l	Diameter of the larger particle
d_l	Diameter of the largest particle
$divJ_{12}$	Diverging flux between particle 1 and 2
D_{12}	Diffusion coefficient for particles
D_∞	Particle diffusion coefficient without the influence of other particles
DAF	Dissolved air flotation
g	Gravitational constant
G	Mean velocity gradient
G_C	Coagulation mixing mean velocity gradient
G_F	Flocculation mixing mean velocity gradient
$G(s,\lambda)$	Hydrodynamic correction to the diffusivity constant
H_A	Fluid shear dimensionless number
k_B	Boltzmann constant
n	Particle number
N_g	Differential settling dimensionless number
P	Power inputted
pH	Potential of hydrogen
pKw	-log of the water dissociation constant
pOH	Potential of hydroxide
r	Particle radius
r_{COR}	Polar coordinate system radius
r_d	Distance between the two particles
r_1	Radius of the larger particle
r_2	Radius of the smaller particle
R_L	Radius of the larger particle
s	Distance size ratio
s_d	unitless separation distance
s_r	Dimensionless separation number
t	Time
T	Temperature in kelvin
U_{s12}	Particle approaching velocity
V	Reactor volume

V_A	van der Waals interaction energy
$V_{p,i}$	volumes of i^{th} size particles
$V_{p,j}$	volumes of j^{th} size particles
V_{IP}	Interparticular potential
$V\Phi_{12}$	Interparticle forces typically obtained by the DLVO theory
X_C	Critical trajectories cross section
α	Short range efficiency factor
α_{Br}	Brownian motion collision efficiency
α_{DS}	Differential settling collision efficiency
α_{emp}	Empirical correction factor
α_{FS}	Fluid shear collision efficiency
β	Long range collision factor
${}^{Br}\beta_{ij}$	Brownian motion long range collision factor
${}^{DS}\beta_{ij}$	Discrete settling long range collision factor
${}^{Sh}\beta_{ij}$	Fluid shear long range collision factor
θ	Polar coordinate system angle
λ	Size ratio
μ	Dynamic viscosity
ρ_L	Liquide density
ρ_P	Particle density

Chapter 1 -Introduction

1.1 Background

Conventional drinking water treatment systems are the most common technology for treating surface waters to produce safe drinking water in North America. Most colloidal particles, clay particles, and natural organic matter (NOM) in surface waters have negative surface charges due to multiple factors such as isomorphous replacement, structural imperfection, preferential adsorption, and ionization of surface groups. The negative surface charges causes repulsion forces between particles resulting in a stable suspension as the particles do not agglomerate (Crittenden et al., 2012). The treatment system typically begins with the coagulation process, where a chemical coagulant, that is generally positively charged, is added to the water to destabilize the colloids and NOM by counteracting the negative surface, reducing the zone of influence of the surface charge, bridging the particles or producing metal oxide flocs that seeps the contaminants out of solution (Crittenden et al., 2012). The flocculation process follows the coagulation process. In the flocculation process, the water is agitated to stimulate the collision between the destabilized particles resulting in their rapid aggregation into larger particles, known as flocs. The typical flocculation process consists of two or three basins in series, with reducing mixing intensity in each subsequent basin. The decreasing mixing intensity in basins in series is known as tapered flocculation, and it is more effective than flocculating in a single basin (Crittenden et al., 2012). The relatively fast mixing rate in the first flocculation basin facilitates the collision between particles resulting in the formation of flocs. The following basins mix the water and suspension at a progressively slower mixing rate to help the formation of larger flocs and to prevent the breakage of the large flocs. The water and floc suspension developed in the flocculation basins progresses into the sedimentation basin. The sedimentation basin is a large basin that is not agitated, where the flocs formed in the first two processes settle out of suspension. Lamella clarifiers or similar systems are sometimes used in sedimentation basins to increase the amount of water that drinking water plants can treat. Coagulation/flocculation/sedimentation are very effective at removing

colloids that cause water turbidity. The clarified water from the sedimentation basin continues into the deep bed filters, which consists of several layers of granular media of different densities and particle sizes. The water flows through the media layers which results in the removal of many particles not removed in the sedimentation basin. The filtration process is followed by the disinfection clear well, the reservoir that stores the filtered water. As the water enters the clear well it is mixed with a chemical disinfectant, and the detention time in the clear well provides the time necessary for the disinfection of the water. The water is then sent into the distribution system with residual disinfectant to prevent the contamination of the drinking water. The removal of particles is important as they can reduce the efficiency of the disinfection process and be carriers of microorganisms (Crittenden et al., 2012). Because of the removal of turbidity, which is caused by particles, is a key part of drinking water treatment and is reflected by the primary (health related) drinking standard for turbidity. The treatment process is summarised in Figure 1-1 below.

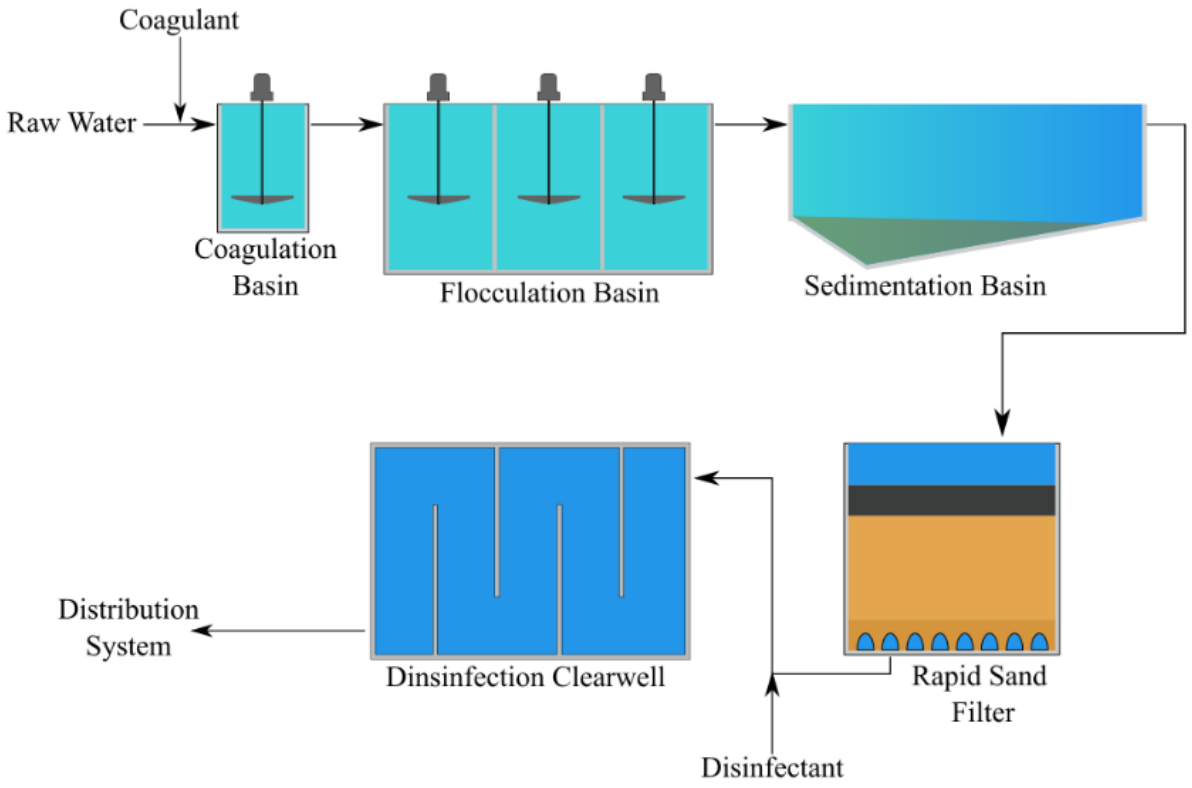

Figure 1-1: Conventional drinking water treatment train.

Conventional drinking water system is the product of many decades of iterations and optimization. Some variations exist between systems, such as the coagulants and disinfectants used, and the type of media used in the deep bed filters. Other variations include changes in some of the treatment units used. Traditional sedimentation basins are large due to the required low hydraulic loading rates. Alternatives to sedimentation are ballasted flocculation units that utilises dense particles to accelerate the floc sedimentation (Cui et al., 2020) or dissolved air flotation (DAF) which separates the flocs by reducing the floc density. Both processes can operate at significantly higher hydraulic loading rates than traditional sedimentation.

In a DAF system, the flocs formed in the coagulation and flocculation processes are contacted with microbubbles forming microbubble-floc aggregates. The aggregates have a net weight less than water, so they rise to the water surface. The microbubbles are produced by releasing supersaturated water into the

treatment stream resulting in the precipitation of microbubbles. The supersaturated stream of water is produced by pressurizing floated water to higher pressures (approximately 4 to 5 atmospheres) in a pressure vessel, known as a saturator, or by using a venturi nozzle to inject air into a recycled floated water stream.

DAF systems are gaining popularity due to increased risks to the drinking water systems caused by climate change. Climate change has caused significant water cycle changes that directly affect drinking water treatment. Increased rainfall intensity (leading to greater agricultural run-off and greater fertilizer pollution) and warmer waters are increasing the occurrence of cyanobacteria, commonly known as blue-green algae (Walker, 2015). In August 2014, there was a very large bloom in Lake Erie near Toledo, Ohio, leading to over 400,000 residents being advised not to consume the drinking water produced by the water plant because it contained cyanotoxins originating from the source water that could not be removed by the treatment plants configuration at that time (Jetoo et al., 2015).

DAF systems are more efficient at removing cyanobacteria cells and algae cells from water compared to sedimentation (Rance Bare et al., 1975), but they also present additional advantages. The second advantage of DAF is the higher hydraulic loading rate than sedimentation. Typical sedimentation hydraulic loading rates are approximately 1.25 to 2.5 m/h for standard sedimentation systems and increase to 6.0 m/h for systems with tube settlers (Crittenden et al., 2012). Conventional DAF systems have hydraulic loading rates of 5 to 15 m/h (Edzwald, 2010), and high hydraulic loading rate DAF systems can have hydraulic loadings up to 40 m/hr (Wang, 2021). The higher hydraulic loading rate for DAF systems results in smaller treatment plant footprints, reducing the size of the building required and thus reducing the construction costs. The third advantage of DAF is the versatility of treating different floc sizes. In conventional sedimentation systems, flocculation aims to produce the largest possible flocs to increase the sedimentation rate. To achieve this, long flocculation times are required. In a DAF system, smaller flocs can be removed because the separation process is governed by the bubbles and not the floc size, thus the accompanying flocculation basins do not need to be as large. A further advantage is that DAF systems tend to have a somewhat higher removal of NOM, which helps reduce the production of potentially harmful disinfection

by-products (Chu et al., 2011; Lin et al., 2020). In addition, DAF systems have denser sludge resulting in lower processing and disposal costs (Crossley & Valade, 2006). Compared to sedimentation, the main disadvantage of DAF is the energy required to pressurize the saturator and pump the water in the secondary stream. In addition, with higher operational costs, DAF systems are more complex, and the operation can be compromised if the operator does not understand their system.

The high energy requirement for DAF system is a function of the treatment process and cannot be reduced by significant amounts, but it can be optimized. The complexity of the DAF system may cause problems on the short term and it can be minimized by appropriately training the plant employees. Even with these two problems, many DAF systems are operated successfully worldwide.

Aluminum sulphate, alum, used to be the primary aluminum-based coagulant used for drinking water treatment because of its effectiveness and relatively low cost, however under cold water conditions it produces fragile flocs which complicate the operation of conventional plants (Camp et al., 1940; Hanson & Cleasby, 1990; Morris & Knocke, 1984). Due to increased regulatory pressure and an insufficient understanding of the effect of temperature on alum-derived compound solubility, many small-scale drinking water plants have resorted to using polynuclear aluminum coagulants, such as polyaluminum sulphate and polyaluminum chloride as observed in Appendix A The polynuclear species are more consistent over the range of operational pH, thus providing the treatment plant with more consistent operation over a broader range of conditions. Polynuclear coagulants are significantly more expensive than alum, and they result in higher residual aluminum concentrations in the product water, which is a health concern (Edzwald, 2020).

A greater understanding of operating DAF units at cold temperatures would benefit drinking water plants operating DAF systems. The operation could potentially be optimized by changing the saturation pressures with decreasing water temperature. Depending on the effective size ratio between microbubbles and flocs, the operating pressures may be increased during the winter to treat the smaller more fragile flocs. The operating pressures could decreased during the summer, resulting in larger bubbles, to treat larger flocs more easily formed in warm conditions.

1.2 Research Objectives

This research aims to study additional variables that treatment plant managers can modify to optimize DAF treatment systems.

- The first phase of the research is tailored to optimize the pretreatment processes of the DAF system for cold conditions using just aluminum sulphate, the most inexpensive coagulant (Barwon, 2009; Mohamed et al., 2020; Teguh et al., 2022; Zarchi et al., 2013). Recent research has shown that the alum solubility limits differ with temperature (Pernitsky & Edzwald, 2003). Edzwald and Haarhoff (2012) recommend that DAF treatment during cold water periods using alum alone should raise the coagulation pH to 7.0 or even 7.5, but there has not been any field research applying this new information to dissolved air flotation performance. This phase will assess the impact of flocculation rate and the effect of cold temperature while incorporating the knowledge of shifting alum solubility limits.
- The second part of the research evaluates the effect of saturator pressure at the microscopic scale to determine an efficient operating pressure. The interaction of flocs and bubbles formed at four pressures ranging from 275 kPa and 610 kPa is evaluated. An increased understanding of the effect of pressure on flocs-bubble aggregates will allow better evaluation of increasing the saturator pressure in DAF treatment plants.
- The expected benefits of this research could be used to optimize the DAF process at cold temperatures. Mixing intensities and flocculation time can be tailored for the treatment in combination with increasing the pH to operate in conditions where dissolved aluminium is less soluble. The saturator pressure can be increased or decreased depending on the interaction between bubbles and flocs knowing the flocs formed at cold temperatures are still weaker than flocs formed at warmer temperatures.

1.3 Research Methodology

Phase 1: Optimisation of DAF pre-treatment

This optimization of the effect of flocculation mixing intensity on the final turbidity was performed using Ottawa River water and a large batch DAF system using aluminum sulphate as the sole coagulant. Experiments were conducted at room temperature (without additional adjustment) and at 1 degree Celsius while adjusting the pH to maintain a constant pOH.

Phase 2 : Microscale Analysis of Bubble and Floc Interaction

This phase studies the interaction between bubbles formed in a DAF jar tester and the flocs formed by coagulation/flocculation pre-treatment DAF jar tester. The sizes of the bubbles formed at multiple pressures, the flocs before DAF, and the floc after DAF treatment were measured to evaluate the effect of bubble size on floc removal.

1.4 Thesis Layout

The current chapter presents background material leading to a set of identified set needs, it outlines the objectives of this thesis and presents the thesis layout. The second chapter of this thesis begins with a literature review studying the pretreatment for gravity separation processes. This includes recent studies demonstrating a shift in the solubility diagrams with respect to temperature. The second part of the literature review studies the flocculation theory to determine the effect of temperature on flocculation. Flocculation is a physical process, but it is dependent on coagulation chemistry. The last part of the literature review reviews the key parameters of DAF as it will be the treatment method used in the research.

The third chapter of this thesis is the material and methods section. The material section covers the challenge water and collection, the reagents, and the two jar test apparatus used for the research. The method section covers the batch test procedures, the analytical methods, the size measurement methods, and the method used to normalize the frequency based results.

The fourth chapter of this thesis is the research manuscript arising from this work. The manuscript begins with a short introduction and an abbreviated methods and materials section. The result of the research is then presented in two parts. The first part covers cold water coagulation, and the second part covers the effect saturator pressure on bubble size and floc removal. Each section of the results includes a discussion. The chapter ends with the conclusions of the study.

The final chapter of the thesis includes a general conclusion and a discussion about additional research needed to properly understand the effect of cold water treatment on conventional drinking water processes.

Chapter 2 -Literature Review

The literature review focuses on coagulation, flocculation, and DAF; these will be first discussed separately and finally together. This chapter concludes with the identified research needs.

2.1 Coagulation

In drinking water plants, coagulation is typically one of the first processes. Coagulation is the process of adding chemical(s) to water to destabilise the suspended and colloidal particles so they can agglomerate and be separated. Colloidal particles are smaller than 10^{-5} meter and because of their small mass their surface charges can have a great impact on their behavior (Bratby, 2016). Most particles found in waters entering drinking water plants have a negative surface charge (Crittenden et al., 2012). The negative charges results in inter-particular repulsive forces due to their similar charges and produces a suspension that is stable and will not separate (Bratby, 2016). Effective coagulation destabilizes of particles by introducing positively charged chemicals to is critical for the agglomeration of particles so that they can become sufficiently large and be separated by gravity.

2.1.1 Coagulation Principles

As discussed above, most particles found in waters entering drinking water plants have a negative surface charge (Crittenden et al., 2012). The negative charges results into interparticular repulsion forces due to their similar charges and produces a suspension that is stable and will not separate (Bratby, 2016). There are four main sources of the surface charge (Benjamin & Lawler, 2013). First, for many inorganic particles such as silts and clays, there is isomorphous replacement where the molecular structure has an ion of different valence charge resulting in net surface charges. The second source of surface charge is structural imperfection where the surface charge forms due to broken bonds on the crystals edges. The third potential source of surface charge is preferential adsorption of ions. Large NOM macromolecules have surface charges originating from ionic surface molecule that change charges with change in pH. The fourth source

of surface charge is the ionization of inorganic surface groups which are dependent on pH. Kaolinite clay for example has a positive surface charge when exposed to acidic conditions below a pH of 3.3 to 4.6 and has a negative surface charge when in conditions where the pH is above 3.3 to 4.6. The negative surface charge results in the presence of an electrical double layer. (Benjamin & Lawler, 2013).

2.1.2 Electric Double Layer

The negative surface charges predominantly attract positive ions in solution and results in an electric double layer condition (Benjamin & Lawler, 2013). A positive layer know as the Stern layer is attached to the particle surface and a second non-attached positive layer diffuses with distance to bulk solution conditions, (Benjamin & Lawler, 2013) as seen in Figure 2-1 The mostly positive charge around the particles results in repulsion forces that prevents the particles from attaching. If the repulsion forces can be supressed, the particles can approach each other significantly for the van der Waals forces to induce attachment. This is the Derjaguin, Landay, Verwet, and Overbeek (DLVO) theory (Bratby, 2016).

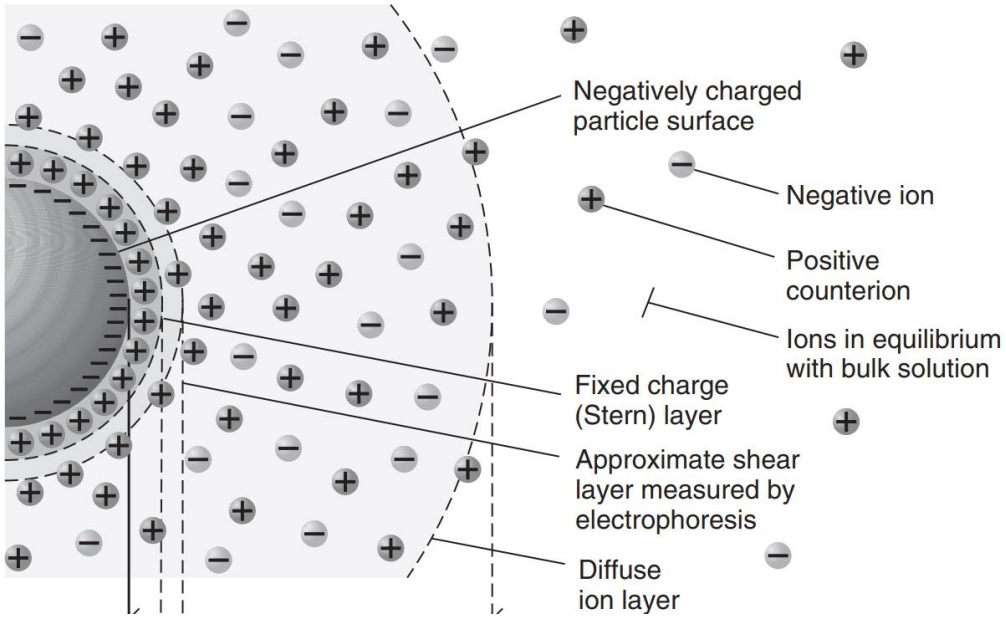

Figure 2-1: Structure of the electrical double layer (Crittenden et al., 2012).

2.1.3 Coagulation Theory

Four primary mechanisms can be implemented for the destabilization of particles in natural waters. The first mechanism is the suppression of the electrical double layer. By supressing the double layer the repulsion forces are less influential and the attracting forces can produce larger flocs that can be separated. This is typically obtained by increasing the ionic strength of the solution an using counter-ions. By increasing the ionic charge of the counter ion, the ionic strength can be reduced with respect to the Schultz-Hardy rule. For drinking water treatment, the ionic strength is regulated thus increasing the ionic strength is not a suitable option (Bratby, 2016). The second mechanism is adsorption and charge neutralization. For adsorption and charge neutralization, the destabilization mechanism is the adsorption of negative charge to neutralize the positively charged double layer (Benjamin & Lawler, 2013). The third mechanism is interarticular bridging which is predominantly a mechanism with polymer coagulants. The longer polymer molecules are adsorbed on the particle surface at one end and extends into solution at the other end. The free end is adsorbed on another particle surface and links the two particles together (Crittenden et al., 2012). The last mechanism is enmeshment, also known as sweep flocculation. Higher concentrations of coagulants are used relative to charge neutralisation resulting in the formation of metal oxide precipitate. The precipitate forms large flocs which removes particle by interception (Crittenden et al., 2012). The removal of particles is important as they can reduce the efficiency of the disinfection process and be carriers of microorganisms (Crittenden et al., 2012).

Coagulation is the addition and mixing of chemicals into the water to destabilize contaminants, resulting in the agglomeration and removal of particles by subsequent processes. The most common types of coagulants in water treatment are aluminum-based and iron-based coagulants. Traditionally, the most commonly used aluminum-based coagulant was aluminum sulphate ($Al_2(SO_4)_3 \cdot 14.3H_2O$), also known as alum. The most widely used iron-based coagulants were ferric chloride and ferric sulphate, which dissociates in water and produces Fe^{3+} cations which hydrate and form iron-hydroxide molecules (Johnson & Amirtharajah, 1983; Stumm et al., 1962).

The hydration of Al^{3+} cations with water forms several different species (such as $Al(OH)^{2+}$, $Al(OH)_2^{+}$, $Al(OH)_{3(aq)}$, $Al(OH)_4^{-}$, $Al_2(OH)_2^{4+}$, $Al_8(OH)_{20}^{4+}$, $Al_{13}O_4(OH)_{24}^{7+}$ and $Al_{14}(OH)_{32}^{10+}$) that in turn can react to form insoluble $Al(OH)_{3(s)}$ that precipitates (Crittenden et al., 2012). The distribution among the various species and $Al(OH)_{3(s)}$ precipitate depends on the solution's pH and the concentration of dissolved aluminum ions (Amirtharajah & Mills, 1982). Accordingly, coagulation results are frequently interpreted using a logC-pH diagram, where C is the molar concentration of aluminum. logC-pH diagrams were developed based on various species' solubility at a given temperature. Figure 2-2 is an aluminum solubility diagram between the pH of 2 and 12 with four aluminum species. The vertical axis is the logarithmic concentration of the aluminum species in terms of $[Al^{3+}]$, and the horizontal axis is the pH of the solution. The aluminum species concentration in solution will approximately be that of the line with the highest concentration at a given pH. The excess aluminum, that above the highest concentration line, will precipitate out of the solution. Thus, the lowest effective coagulant dose and the final aluminum concentration are a function of dose and pH. Based on Figure 2-2 the lowest theoretical Al dose that can be used is approximately $5x10^{-7}$ mol/L at a pH of 5.7.

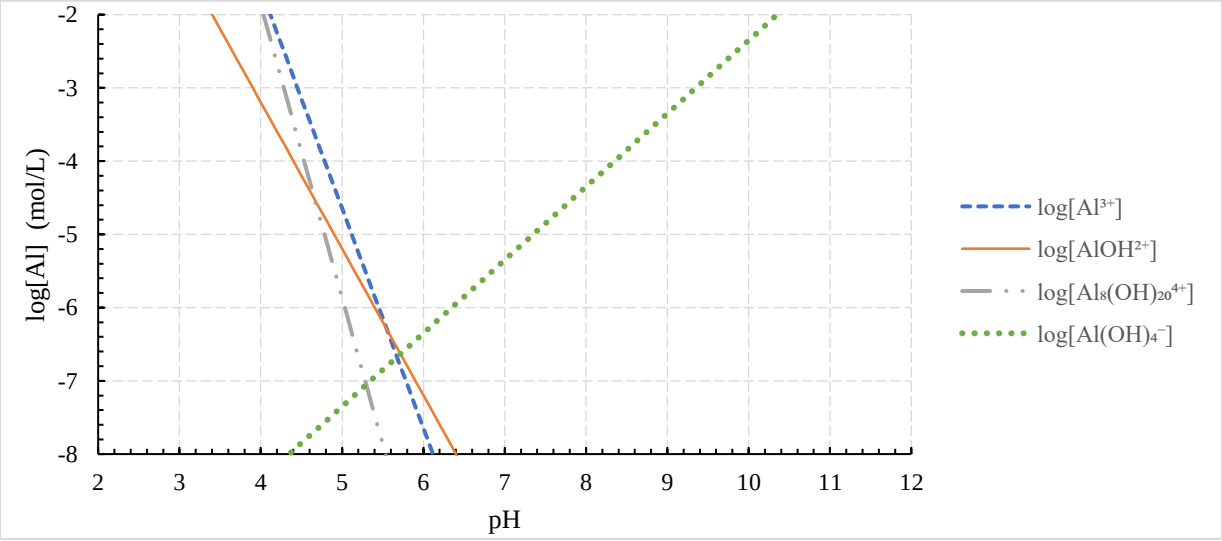

Figure 2-2: Typical alum solubility diagram at room temperature.

2.1.4 Amirtharajah & Mills logC-pH diagrams

Amirtharajah & Mills (1982) compiled the results of 18 publications, each investigating boundary conditions found within the alum solubility diagram. Figure 2-3 shows the boundary condition they studied, and Figure 2-4 is a summary graph differentiating different zones with different agglomeration mechanisms within the solubility diagram.

Boundaries ① and ② were studied by Matijevic (1973). Boundary ① is the limit at which alum precipitates in a pH-adjusted distilled water solution while boundary ②is the limit at which alum precipitate in a pH-adjusted distilled water solution containing 2g/L of Ludox AM, a silicate sol solution. The solutions were analyzed after 24 hr and maintained at 25 ºC. Matijevic (1973) claimed that coagulation of the silica sol was observed in the zone between the boundary ① and boundary ②, while large rapidly settling flocs were observed in the high pH zone between boundary ② and boundary ①. Given the later, it is not clear why boundary ② is higher than boundary ①. Boundary ③, studied (Hanna & Rubin, 1970) is the limit at which an *Escherichia Coli* (*E. coli*) suspension coagulated with alum settles within an hour at 25ºC. At concentrations above the boundary, the *E. coli* suspension quickly settled. Hanna and Rubin (1970) observed that for conditions below the boundary ③ and at pH lower than 5.8 the solution flocculated slowly; at pH above 5.8, the solution did not flocculate. Yet the Figure 2-2 shows that at pHs above 5.8 the degree of precipitation decreases with increasing pH, but there is some precipitation. Boundaries ④ and ⑤, were studied by Rubin & Kovac (1974). Boundary ④ is the critical pH for titanium dioxide solutions flocculate with alum which is an extrapolation. Boundary ⑤ is entirely based on experimental data, it has two separate curves at the lower concentration range. The lowest is the solubility limit for a solution with 91.9 mg/l of titanium dioxide while the upper limit is for a solution with 3.2 mg/L of titanium dioxide. Similar observations were documented for conditions below boundary ④, corresponding with the observation of Hanna and Rubin (1970). Boundary ⑥ studied by Packham (1962), indicates the coagulant dose at a given pH to reduce the initial turbidity of synthetic water mixture by 50% after 10 min. Organic matter in the solution did not affect the results compared to synthetic water containing clay without organic matter.

Boundary ⑦, studied by Matijević & Stryker (1966), separates areas of coagulation with a zone of stability for the silver iodine sol using alum as the coagulant. Boundary ⑦ corresponds with boundary ⑤ from Rubin & Kovac (1974). Boundary ⑧, studied by Hayden & Rubin (1974) represents the right-hand side of the solubility diagram such as boundary ①, ③, and ④. Hayden & Rubin's primary objective was to determine the effect of the sulphate molecule in alum. The sulphate increases the range of flocculation in acidic conditions when compared with coagulation using aluminum nitrate coagulants. Boundary ⑨ was based on the work of (McCooke & West, (1978) which delineates a zone in which kaolin clay suspension coagulated with alum is stable. Finally, note that rectangular zone of AWWA practice corresponds to Al concentrations that are significantly higher than the minimum solubilities.

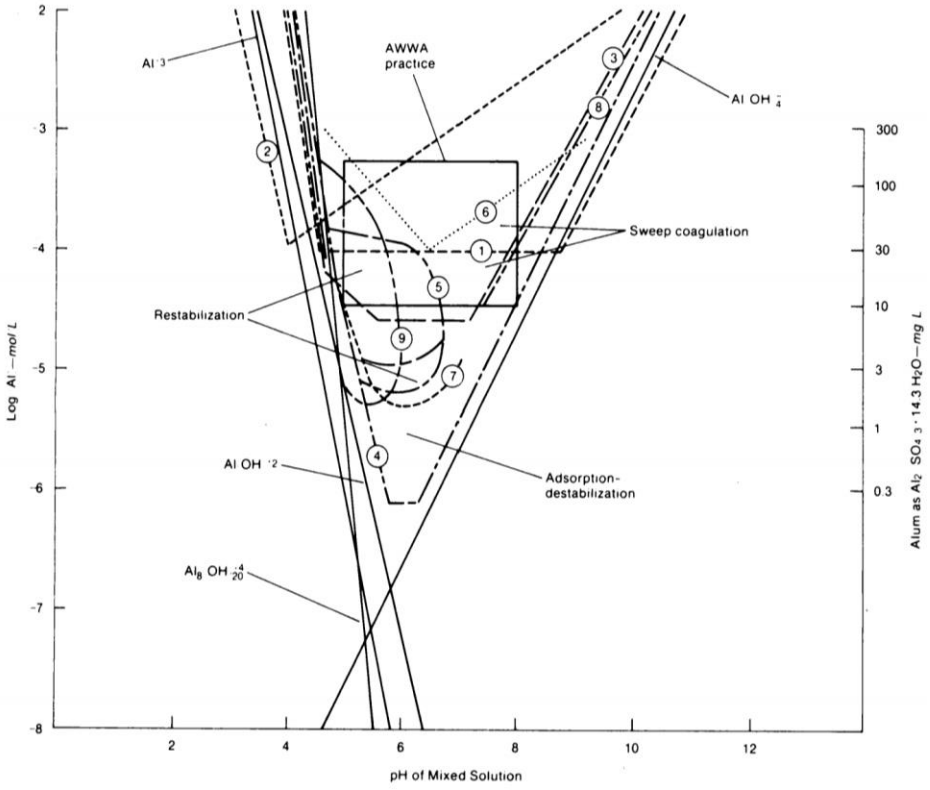

Figure 2-3: Aluminum solubility boundaries at 25ºC studied by Amirtharajah & Mills (1982).

A few essential observations can be made about the characteristics of alum coagulation based on the above diagrams and the above mentioned research. First, if there are no contaminants, aluminum flocs have difficulty forming, as seen with boundary ①. It should be noted that boundary ① also corresponds with the top end of boundary ⑤ and ⑨. Depending on the particles being removed, the zone of stabilization changes concentrations and shape. There is a zone of rapid flocculation on the right-hand side of the destabilization zone above the solubility limits of the aluminum hydroxides. Slow flocculation occurs for concentrations below the solubility envelope and at low pH values, including areas below the hydroxide solubility limits. The flocculation at lower pH and below the solubility limits are associated with coagulation with hydrogen. It should also be noted that positively charged aluminum ions are in suspension, which may result in charge neutralization. The destabilization mechanism boundaries studies were summarized in Figure 2-3. At aluminum concentration substantially higher than the lowest solubility limits there are rapid flocculation zones that produce large flocs, they are associated with the sweep flocculation mechanism. While the slow flocculating conditions observed for smaller aluminum doses were the result of smaller flocs associated with the charge neutralization mechanism. And for intermediate aluminum doses there are zones were a combination of charge neutralization and sweep flocculation prevail. All the analyses used in the graph construction were performed near or at room temperature and they did not consider the effect of temperature.

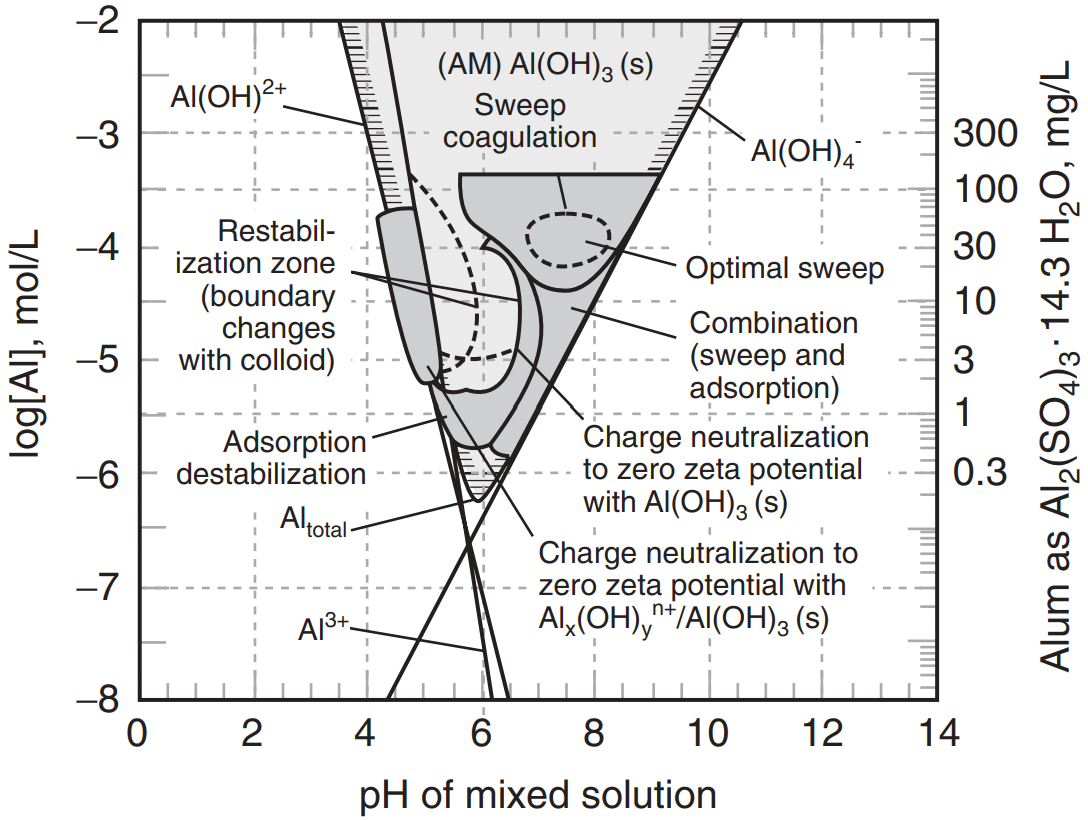

Figure 2-4: Amirtharajah & Mills (1982) final diagram, after Crittenden et al (2012).

The pC-pH diagrams for aluminum species concentration lines present the theoretical boundary conditions delineating soluble and insoluble conditions. The Al concentrations required for practical separations are often higher. As seen from Boundary ① and Stumm & O'Melia (1968), the formation of flocs requires a nucleation site or high concentration of coagulants. It should also be noted that the lower portion of Amirtharajah & Mills (1982) solubility diagram consists of charge neutralization. Charge neutralization may not be favorable for drinking water treatment plants as the flocculation process is slower than the sweep flocculation process. In addition, the solubility diagram is theoretical and the aluminum concentration required at water treatment plants are generally much higher (AWWA practice in Figure 2-2) and it varies depending on the water because of other ions/contaminants present. For example, at Ottawa's Britannia water treatment plant operates well with a typical alum dose of 34 mg alum/L and a pH~6, yet according to Figure 2-3 this a borderline re-stabilization condition.

2.1.5 Alternative Aluminum-Based Coagulants

The alternatives to traditional alum are polynuclear coagulants. The most common are polyaluminum sulphate, polyaluminum chloride and polyaluminum silica sulphate. Polyaluminum coagulants are favored by plants as they are less sensitive to temperature and pH variations(Go et al., 2021) and are effective at removing natural organic matter from solution (Liu et al., 2019; Tafvizi & Husain, 2022).

Polynuclear coagulants are stable on a wider pH range compared to alum (Xu et al., 2011). The wide pH range and stability over varying treatment conditions make polyaluminum coagulants desirable for drinking water plants. The author gathered from municipal drinking water reports the coagulants used by 72 Ontario conventional drinking water plants servicing over 1000 persons (Appendix A). 53% of plants use advanced coagulants, mostly polynuclear aluminum variants, only 19% of plants use alum without a flocculation aid. Low basicity polyaluminum sulphate does not exhibit significant variation in its solubility diagram with respect to pH compared to alum (Pernitsky & Edzwald, 2003). Alum has a significant shift in solubility with respect to temperature. The change in solubility of alum was not known in the twentieth century and resulted in difficult winter operations. An advantage of alum is its lower solubility relative to polyaluminum coagulants which leads to lower aluminum residuals in the treated water (Edzwald, 2020).

New Health Canada guidelines recommend lowering the aluminum operational guidelines for drinking water to 0.05 mg Al/L (log[Al]=-5.73) (Health Canada, 2019). The enforcement of this standard will cause problems at many drinking water plants using polyaluminum coagulants since these coagulants have solubility limits near or above the proposed Health Canada operational guideline (Pernitsky & Edzwald, 2003). Alum-derived aluminum compounds are less soluble than compounds formed with polyaluminum coagulant producing a wider pH range for operations (Edzwald, 2020). A coagulant which is effective over a wide range of pHs is better for drinking water systems operation as the water quality of many water sources may vary significantly over time. Two primary causes for sporadic changes in raw water quality are observed in river systems. The first is increased flow rate, such as spring snow melt and

heavy storms which causes increased sediment loads in the raw waters (Lane, 1955). The second major cause of variation is man-made water control structures, such as hydroelectric dams (Kuriqi et al., 2021). There is the potential for increased sediment load downstream of a hydroelectric dam when the flood gates are open. The other water control structure affecting drinking water plants are locks in canal systems. Depending on the waterbody, algal blooms can occasionally increase the sediment load and change the chemistry of water entering the treatment plant, stressing the treatment system.

2.1.6 Cold Water Operation with Alum

Alum has a wider pH operating range compared to polyaluminum coagulants and its Al solubility is below the proposed new aluminum aesthetic Canadian operational guideline (Pernitsky & Edzwald, 2003). The effect of temperature on alum solubility was not well understood, causing less than optimal treatment at cold temperatures (Camp et al., 1940; Hanson & Cleasby, 1990; Morris & Knocke, 1984). The pC-pH diagrams presented thus far do not consider the shift in solubility of alum with respect to temperature. pC-pH diagrams are drawn based on the stoichiometric equation of the various aluminum species that form $Al(OH)_3$, which precipitates, and the equilibrium constants of these equations. These equations are used to establish the possible limits of the solubility envelope (Figure 2-1). This basic chemistry information in the pC-pH diagrams is complimented with the results of coagulation/flocculation experimental and plant data (Figure 2-2 and 2-3). The values of the equilibrium constants are available for temperatures like 20 and 25°C, and they were used in generating the solubility diagrams for room temperature presented in section 2.1.1. As far as the candidate was able to ascertain there is not a complete set of values available for the relevant equilibrium constants at low temperature, accordingly it is not possible to produce a theoretically based pC-pH diagram for low temperatures. However, as these solubility diagrams are important to interpret low temperature data a number of researchers have used low temperature experimental data to estimate the corresponding solubility diagrams. Figure 2-5 through 2-7 are examples the estimated solubility values based on experiments from the literature at warm and cold water

temperatures.

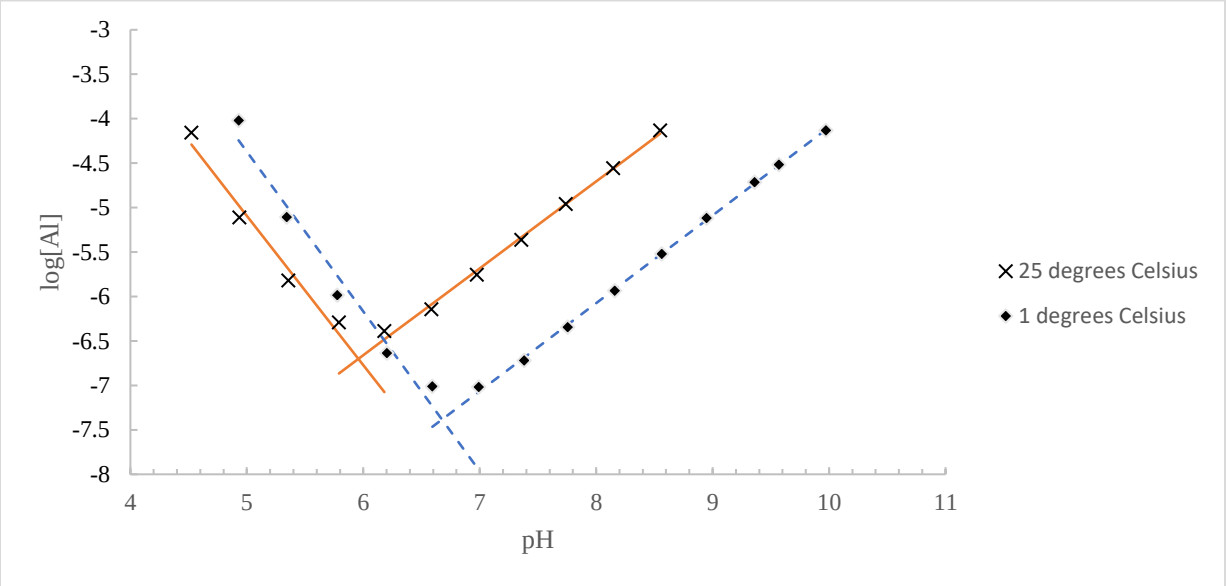

Figure 2-5: Aluminum solubility for the 1ºC and 25ºC, data from May tests by Hanson & Cleasby, (1990).

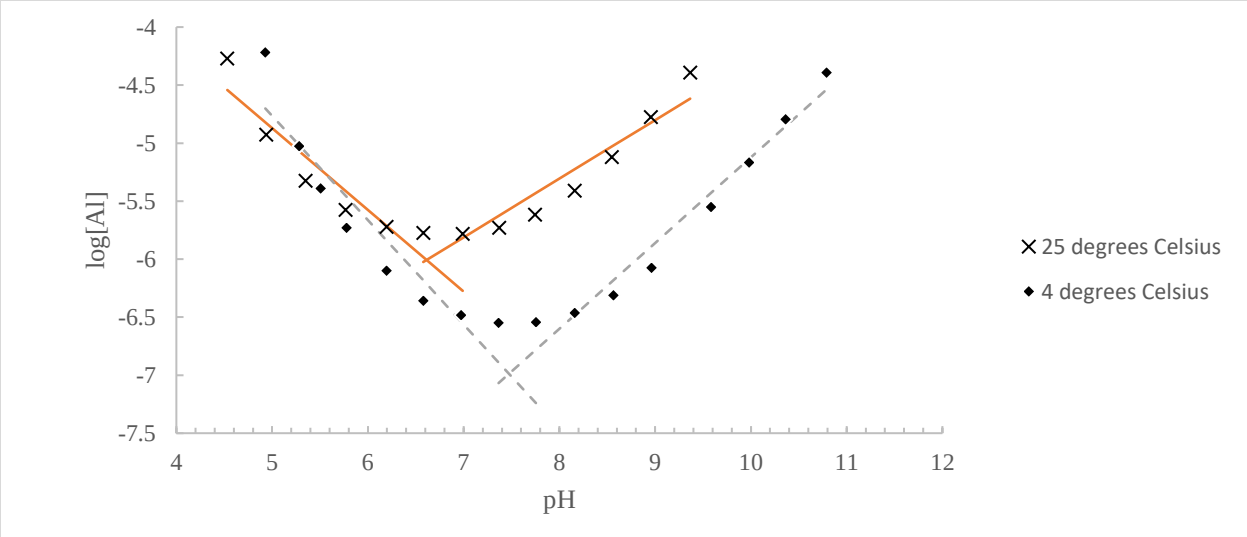

Figure 2-6: Aluminum solubility with for the 4ºC and 25ºC, based on data from Smith and Martell (source: Hanson & Cleasby, 1990).

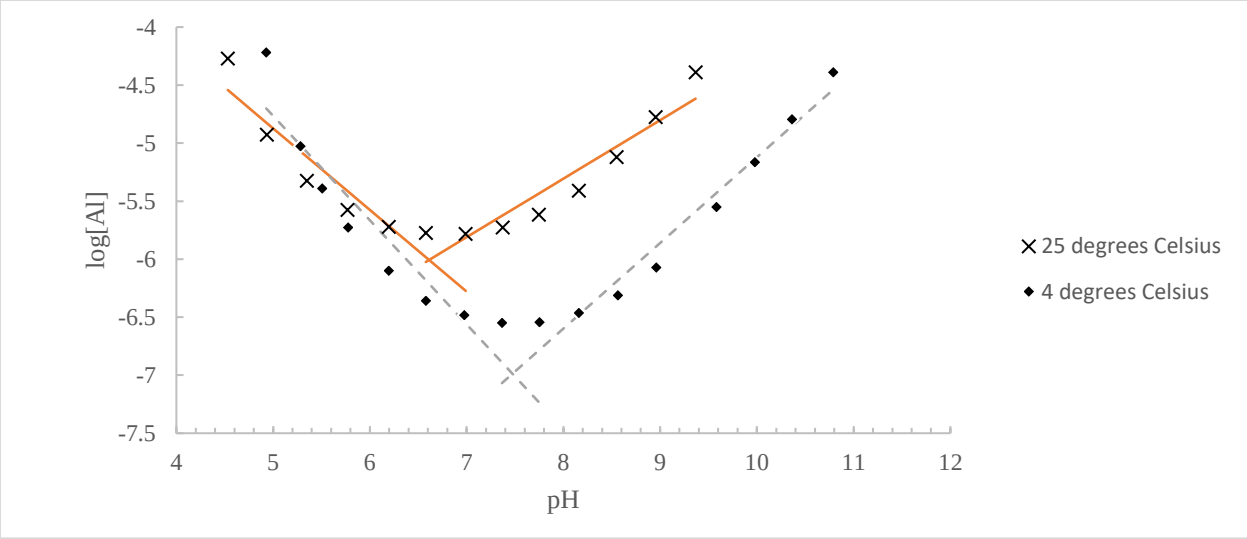

Figure 2-7: Aluminum solubility for the 4ºC and 25ºC, based on Van Benschoten & Edzwald (1990).

It can be observed from Figures 2-5, 2-6, and 2-7, that a decrease in solubility and the point of minimum solubility is located approximately one pH higher for the cold-water series compared to the warm weather series. Morris & Knocke (1984) reported that operations were difficult at cold temperature and Camp (1940) showed operational conditions at cold temperatures. The shift of solubility limits of alum changes with temperature causes problems with treatment if the pH is not adjusted (Hanson & Cleasby, 1990).

Two theories have been proposed to explain the cold-water operations of aluminum-based coagulants in cold water. The first theory proposed that $AlO_4Al_{12}(OH)_{24}(H_2O)_{12}^{7+}$, known as Al_{13}, solubility shifts significantly with temperature (Feng et al., 2008). Al_{13} is found in high concentrations in polynuclear aluminum based coagulant (Mustereț et al., 2021; Tian et al., 2018; Wang et al., 2019), but is not found in significant quantities in alum derived products (Van Benschoten & Edzwald 1990). The second theory, proposed by Hanson & Cleasby (1990), is that coagulation with alum is pOH dependent, not pH dependent. Equation 2.1 shows the relation between pH and pOH, while equation 2.2 is the relation of pK_w, the negative log of the water dissociation constant, with temperature (Bratby, 2016).

$$pH + pOH = pK_w \quad (2.1)$$

$$pK_w = 0.01706 \cdot T + \frac{4470.99}{T} - 6.0875 \quad (2.2)$$

where T is the temperature in Kelvin.

Table 2-1 tabulates typical pK_w with temperatures between 0 and 25°C.

Table 2-1: Relation of pK_w with temperature.

Temperature (ºC)	pK_w
0	14.94
2	14.86
4	14.77
6	14.69
10	14.53
15	14.34
20	14.17
25	13.99

To investigate the claims of constant or near constant pOH for satisfactory separation made by Hayden & Cleasby (1990), the candidate performed a number of linear regressions to determine the minimum solubility pOH using data from several studies. Table 2-2 is a tabulation of the linear regressions of the left hand side and right hand side of Figures 2.4, 2.5, and 2.6 to determine the pOH of minimum solubility, i.e., the pOH at which the lines simulating the low pH (left side) and high pH (right side) solubilities intersect.

Table 2-2: Analysis of the effect of pOH.

Study	Temp. (°C)	Solubility line	Solubility line Slope	Solubility line Intercept	Min. solubility (log Al)	Min. solubility (Intercepting) pH	pK_w	Min. solubility pOH
May	25	Left side Right side	-1.681 0.978	3.314 -12.530	-6.4	5.96	13.998	8.04
	4	Left side Right side	-1.797 0.989	4.616 -13.986	-7	6.68	14.748	8.07
Data of Smith and Martell	25	Left side Right side	-0.704 0.505	-1.352 -9.345	-5.8	6.61	13.998	7.39
	1	Left side Right side	-0.898 0.738	-0.273 -12.507	-6.6	7.47	14.895	7.42
Van Benschoten and Edzwald	25	Left side Right side	-1.464 0.953	2.296 -12.200	-6.3	6.00	13.998	8.00
	4	Left side Right side	-1.504 1.060	3.355 -13.700	-6.6	6.65	14.748	8.10

From Table 2-2, it is possible to see the pH of minimum solubility changes with pH while the pOH of minimum solubility is more consistent. The difference in pOH can be caused by the change of solubility of alum with temperature or an error in pH readings. The new perspective on the change of alum solubility highlights the need to study the performance of coagulation/flocculation-based systems in terms of pOH. It should be highlighted that lower-temperature solubility envelopes indicate a lower solubility level than that for 25ºC. As it will be covered in sections 2.2.3.4 and 2.2.4.4, flocculation is affected by temperature minimizing the effect of the lower final solubility.

As with warm water conditions, the solubility diagram for cold waters represent a theoretical limit for drinking water treatment and the operating conditions may require higher concentrations than the solubility limits. The cold water conditions have not been studied as intensively as warm water treatment thus to the author's knowledge, exact flocculation regimes boundary have not been determined.

2.1.7 Alternative Coagulants

Alum and aluminum-based coagulant are common for drinking water treatment but there are multiple other alternatives. The selection of the coagulant is based on performance assessments, i.e., jar tests or pilot tests, and a cost analysis. Iron based coagulant are also fairly common. For simple iron salt coagulants, there is ferric sulfate ($Fe_2(SO_4)\cdot 8H_2O$), ferrous sulphate ($FeSO_4\cdot 7H_2O$), and ferric chloride ($FeCl_3$). There are also polymerized ferric coagulants such as polyferric sulfate. Alternatively, there are synthetic organic polymers that can be used for coagulation with various molecular weights and charge density. There is also non-organic polymers such as activated silica. The use of polymer would theoretically lead to lighter flocs that would be more amenable for flotation, however, they have a high unit cost and its use in drinking water application is restricted in many jurisdictions because of health concerns. Less commonly used in North America but natural polyelectrolytes such as some seed extracts or starches, and chitosan are capable of coagulation and successful drinking water treatment (Bratby, 2016).

2.2 Flocculation

Flocculation is the physical process of floc formation. For flocculation to occur, the particles must get closer, collide and agglomerate, which all require proper destabilization (Crittenden et al., 2012). Flocculation is classified as perikinetic or orthokinetic flocculation (Han & Lawler, 1992). Perikinetic flocculation occurs when the flocculation influences microscale particles. Its driving mechanism is Brownian motion which was first studied by the Scottish botanist Robert Brown in 1827 (Crittenden et al., 2012). Brownian motion is caused by the random interaction between molecules resulting in chaotic microscopic movements. Orthokinetic flocculation is macroscale flocculation governed by differential fluid shear and differential settling (Benjamin & Lawler, 2013). Differential shear flocculation is the primary flocculation mechanism that occurs in the flocculation basin of drinking water plants. The slow mixing in the flocculation tanks produces a velocity gradient between particles promoting the collision between flocs, some of which result in the formation of larger aggregates. The final flocculation mechanism is differential

settling which occurs in gravity separation basins. Larger flocs settle quicker than smaller flocs; this difference in movement results in larger flocs colliding with smaller flocs. The term sweep flocculation comes from this mechanism where the larger flocs sweep the smaller flocs out of suspension.

2.2.1 Flocculation Theory

Flocculation theory is a compilation of years of research explaining the process of particle flocculation. The flocculation theory is modelled by a modified Smoluchowski equation that introduces the collision frequency factors and the collision efficiency factors (Han & Lawler, 1992; Smoluchowski, 1917). The collision frequency factor is the frequency at which two particles collide if there is no interparticle interaction. Interaction between particles is negligible if the distance between particles is sufficient to prevent interaction due to interparticle hydraulic forces or van der Waal forces. A long-range interaction model represents the collision frequency factor. The collision efficiency factor is a correction to the collision frequency factor considering short-range particle interactions. The short-range interactions are interparticle hydraulic forces and van der Waal forces. The interparticle hydraulic forces result from forcefully displacing the water between the particles. The van der Waal forces are caused by surface charges between particles and depend on efficient coagulation processes. A short-range interaction model represents the collision efficiency factor. The flocculation theory is covered in detail to investigate the individual effects on flocculation and then the effect of temperature on individual flocculation factors, which would result in compromised flocculation due to changes in temperature.

2.2.1.1 The Smoluchowski Equation

The Smoluchowski equation is the core model of the flocculation theory. The Smoluschowski equation is based on work published by Marian Smoluschowski on the population balance of particles in suspension influenced by flocculation (Smoluchowski, 1917). The equation states that the rate of change of the number of particles of a particular size with respect to time is the difference between the rate of formation due to the agglomeration of smaller particles and the rate of loss of particles (of that particular

size) due to agglomeration with other particles. Below is the modern interpretation of the Smoluchowski equation with a few additional terms (Benjamin & Lawler, 2013).

$$r_k = \left(\frac{1}{2}\alpha_{emp} \cdot \sum_{\substack{all\ i\ and\ j \\ such\ that \\ V_{p,i}+V_{p,j}=V_{p,k}}} \alpha_{ij} \cdot \beta_{ij} \cdot n_i \cdot n_j \right) - \left(\alpha_{emp} \cdot n_k \cdot \sum_{all\ i} \alpha_{ik} \cdot \beta_{ik} \cdot n_i \right) \qquad 2.3$$

where r_k is the formation rate of k size particles due to the flocculation of i, j, and k size particles, particles;. α_{emp} is an empirical correction factor, dimensionless; α_{ij} and α_{ik} are the short-range efficiency factors/functions accounting for short-range particle interaction between particles of i^{th} and j^{th} size and the i^{th} and k^{th} size, respectively, dimensionless; β_{ij} and β_{ik} are long-range collision frequency factors/functions for the interaction between the i^{th} and j^{th} size particle and the i^{th} and k^{th} size particles, respectively, dimensionless; and n_k is the number concentration of k^{th} size particles. $V_{p,i}$ and $V_{p,j}$ are the volumes of i^{th} and j^{th} size particles, meters.

For flocculation, two types of forces are considered within the Smoluschowski equation. The forces that result in the particles getting closer to one another, resulting in flocculation, and the forces that inhibit the flocculation between two particles. The long-range force model only considers the forces that result in the particles getting closer. In contrast, the short-range model corrects the long-range models by considering the hydrodynamic and van der Waals effects.

2.2.2 Collision Frequency

Long-range collision frequency models represent the rate of collision between particles under a specific transport mechanism without the effect of short-range forces, such as hydrodynamic forces or van der Waal forces. Long-range interactions follow a rectilinear model, as seen in Figure 2-8. In the rectilinear models, the particles will collide if the distance between the two paths at the time of possible collision is less than the sum of the two radiuses. If the particle's trajectory is outside the critical zone, the trajectory is

open, and collision will not occur. The following subsections cover the long-range models for the Brownian motion transportation regime, the fluid shear transportation regime, and the differential settling regime. The net rate of particle formation is the summation of the contribution of these three regimes.

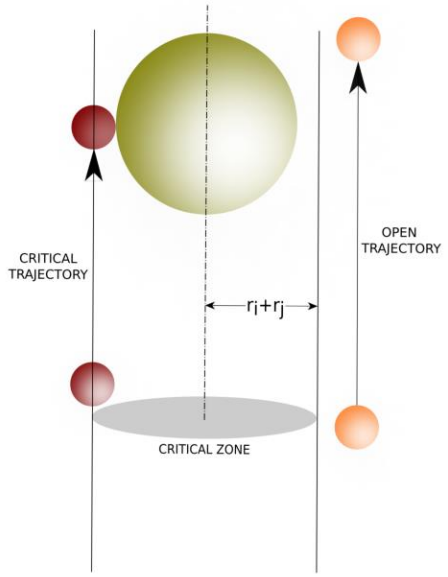

Figure 2-8: Rectilinear flocculation after Han & Lawler (1992).

2.2.2.1 Brownian Motion

Brownian motion is the random movement of particles caused by molecular collision. The most common explanation of Brownian motion is the diffusion of particles from a high concentration zone to a lower concentration zone. At the microscale, diffusion is defined by Fick's law, where the concentration gradient is the driving force of diffusion. Brownian motion is random in every direction, but it is easier for particles to move from high-concentration zones to low-concentrations because, in the zone of high concentrations, the particles are constantly redirected by the frequent intra-particle collisions. (Metcalfe et al., 2012).

The collision frequency for Brownian motion is determined by Fick's law which yields the flux of i^{th}-size particles crossing the surface area of j^{th}-sized particles. The resulting equation is the collision frequency for Brownian motion (Benjamin & Lawler, 2013):

$$ {}^{Br}\beta_{ij} = \frac{2k_B T}{3\mu}\left(\frac{1}{d_i} + \frac{1}{d_j}\right)(d_i + d_j) \qquad 2.4 $$

where ${}^{Br}\beta_{ij}$ is the collision frequency function between the i^{th} and the j^{th} size particles to volumetrically sum up to the volume of k^{th} size particle caused by Brownian motion; k_B is Boltzmann's constant, 1.38×10^{-16} g cm^2/s^2K; T is the temperature in Kelvin; μ is the dynamic viscosity of the fluid matrix, Pa s; and d_i and d_j are the diameters of i^{th} and j^{th} size particles, respectively, in centimeters.

Keeping the temperature constant, the only other variable in the collision frequency function by Brownian motion is the particle size. The function is minimized when both particles are the same size and vary by less than two orders of magnitude across the range of typical particle sizes.

2.2.2.2 Fluid Shear

Fluid shear is the flocculation mechanism that plants operators and designers have the most significant control over. Fluid shear is the product of velocity gradient and the particle sizes to the power of three. The faster-flowing particles with trajectories that cross the trajectory of slower particles will produce larger particles if collision and attachment occur. The derived equation for collision frequency is (Friedlander, 1977; Han & Lawler, 1992; Smoluchowski, 1917):

$$ {}^{Sh}\beta_{ij} = \frac{1}{6} G(d_i + d_j)^3 \qquad 2.5 $$

where ${}^{Sh}\beta_{ij}$ is the collision frequency between i^{th} and j^{th} size particles which the sum of volumes add up to k^{th} size particles due to fluid shear, dimensionless; G is the velocity gradient, s^{-1}; and d_i and d_j are the diameters of i^{th} and j^{th} size particles, respectively, cm.

Comparing the equation for fluid shear collision frequency and Brownian motion collision frequency, the function of fluid shear depends on the sum of particle sizes to the power of three. In contrast, Brownian motion-controlled collisions are proportional to the sum of particle sizes to the power of one. Thus, it is possible to conclude that long-range function in respect to fluid shear will increase rapidly as the particle size increases. In addition, the collision frequency for fluid shear is a function of the velocity gradient to the power of one.

2.2.2.3 Differential Settling

Assuming all particles in a suspension have the same density. Larger particles will settle quicker than smaller size particles resulting in large particles intercepting the path of the smaller particle. The equation was originally derived in German and re-derived and presented in English by Friedlander (1977). This equation is:

$$^{DS}\beta_{ij} = \frac{\pi g}{72\mu} \cdot \left(\rho_p - \rho_{\mathrm{L}}\right) \cdot \left(d_i + d_j\right)^3 \cdot \left|d_i - d_j\right| \qquad 2.6$$

where $^{DS}\beta_{ij}$ is the differential settling collision frequency constant of i^{th} and j^{th} size particles of which their volume sum up to that of k^{th} size particles, dimensionless; g is the gravitational constant, m/s^2; μ is the dynamic viscosity of the fluid matrix, (Pa·s); ρ_p and ρ_L are the density of the particle and the liquid matrix, respectively, $kg \cdot m^{-3}$; and d_i and d_j are the diameter of i^{th} and j^{th} size particle respectively, cm. Keeping temperature constant, the first two terms on the right-hand side are constant. Accordingly, the size of the particles dramatically influences the collision frequency function for discrete settling, especially when the difference in diameter is significant. When the particles of interest approach the same size, the collision function approaches zero and becomes zero when the two particles are the same size. Due to the nature of flocs, their particle density is slightly above the density of water. This results in very slow settling.

2.2.2.4 The Effect of Temperature on Collision Frequency

Analyzing the equations for Brownian motion, fluid shear, and differential settling collision frequency functions, only a few parameters are influenced by temperature variations, namely temperature directly and viscosity. For Brownian motion, the temperature in Kelvins is in the denominator of equation 2.4. This direct effect has less influence on the collision frequency for Brownian motion than the effect of changing dynamic viscosity over the normal seasonal water temperature change. For a temperature change from 25°C to 5 °C, the temperature in degrees Kelvin decreases by approximately 6.7%. For the same change in temperature, the dynamic viscosity goes from 8.902×10^{-3} $^{g}/_{cm \cdot s}$ at 25 °C to 1.519×10^{-2} $^{g}/_{cm \cdot s}$, a 41% increase. The combined effect of these changes reduces ${}^{Br}\beta_{ij}$ by approximately 45%.

The only variables in the fluid shear collision frequency function are the floc size and the velocity gradient. The velocity gradient used to describe the flocculation theory is linear for simplification. In actual flocculation conditions in a drinking water plant, the velocity gradient used is the (root mean square) velocity gradient (G). The equation for G_{RMS} is (Crittenden et al., 2012):

$$G = \sqrt{\frac{P}{\mu \cdot V}} \qquad 2.7$$

Where P is the power inputted in the body of water, watts; V is the volume of water, m^3; and μ is the dynamic viscosity, Pa·s. The change in dynamic viscosity is thus a factor, but the effect is not as significant as its effect on Brownian motion. The reduction of the fluid shear collision frequency function is approximately 23% for a water temperature decrease from 25 °C to 5 °C.

Finally, the differential settling collision frequency function is inversely proportional to the dynamic viscosity, so a change from 25 °C to 5 °C will result in a 41% decrease in ${}^{DS}\beta_{ij}$.

2.2.3 Collision Efficiency

Long-range frequency models represent particles in bulk suspension where other particles do not influence individual particles. Thus, a collision with the long-range model occurs when the two particles cross paths. Short-range forces, such as hydrodynamic and van der Waal, affect the particle paths as the particles approach each other. As the distance between two particles decreases, the short-range forces increase and inhibit the collision of two particles. The short-range model corrects the number of trajectories at which the successful attachment of two particles occurs. The short-range interaction follows a curvilinear trajectory model, as shown in Figure 2-9 below. In the long-range model, the collision occurs if the linear trajectory crosses the r_i+r_j cross-section. Due to short-range forces, some of the trajectories that would cause a collision in the long-range regime will deviate into an open trajectory. The following sections discuss the Hamaker constant first, as it is a term in all collision efficiency models. This is followed by examining the three flocculation mechanisms regarding short-range collision efficiency factors. The effect of temperature on the short-range models is then discussed.

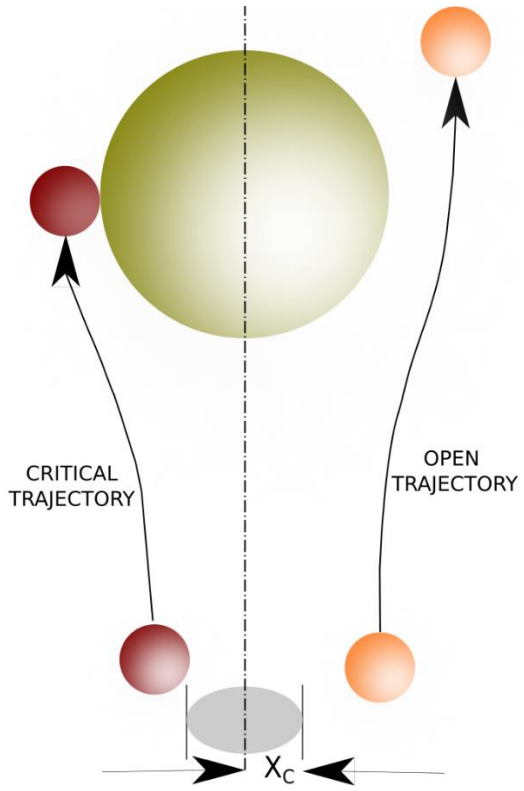

Figure 2-9: Curvilinear flocculation trajectory after Han & Lawler (1992).

2.2.3.1 Hamaker Constant

The Hamaker constant (A) is a coefficient relating the separation distance between two interacting particles and the van der Waals interactive force (Donaldson & Alam, 2008). The value of the Hamaker constant depends on the fluid medium and the particles themselves. The Derjaguin, Landay, Verwet, and Overbeek (DLVO) theory explains that particles that are not adequately destabilized will have a repulsion force more significant than an attractive force and thus have a very low Hamaker constant.

2.2.3.2 Brownian Motion

The collision efficiency interaction for Brownian motion was first described by Equation 2.8 which was derived by (Spielman, 1970).

$$\frac{\delta n_2}{\delta t} = -div\, J_{12} = \frac{1}{r^2}\frac{\delta}{\delta r} r^2 \left(D_{12}\frac{\delta n_2}{\delta r} + \frac{n_2}{d}\frac{dV_{IP}}{dr} \right) \quad 2.8$$

Which states that $\frac{\delta n_2}{\delta t}$ the rate of change of the number (n_2) distribution with respect to time (t) is equal to the negative divergence between two interacting particles; it is a function of r, the separation distance, meters; D_{12}, the diffusion coefficient between the two particles; and V_{IP}, the particles interaction potentials. The particle interaction potential is a function of the Hamaker constant. Valioulis & John (1984) elaborated with additional boundary condition as seen in Equation 2.9

$$\alpha_{12} = \left(1 + \frac{r_2}{r_1}\right) \int_{1+\frac{r_2}{r_1}}^{\infty} \left(\frac{D_\infty}{D_{12}}\right) \exp\left(\frac{V_A}{k_B T}\right) \frac{dt}{s_r^2} \quad 2.9$$

Where α_{12} is the collision efficiency; k_B is the Boltzmann constant; T is the temperature in Kelvin; s_r is a dimensionless separation function; D_∞ is the particle diffusion coefficient without the influence of other particles; V_A is the van der Waals interaction energy; and the remainder are of the variables are as defined previously.

Han & Lawler (1992) presented the simplified Equation 2.11 to calculate the collision efficiency using the size ratio (λ), to evaluate the effect of differential particle sizes. The size ratio is defined by equation 2.10, where r_1 and r_2 is the radius of the larger and smaller particles, respectively. Equation 2.11 calculate the Brownian motion collision efficiency between two particles considering the size of the larger of the two particles. The coefficient values for Equation 2.11 are presented in Table 2.3. The table is a tabulation based on solutions of differential equations which describes Brownian motion collision efficiency, with different initial conditions.

$$\lambda = \frac{r_2}{r_1} \quad 2.10$$

$$\alpha_{Br} = a + b\lambda + c\lambda^2 + d\lambda^3 \quad 2.11$$

Table 2-3: Factors for Equation 2.11 after Han & Lawler (1992).

Diameter of the larger particle (r_1) (μm)	a	b	c	d
0.1	1.025	-0.626	0.516	-0.152
0.2	1.007	-0.860	0.870	-0.322
0.6	0.976	-1.155	1.342	-0.554
1.0	0.962	-1.263	1.522	-0.645
2.0	0.943	-1.383	1.725	-0.748
6.0	0.916	-1.533	1.991	-0.887
10	0.905	-1.587	2.087	-0.936
20	0.891	-1.658	2.221	-1.009
60	0.871	-1.739	2.371	-1.090
200	0.863	-1.775	2.439	-1.125

Figure 2-10 demonstrates the effect of the radius of the larger particle (R_L) and the size ratio between the two particles on the collision efficiency. The vertical axis is the collision efficiency, while the horizontal axis is the size ratio between the two colliding particles. The separate lines represent the size of the largest of the two interacting particles. The short-range efficiency for Brownian motion reduces as the particles become larger. In addition, the collision efficiency decreases as the size of the two particles converges (size ratio = 1).

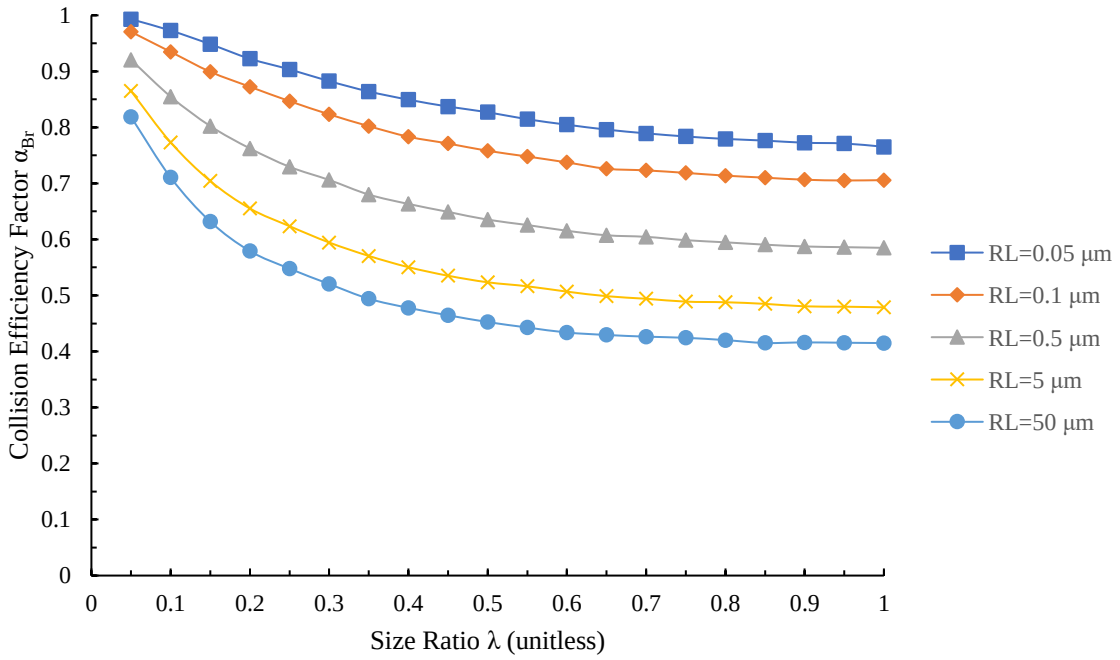

Figure 2-10: Brownian motion collision efficiency factor at 21ºC and a Hamaker constant of 40.6 zJ, adapted from Han & Lawler (1992).

The graph uses a Hamaker constant of $10k_BT$, equal to 40.6 zJ. is for temperature of 21ºC (or 294.1 Kelvin), k_B is the Boltzmann constant. If the Hamaker constant increases to 101.5 zJ, the collision efficiencies will increase by 0.1 when the size ratio is one. In contrast, with a decrease of the Hamaker constant to 10.15, the efficiencies would decrease by a factor of 0.1 at the size ratios of 1 (Han & Lawler, 1992).

2.2.3.3 Fluid Shear

The short-range fluid shear interaction is described by a set of differential equations derived by (Adler, 1981). The differential equations describe the trajectory of two sphere with inter-particular forces. The inter-particular forces are presented by the dimensionless factor, H_A, defines as:

$$H_A = \frac{A}{18 \cdot \pi \cdot \mu \cdot d_l^3 \cdot G} \qquad 2.12$$

where A is the Hamaker constant, J; μ is the dynamic viscosity, (Pa·s); d_l is the diameter of the largest of the two particles, cm; and G is the velocity gradient, s^{-1}. Han & Lawler (1992) presented the graphically the collision efficiency factor, α_{FS}, prediction as a function of the size ratio (λ) and log(H_A) (Figure 2-11). The effect of the inter-particular forces is represented by individual curves on the graph.

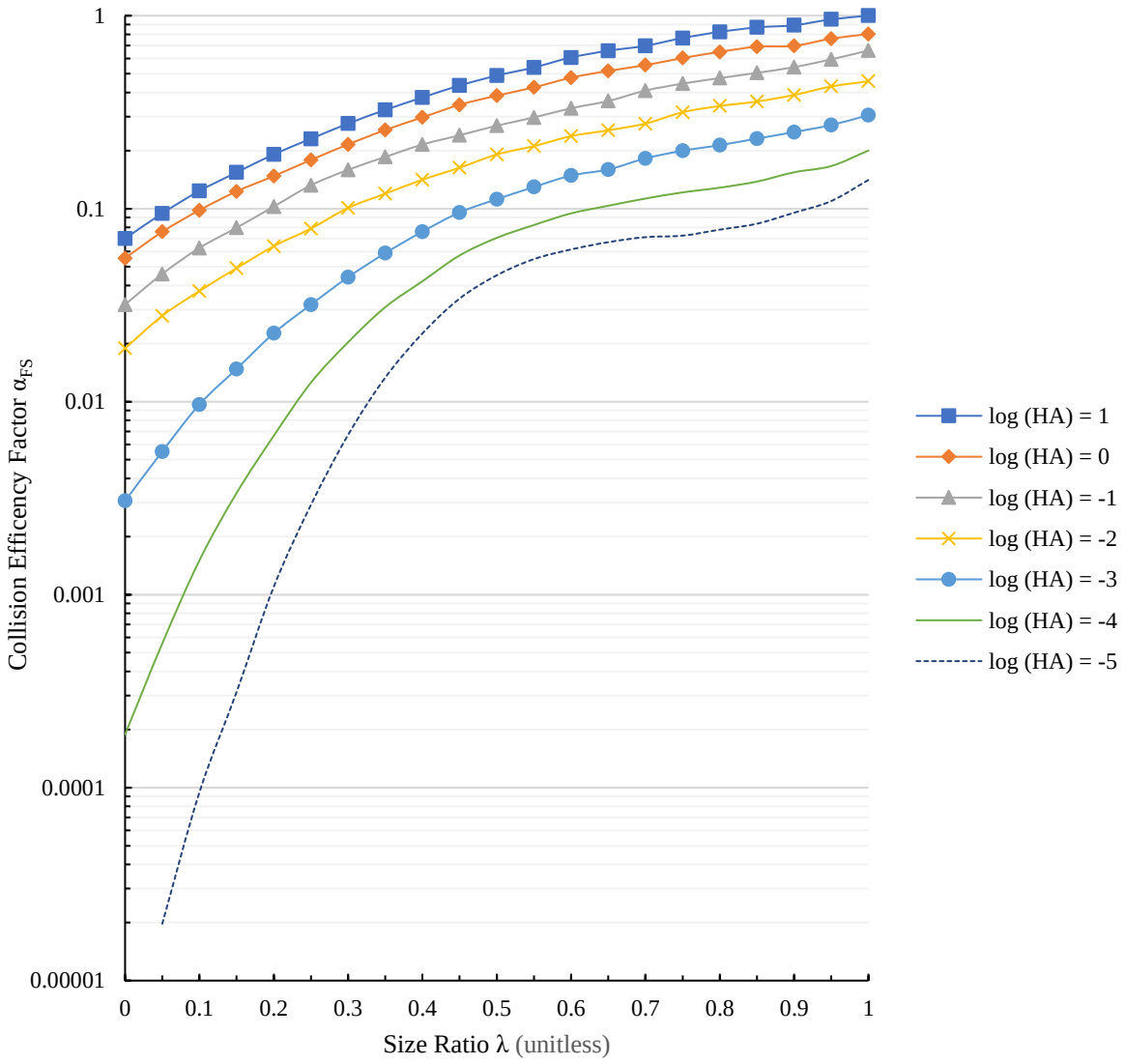

Figure 2-11: Fluid shear collision efficiency factor adapted from Han & Lawler (1992).

As shown in Figure 2-10, the collision efficiency varies between values from 0.1 to 1 for similar size particles (i.e., $\lambda \sim 1$) and decreases to 10^{-3} to 10^{-4} for very different particle sizes. If the particles are adequately destabilized, the relative particle ratio size is near one, the shear rate is low (resulting in a high H_A value), and the large number of the collisions lead to particles/flocs combining to create flocs. If the particles are not destabilized, which results in a low Hamaker constant, the collision efficiency correction can be significant, and only a small fraction (1/1000 to 1/10,000) of the collision results in the formation of new larger particles.

2.2.3.4 Differential Settling

The collision coefficient efficiency function for differential settling was derived by Han and Lawler (1991). The function was derived by analyzing the interaction of particles using the coordinate system shown in Figure 2-12. θ and r_{COR} are the two parameters of the coordinate system used. The vertical axis follows the direction of gravity, while the X axis is the orthogonal distance between the path of the larger particle and the smaller particle.

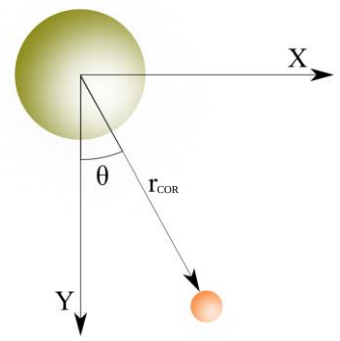

Figure 2-12: Coordinate system used for differential settling computations by Han & Lawler (1992).

The following differential equation represents the rate of change of the distance between the two particles distance with respect to influencing factors:

$$\frac{dr_{COR}}{d\theta} = s \cdot \frac{-cos\theta \cdot L(s,\lambda) \cdot U_{s12} - \frac{D_{12}}{k_B T} \cdot G(s,\lambda) \cdot \nabla\Phi_{12}}{M(s,\lambda) \cdot sin\theta \cdot U_{s12}} \quad 2.13$$

where L(s,λ) and M(s,λ) are hydrodynamic correction factors to Stokes' relative settling velocities, dimensionless; D_{12} is the diffusion coefficient for particles, m^2/s; G(s,λ) is the hydrodynamic correction to the diffusivity constant for particles moving parallel to their line of centers, dimensionless; $V\Phi_{12}$ is the interparticle forces typically obtained by the DLVO theory, J; T is the temperature in Kelvin; k_B is the Boltzmann's constant, $1.38x10^{-16}$ g cm^2/s^2K; λ is the size ratio between the smaller and the larger particles, dimensionless; U_{s12} is the approaching velocity of the particle in the r direction at s_d separation distance; and s_d is the unitless separation distance. The value of s is calculated by:

$$s_d = \frac{2r_d}{r_1 + r_2} \quad 2.14$$

where: r_1 and r_2 is the radius of the larger and smaller particles, respectively; and r_d is the distance between the two particles.

The differential equation was numerically solved using varying initial conditions to determine the critical trajectories cross section (X_C) and thus the collision efficiency factors α_{DS}. The relation between X_C and α_{DS} is presented by equation 2.12 (Benjamin & Lawler, 2013).

$$\alpha_{DS} = \frac{X_C^2}{\left(\frac{d_i}{2} + \frac{d_j}{2}\right)^2} \quad 2.15$$

where d_i and d_j are the diameter of the intersecting particles.

The collision efficiency factor was presented graphically (Figure 2-12) as a function of the size ratio evaluating the effect of inter-particular and hydraulic forces, Hamaker constant, density, and particle

size. All the relations were reduced to one graph using the function the dimensionless number N_g, defined as

$$N_g = \frac{48 \cdot A}{\pi \cdot g \cdot \left(\rho_p - \rho_l\right) \cdot d_l^4} \qquad 2.16$$

where A is the Hamaker constant, J; g is the gravitational constant, m/s^2; ρ_p and ρ_l are the particle and liquid matrix densities in kg/m^3, respectively; and d_l is the diameter of the largest of the two particles, m. The value of N_g has a significant impact on the performance of differential settling. When $\log N_g$ is near 0 the effect of the size ratio is minimal compared to the impact when $\log N_g$ is significantly negative. As the value of N_g decreases, the collision efficiency is hindered dramatically. The HYD line in Figure 2-13 represents the collision efficiency factor only considering the hydrodynamic forces without any van der Waal interactions.

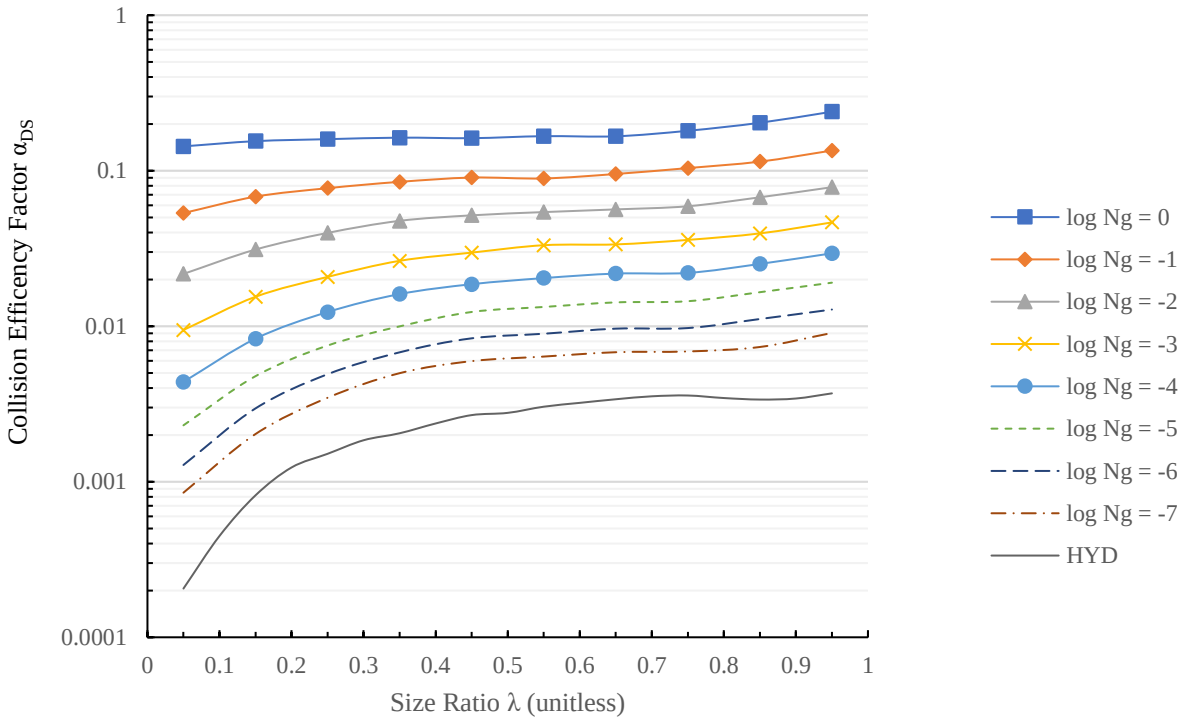

Figure 2-13: Differential settling collision efficiency factor as a function of the particle size ratio adapted from Han & Lawler (1992).

Compared to the fluid shear and the differential settling collision efficiency, the collision efficiency for Brownian motion is relatively low compared to the other mechanisms. The other mechanisms are results of faster moving particles resulting in higher interparticular hydraulic forces and are more dependent on proper particle destabilization (Han & Lawler, 1992).

2.2.3.5 Effect of Temperature on Collision Efficiencies.

Compared to the long-range model, the effect of temperature does not seem as significant. For the Brownian motion collision efficiency, the diffusion coefficient will reduce with temperature. For the fluid shear collision efficiency, both the viscosity and G will be effected by temperature. For the differential settling, the liquid density will vary slightly. The most important parameter that is present in the equations describing of Brownian motion, fluid shear, and differential settling on the collision efficiency is the

Hamaker constant. As discussed in section 2.2.3.1, the Hamaker constant is a relation between the van der Waals forces between particles and the distance between the interacting particles. The DLVO theory states that the van der Waals interaction is dependent on the destabilization by coagulation. By reducing the repulsion forces, the attraction between particles is increased. Inefficient particle destabilization could reduce the collision efficiency of flocculation by over 99% if the particles are not properly destabilized (Benjamin & Lawler, 2013). If coagulation conditions are inefficient, such as the coagulation occurs in less ideal pH levels, it will result in significantly lower Hamaker values and flocculation will not be efficient. As discussed in section 2.1.3, recent research suggests that the optimal pH for coagulation shifts with temperature. Thus, ideally cold temperatures should not affect flocculation compared to inefficient destabilization caused but non-optimal coagulation conditions.

2.2.4 Historical results of cold-water drinking water operations

The effect of temperature on flocculation was first researched by (Velz, 1934). Velz (1934) observed that a higher coagulant dose was required for satisfactory color removal during the Summer than in the Winter. However, this apparent contradiction of superior Winter performance can be explained. Because of the relatively high raw water pHs (6.9 to 7.8), the pH of the coagulated Winter water is within the lower end of the solubility envelope for those temperatures. During the Summer, because of the warmer temperatures the solubility envelope shifts to the left (lower pHs) and the dose used during the Winter is now outside the solubility envelope. Thus, in order to move to within the solubility envelope the coagulant dose had to be increased. This also means that during the summer sweep flocculation is much more important. Camp et al. (1940) determined that temperature did not affect flocculation. They determined the effect of temperature on settling based on the settling curves and adjusted the curves to 10^{o}C to eliminate the variations due to viscosity (Camp et al., 1940). Morris and Knocke (1984) clearly demonstrated that turbidity removals by coagulation/flocculation/sedimentation at 1^{o}C were significantly worse than those at 5 and 20^{o}C, and the impact of temperature was more severe for low turbidity waters. Hanson & Cleasby (1990) studied the effect of temperature on the hydrodynamics and chemistry of water treatment with

coagulation and gravity separation. Hanson & Cleasby (1990) observed improved treatment while operation at constant pOH as opposed to constant pH. As treatment plants operate at cold temperatures a significant portion of the year in Canada, additional research on the coagulation, flocculation and gravity separation with conventional coagulants is necessary.

2.3 Dissolved Air Flotation

An alternative to conventional drinking water treatment train is replacing the sedimentation process with a dissolved air flotation (DAF) process. Regarding physical mechanism, sedimentation and dissolved air flotation are solid-liquid separation processes taking advantage of gravity, thus called gravity separation processes. As discussed earlier, the two preceding processes (coagulation and flocculation) are designed to destabilize the particles and produce flocs. When used in conjunction with sedimentation the coagulation and flocculation units are designed and operated to produce large flocs (diameter > 100μm) that settle to the bottom of the sedimentation basin during the sedimentation process. For the dissolved air flotation process, flocs enter a contact basin where microscopic bubbles attach to the flocs forming floc-bubble aggregates. The aggregates flow into the separation basin, where they rise to the surface producing a semi-solid mass, and the clarified water flows downward in the separation basin. The process used to remove the flocs from the top of the separation basin varies depending on the designer of the treatment process. DAF efficiently treats water with turbidity values less than 100 NTU (Valade et al., 2009). For DAF the incoming flocs do not have to be so large, so the flocculation does not need to be as extensive, so often there are only two flocculation basins in series and they have shorter detention times (Edzwald & Haarhoff, 2012). For the effective operation of DAF systems is that the incoming flocs are effective in forming the bubble-floc aggregates.

Figure 2-14 shows a typical dissolved air flotation treatment train in a dead-end saturator configuration with its auxiliary equipment.

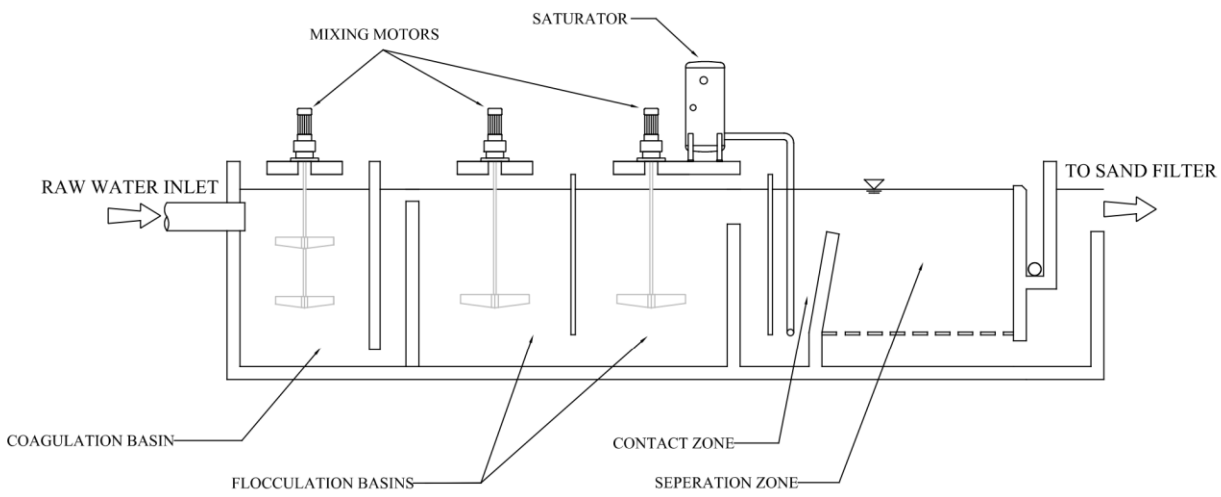

Figure 2-14: Dead-end dissolved air flotation configuration.

2.3.1 Floc Sizes for DAF systems

Floc sizes are a significant variable for gravity separation processes. The optimal floc size for dissolved air flotation has been debated among researchers. Some research indicates that smaller flocs, in the size range of 15 to 25 μm, are favourable but acknowledge the removal efficiency is high for large flocs (Park et al., 2001). The problem with large flocs is the floc breakup as the floc rises. (Edzwald, 1993, 2010). Other research proposes that the floc size should be as close as possible to the bubble size (Park et al., 2001). Edzwald and Haarhoff (2012) states that the flocculation process before DAF treatment should target flocs between 25 and 50 μm of size as they demonstrate high collision efficiency with microbubbles. While additional research indicates that large flocs are optimal as they have greater collision efficiency, and larger flocs have lower densities (Fukushi et al., 1995; Tambo & Watanabe, 1978).

Considering that dissolved air flotation bubble concentrations are in the range of 75,000 bubbles per millilitre (Edzwald & Haarhoff, 2012), the increased collision efficiency and reduction of particle density in exchange for floc breakage may be advantageous for operations. Depending on coagulant doses, flocs were observed to have a mean floc size of around 50 μm for water flocculated with 41.7 mg/l of alum

in a DAF pilot plant, while the floc size reduced to a mean floc size of 25 μm for water treated with 15.5 mg/l in the same pilot plant (Gorczyca & Zhang, 2007). The average floc size will depend on water chemistry, temperature, and pretreatment methods. There are two main methods to measure floc sizes, the first is using direct measurements with a camera (Fan et al., 2020; Jarvis et al., 2005; Gonzalez-Galvis et al., 2022; Sun et al., 2016) and the other is measuring the shadow the floc cast on an camera (Alam et al., 2011; Alansari & Amburgey, 2020; Fitria et al., 2014; Govoreanu et al., 2009; Li et al., 2006; Verberk et al., 2007; G. R. Xu et al., 2008; Yu et al., 2006). The main advantage of directly measuring the floc size with a camera is that the flocs are measured in-situ with minimal disturbance but the focus length may be long and the floc size is slightly inaccurate. The advantage of measuring the shadow cast by the floc is that the measuring cell is a know distance of the camera sensor reducing the inaccuracy but the pumping and transportation methods may cause floc breakage.

2.3.2 Bubble Size

The mean bubble size in a dissolved air flotation system varies with pressure, flow rate, types of nozzle and relative position in the contact and separation basin. (de Rijk et al., 1994; Gorczyca & Zhang, 2007; Haarhoff & Edzwald, 2004; Leppinen & Dalziel, 2004; Zabel, 1983). Table 2-4 is a compilation of multiple studies that measured bubble size in DAF systems. The flow rate should only be used to compare results within an investigation, as different studies measure flowrate differently. For a given flowrate, the bubble size decreased with the increased saturator pressure as expected. The system flowrate also had an impact on the bubble size. It is possible that the increase flowrate decreased the bubble concentration and in turn reduce the agglomeration between bubbles (Edzwald & Haarhoff, 2012). The mean/median bubble sizes observed in the common operating range of saturated pressure varied between 30 μm and 70 μm.

Table 2-4: Dissolved air flotation bubble size from literature.

Bubble Size (μm)	Saturated Water Pressure (kPa)	System Water Operational Flow Rate (l/min)	Nozzle	
40-90	485	-	Needle Valve	Zabel, 1983
20-50	485	-	Proprietary Nozzle	
106[a]	350	0.83	Needle Valve	de Rijk et al., 1994
83[a]	350	1.25	Needle Valve	
56[a]	350	1.67	Needle Valve	
72[a]	500	0.83	Needle Valve	
51[a]	500	1.25	Needle Valve	
49[a]	500	1.67	Needle Valve	
47[a]	620	0.83	Needle Valve	
41[a]	620	1.25	Needle Valve	
37[a]	620	1.67	Needle Valve	
32[b]	600	-	-	Haarhoff & Edzwald, 2004
82[b]	200	-	-	
62[b]	500	-	-	

[a] Median bubble diameter,
[b] Mean bubble diameter

In addition to pressure and the types of valves used, the bubble size varies depending on the location in a DAF system and the DAF system design. Leppinen & Dalziel (2004) observed the smallest median bubble sizes just under the surface near the separation zone inlet. The smallest bubbles were measured in the contact zone, but large macrobubbles (>150 μm) (Edzwald, 2010) were also present, increasing the mean bubble size.

The effect of pressure on bubble size has been researched by Zhang et al. (2015) while the effect of bubble size against final turbidity was researched by Gonzalez-Galvis & Narbaitz (2020). Recently, direct measurement of bubble size and floc size using unintrusive methods were used by Marega & Reali (2023). They found an increased floc diameter with time up even after 16 minutes of flocculation. They also observed an increase in efficiency with increased recycle ratio. As all treatment plants are slightly different, operating pressures can provide some initial guidelines but knowing the interaction between flocs and bubbles at a microscopic range could allow individual plants to optimize their DAF operations. The

interaction between flocs and bubbles in a DAF systems have been modeled with a single-collector collision theory (Malley & Edzwald, 1991) and with the population balanced model of bubbles and floc in a turbulent flow condition (Fukushi et al., 1995). In a DAF plant, the non laminar conditions result in a better representation from the population based model (Fukushi et al., 1995). At a microscopic scale, the interaction between flocs and bubbles are similar to the principles described by the flocculation theory. The main driving forces are the fluid shear interactions in the contact zone and the differential settling in the separation zone (Gregory et al., 1999). The potential attachment between bubbles and flocs is more favorable when the particles are of similar size and of opposite charges (Han et al., 2007; Leppinen, 1999).

2.3.3 Flow Pattern

Stoke's law can be used to calculate the bubble rise velocity of different size bubbles and compare their rise velocity at different temperatures (Table 2-3). Stokes's law's assumption of constant particle size is valid for microbubbles since they maintain a spherical shape compared to macro bubbles that deform into shapes with higher drag coefficients (Cliff et al., 1978). Table 2-5 assumes laminar flow regime for demonstration purposes.

Table 2-5: Bubble rise velocity at cold and warm temperatures.

Bubble Size (μm)	2°C	20°C
	Rise Velocity (m/h)	Rise Velocity (m/h)
10	0.117	0.195
20	0.468	0.781
30	1.05	1.76
40	1.87	3.12
50	2.92	4.88
60	4.21	7.03
70	5.73	9.57
80	7.48	12.5
90	9.47	15.8
100	11.7	19.5
120	16.8	28.1
140	22.9	38.3
150	26.3	43.9
160	38.4	47.9
170	41.2	51.3
180	43.9	54.8

Rise velocity decreases with temperature as a function of the increased viscosity. The bubble rise velocity brings forward another question with DAF. Edzwald & Haarhoff (2012) state that smaller bubbles are preferred for DAF to enhance the formation of floc-bubble aggregates. Thus, the DAF hydraulic loading rate could be limited to the rise velocity of the desirable size bubbles. Aquadafs, DAF systems manufactured by SUEZ, are known to operate at high hydraulic loading rates, as high as 40 m/h, which would require bubbles approximately 170 μm in diameter at 2 ºC.

Flow in a DAF tank differs depending on the presence of bubbles, the hydraulic loading and the quantity of air in the recycle stream (Lundh et al., 2002). The flow will spin in a circular pattern in the separation zone if no induced bubbles are in the stream (Lundh et al., 2002). The induction of air bubbles

in the stream causes stratification in the separation zone (Lundh et al., 2002). Water entering the separation zone contains more air, reducing this fluid's density. The air-enriched water flows on top of the denser water under the float layer as the water flows horizontally across the top section of the separation zone. As the floc particles collide with microbubbles in the separation zone, the plume of bubbles acts as a filter (Lundh et al., 2002). As the air content of the water decreases, the stratification reduces to the point where short-circuiting occurs (Lundh et al., 2002).

Kiuru (2001) divided DAF systems based on three generations corresponding with the flow pattern and the physical principles governing clarification operation. The mining industry developed the first generation DAF systems. Their design was governed by the bubble rise velocity and thus they had shallow but long separation zones. The second generation of DAF systems consisted of a deep and broad tanks that were significantly shorter than the first generation. The flow through the separation zone is more vertical, close to 40 degrees from horizontal. In contrast to the first generation, the second generation of DAF tank maintained a layer of bubbles the entire length of the tank. It was observed that increased efficiency was possible with a second-generation DAF because the bubble cloud at the top of the tank acts as a filter. The third generation DAF systems can reach a high hydraulic loading rate since a thicker cloud of bubbles is maintained. The deeper cloud of bubbles is thus acting as a filter, such as a sand filter. The flow is directly vertical in the separation zone.

Considering the hydraulic loading of the three generations, bubble size alone does not govern the entire operation of the DAF system. Two factors affecting the performance are the flow pattern and the filtering effect of the bubble cloud (Leppinen and Dalziel 2004).

2.3.4 Macrobubbles

Macrobubbles are bubbles with a diameter greater than 150 micrometres (Edzwald, 2010), which are problematic for DAF systems. First, they consume a large quantity of air that would otherwise be

allocated to form microbubbles. Second, the rapid rise velocity of the macrobubbles breaks up floc-bubble aggregates.

Table 2-6 is a quantification of the number of microbubbles that could be formed per 0.5, 1, and 2 mm macro bubbles assuming the macro bubbles maintain a spherical shape (Cliff et al., 1978).

Table 2-6: Number of microbubbles of different sizes with the same total volume as macrobubbles of 500um, 1000um and 2000um diameter.

For a 500µm diameter macrobubble		**For a 1000µm diameter macrobubble**		**For a 2000µm diameter macrobubble**	
Microbubble diameter (µm)	# of Microbubbles with the total volume as a 500µm diameter macrobubble	Microbubble diameter (µm)	# of Microbubbles with the total volume as a 1000µm diameter macrobubble	Microbubble diameter (µm)	# of Microbubbles with the total volume as a 2000µm diameter macrobubble
30	277	30	1111	30	4444
40	156	40	625	40	2500
50	100	50	400	50	1600
60	69	60	277	60	1111
70	51	70	204	70	816
80	39	80	156	80	625
90	30	90	123	90	493

Macro bubbles should be avoided in DAF contact and clarification basins. The rapid rise velocity of macro bubbles makes them inefficient at removing flocs from suspension and reduces the quantity of air that can produce microbubbles acting as a filter for the flocs (Edzwald, 2010). It also reduces the effective air content of the water as the macro bubbles rapidly rise to the surface and releases the air into the atmosphere, possibly disrupting the flow pattern in the separation zone that is formed when the influent

water has a high concentration of microbubbles(Lundh et al., 2002), which permits the operation at high hydraulic loading relative to the individual bubble rise velocity.

2.4 Cold Temperature DAF Operation

DAF treatment is advantageous for gravity separation compared to sedimentation as it is efficient at removing small particles (Edzwald & Haarhoff, 2012; Malley & Edzwald, 1991), and in particular the smaller and more fragile flocs formed at cold temperatures (Hanson & Cleasby, 1990). Table 2-7 list some Canadian treatment plants, their operating conditions and coagulants used.

Table 2-7: Coagulant during with in several Canadian DAF plants.

City	Province	Winter Water Temperature (ºC)	Coagulant	Coagulation/Flocculation Aid
Penticton	British Columbia	2 – 6	Aluminum Chlorohydrate	LT 7990 cationic epi-amine coag aid
Kelowna	British Columbia	~4	Polyhydroxy Aluminum Chloride	Isopac
Wetaskiwin	Alberta	~2	Aluminum Sulphate and Aluminum Chloride[1]	Polymer[2]
Winnipeg	Manitoba	2	Ferric Sulphate	None
Deseronto	Ontario	~3	Polyaluminum Chloride	Polymer[2]
Smith Falls	Ontario	2 - 6	Polyaluminum Chloride	Norfloc 122 non-ionic polyeletrolyte
St John's Bay Bulls Big Pond Facility	Newfoundland and Labrador	~1.4	Aluminum Chlorohydrate	None
St John's Petty Harbour Long Pond Facility	Newfoundland and Labrador	~2.7	Aluminum Chlorohydrate	None
Aylmer	Quebec	2-5	Polyaluminum Sulphate	Cationic polyacrylamide polymer.

[1] Aluminum chloride dose varies between 100 and 210 mg/L.
[2] Polymer type not specified.

Most of the Canadian plants are operating with polynuclear aluminium coagulants with or without polymers. The only DAF plant in Canada that operates with alum as the sole coagulant is the Belleville WTP, and the DAF units are not operated during the Winter as they are intended for algal and cyanobacterial cell removal. All of the plants surveyed used the same chemicals throughout the year, but the doses were generally slightly higher during cold water conditions. The chemical dosages at the Wetaskiwin WTP were unusual in that they were much higher than at the other plants. During cold water conditions only the Wetaskiwin WPT operates using alum, but it is in conjunction with very high aluminum chloride concentrations (>120 mg/L) plus approximately 10 mg/L of diallyldimethylammonium chloride. And somewhat surprisingly, the chemical dosages were somewhat higher during the summer.

Malley & Edzwald (1991) compared DAF to conventional sedimentation. They compared the two methods for turbidity removal, flocculation time, DOC removal, UV absorbance, true colour and disinfection by-product precursors. DAF performed better than conventional sedimentation for turbidity removal, especially when the temperature reduced to 4ºC. DAF is more efficient than conventional sedimentation to treat waters with low turbidity (<20 NTU) that contain high levels of humic acids. DAF and conventional treatment performed equally well for the removal of DOC, true colour, UV absorbance as well as disinfection by-product formation potential. Edzwald and Haarhoff (2012) recommend that DAF treatment during cold water periods using alum alone should raise the coagulation pH to 7.0 or even 7.5, but there has not been any field research clearly demonstrating the impact of coagulation pH of cold water DAF performance.

The predominant forces acting on a particle in water are the gravitational force, the drag force and the buoyant force. It should be noted that two of the forces are a function of water density which is itself a function of temperature. Water increases density from 997 kg/m^3 at 25°C to 1000 kg/m^3 at 4°C (Crittenden et al., 2012). For both sedimentation and flotation, the drag force is hindering the separation process equally for the same particle size. The disadvantage for flotation is that the drag force is dependent of the cross sectional area which consist of the cross sectional area of the floc-bubble aggregates, while for

sedimentation only the cross-sectional area of just a floc must be considered. As per the buoyancy force, the water density increase, caused by the temperature decrease, would result in a greater upward component reducing the impact of the gravitational force. So it should be advantageous for flotation.

2.5 Research Needed

Using DAF for treatment of cold waters has not been researched significantly, and particularly using alum as the sole coagulant. Presently, most Canadian drinking water plants with DAF systems are not operating with alum, thus operating with more expensive coagulant for a treatment system that is inherently more energy intensive. Although temperature has a significant impact on the collision frequencies and collision efficiencies of the various mechanism considered by Smoluchowski flocculation models, the most critical variable in the calculation of collision efficiencies is Hamaker constant. And as it is primarily a function of the quality of the coagulation, the efficiency of the coagulation seems more important than the flocculation. So the solubility of aluminum at lower temperatures is critical as it differs from that at room temperature. Considering the new information about shifting solubility limits with temperature (Edzwald, 2020), the treatment of cold waters using DAF with alum by increasing the pH seems to be feasible. In fact, this has been recommended by Edzwald and Haarhoff (2012), but there does not seem to be studies experimentally demonstrating the impact of pH adjustment on DAF performance. This needs to be studied. Cold-water optimization for alum can result in cost savings for the treatment plant as alum is the least expensive conventional, inorganic coagulant.

The second main research need identified is a study on the effect of bubble size on floc removal to further understand the interaction between bubbles and flocs. The literature does not directly compare bubble size against the flocs removed. This information will be valuable and important. First, knowing the effect of bubble size on floc removal efficiency could provide the knowledge to reduce the pressure in some dissolved flotation plants. Second, having factual information can help demonstrate the need to increase the saturator pressure in some dissolved air flotation plants in order to improve their performance.

Chapter 3 - Materials and Methods

This chapter discusses the materials and methods used in this research. It includes a description of the water sampling methods, the materials used for the analysis, the testing equipment and methods, the analytical methods, and the experimental plan.

3.1 Materials

This section covers the materials used for the research. It begins with the challenge water, followed by the reagents, and by descriptions of the two dissolved air flotation batch testing equipment used. The first is a small scale (one-litre) batch configuration referred to as the DAF Jar tester, and the second is a 20 L batch testing configuration referred to as the LB-DAF system.

3.1.1 Challenge Water

Ottawa River water was used for the experiment as it is easily collected, and many treatment plants use it for drinking water production. The water for the cold water experiments were collected from the Aylmer drinking water plant laboratory in Gatineau, Quebec during the spring of 2019. The water for the floc size and bubble size experiment was collected from the rivers edge during the winter of 2020. The water collected from the river was collected with a submersible water pump (062-4146-2, Mastercraft, Toronto, ON) placed in the water five meters from the river's shore where the river was a meter deep. The pump was placed inside a 19 litre (5 US gal) high density polyethylene (HDPE) bucket (PR19003802, Home Depot, Atlanta, GA) to prevent collecting unrepresentative riverbed sediments. The pump was operated for five minutes without disturbance prior to collection to obtain a representative river sample. The collected water was transported in 19-L HDPE buckets. The water was stored in either 19-L HDPE buckets or 208-L HDPE barrels (S-10757, Uline, Pleasant Prairie, WI) kept in a temperature-controlled room at 1ºC±1ºC. Turbidity was maintained in the barrel by mixing the barrel with a 1,500 mm long stirring

instrument for two minutes before transferring the water to HDPE buckets and use in the experiments. To maintain the turbidity levels constant in the HDPE bucket before transferring the testing apparatus, a 450 mm long stainless-steel tube was used to agitate the water. As a low turbidity, low alkalinity, relatively high colour and NOM water Ottawa River water it is more amenable to treatment by DAF than by sedimentation (Edzwald and Haarhoff, 2012)

3.1.2 Chemicals

The main consumables used in this study were the aluminum sulphate coagulant and the chemicals used for water characterization and pH adjustments. The entire research used a commercial grade liquid aluminum sulfate coagulant (ALS, Kemira, Montreal, QC). The coagulant has an aluminum concentration of 4.3±0.1% Al^{3+} with low basicity (0.1±3%) and a pH of 2.0. The pH was increased with sodium hydroxide (ACS grade, VWR Chemicals, Mississauga, ON) and reduced with hydrochloric acid (ACS grade, Fisher Chemical, Ottawa, ON).

Potassium hydrogen phthalate (ACS grade, VWR Analytical, Mississauga, ON) was used to prepare the calibration solutions for the dissolved organic carbon (DOC) analysis. Sodium persulfate with 99% or greater purity (Anachemia, Mississauga, ON) and phosphoric acid (ACS grade, Fisher Chemical, Ottawa, ON) were used as reagents for the DOC analyzer. EDTA and Hach Standard Hardness Solutions were used with a Hach ManVer 2 hardness indicator and hardness buffer (Hach, Loveland, CO) to measure the water hardness. The pH meter was calibrated with 4.00, 7.00, and 10.00 pH reference standards that were NIST traceable (VWR Chemicals, Mississauga, ON)

3.1.3 DAF Jar Tester

A 1-L dissolved air flotation jar test (PFJT, Capital Controls Ltd., Didcot, Oxon, England) was used for some of the experiments. The jar test vessel (Figure 3.1) consists of a graduated acrylic cylinder with three sampling ports and a motor assembly connected to a shaft with a rectangular paddle. The coagulation, flocculation, and flotation steps are conducted in the same vessel. In addition, the system included an 8-L

saturator (pressure) tank, a needle valve-based pressurized water delivery assembly (Figure 3-2), and a portable air compressor (TAW-0308, HDX, Atlanta, GA) were used. The jar test vessel is constructed of an acrylic cylinder with an internal diameter of 9 cm and has a total volume of 1.4 litres. The cylinder walls gradations at 0.02 L intervals serve to indicate the volume being used. The bottom of the vessel is conical shaped and has a sampling port at the bottom of the cone. Additional sampling ports are located 25 and 75 mm from the bottom of the vessel. The sample ports are constructed with acrylic tubes with an inside diameter of 5 mm and a silicon tube with an inside diameter of 6 mm. After each use, the sampling ports were flushed and closed with plastic pinched clamps on the silicon hoses. An electric motor assembly, with ten incremental speed selections, fits on the top of the acrylic cylindrical vessel. A metal shaft, attached to the motor, terminates with a rectangular paddle to mix the sample. The paddle is 2 cm tall and 6 cm wide and is attached to the shaft at its center point. The motor assembly has an opening in its support plate to permit the addition of coagulant.

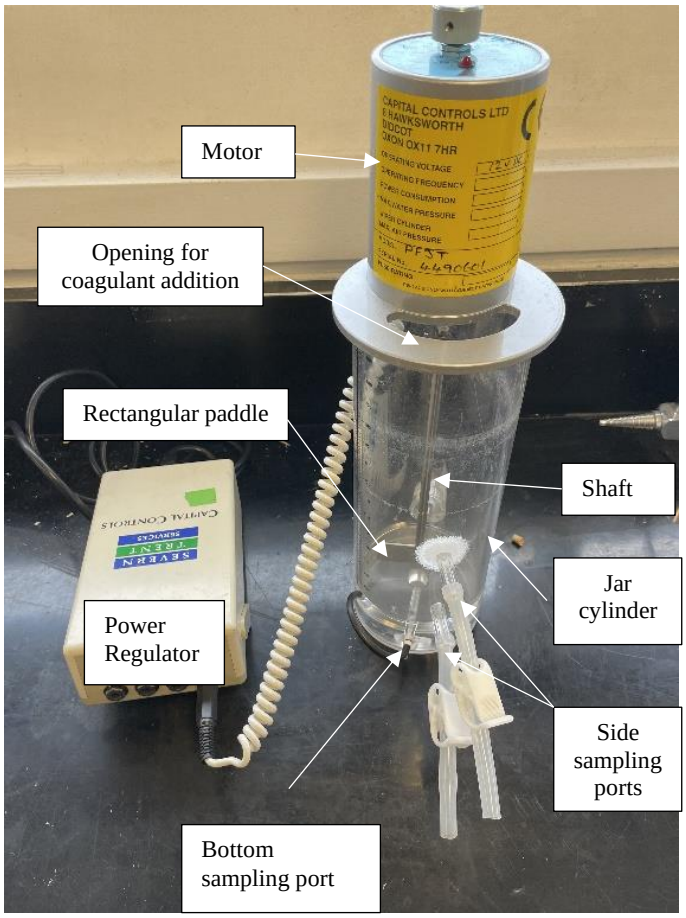

Figure 3-1: Small-scale jar test apparatus.

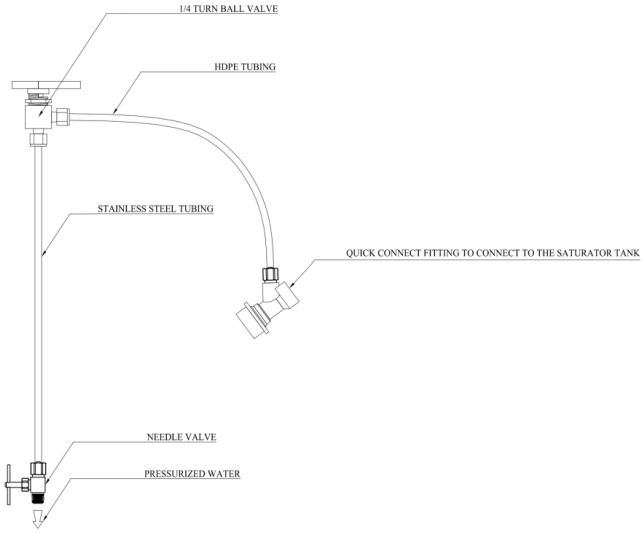

Figure 3-2: Needle valve-based assembly for the delivery of the pressurized water to the jar tester vessel.

For the flotation step, the saturated water is introduced into the jar test vessel, it is produced in an aluminum pressure vessel that acts as a non-packed, dead-end saturator. The vessel is fitted with four flush-faced male fittings. The pressurized water delivery valve assembly is attached to one fitting, and another fitting is equipped with a 100 PSI (690 kPa) pressure gauge. To prepare the saturator for the experiment, the vessel was filled with deionized water and then pressurized. The saturator was pressurized with a 7.6 L (2-gallon) electric air compressor (TAW-0308, HDX, Atlanta, GA) connected with a polyurethane air hose through one of the flush mount fittings on the saturator vessel. The saturator was then disconnected and manually shaken vigorously until the pressure stopped decreasing and for an additional 60 seconds thereafter. The saturated water was injected with a needle valve-based assembly (Figure 3-2) consisting of a 0.64 cm (¼ inch) brass needle valve attached to a 0.64 cm (¼ inch) stainless steel tube which connects to a ¼ turn Swagelok ball valve. The valve is connected to a high-density polyethylene hose terminating with a quick connect flush face female fitting that matches the saturator's fitting.

The small-scale DAF jar test's configuration utilizes the cylindrical acrylic vessel and the eight-litre saturator. In the original equipment the supersaturated water was introduced through a high-density polyethylene tube with an inside diameter of 1 mm. The original system was not used as it did not provide representable results compared to DAF treatment plants.

3.1.4 LB-DAF apparatus

The LB-DAF is a large-scale batch-style dissolved air flotation testing setup developed in our lab (Gonzalez Galvis, 2019; Gonzalez-Galvis and Narbaitz, 2020). The system consists of a 20-L baffled circular tank mixed with a variable-speed electric motor and the same pressurized water production system used for the small-scale jar tests (Figure 3-3). Again, the coagulation, flocculation, and flotation processes occurred in the same tank. Detailed information about LB-DAF is available from the developer's thesis (Gonzalez-Galvis, 2019). From the series of impellers available, the square 10 cm by 10 cm square impeller was used as it is the most studied impeller by Gonzalez-Galvis (2019).

a)

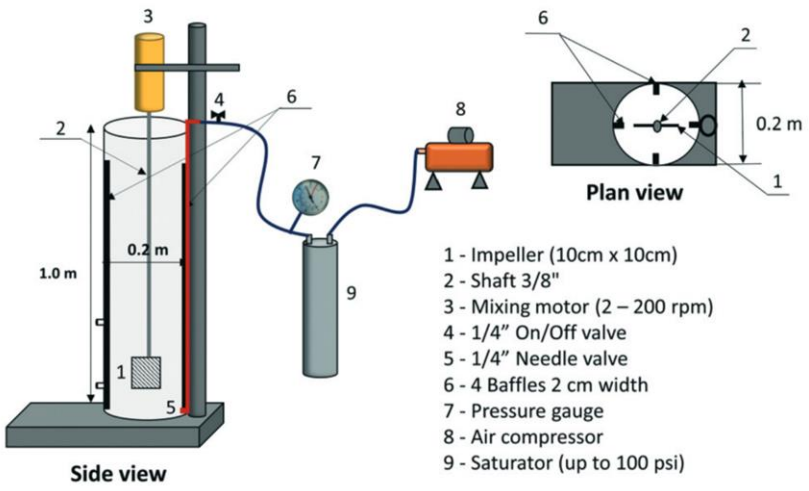

b)

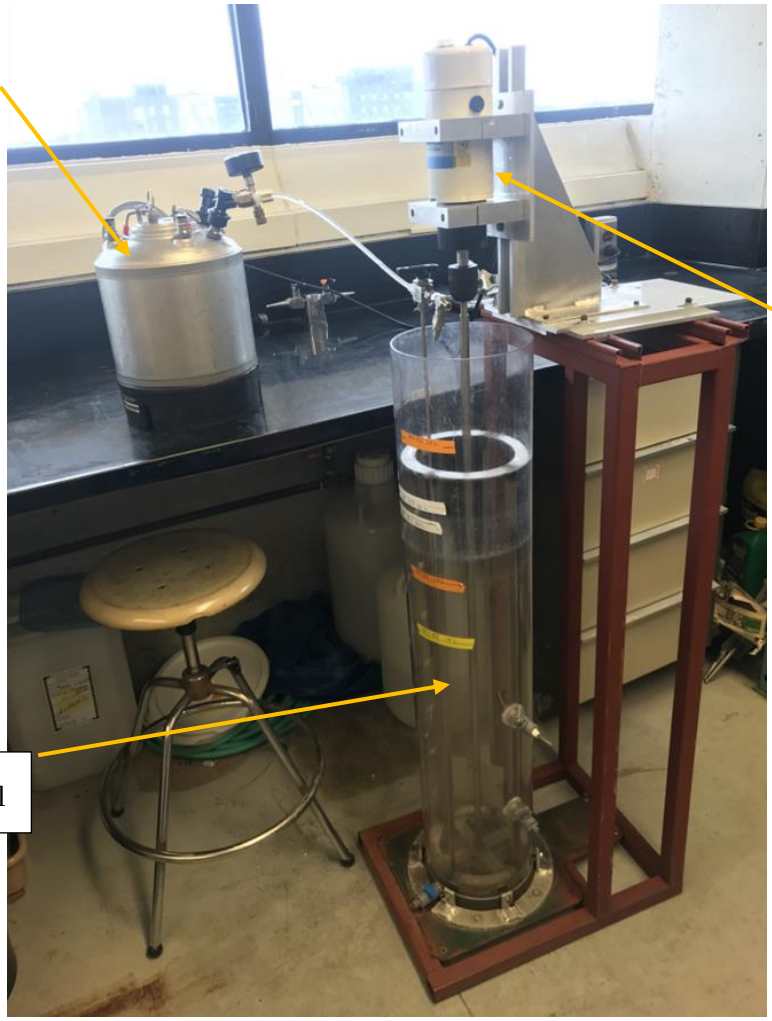

Figure 3-3: Large volume bench-scale dissolved air flotation apparatus a) schematic, from Gonzalez-Galvis (2019) b) photo of the apparatus.

3.2 Experimental Methods

This section covers the standard experimental methods used for the research. If the methods were modified during the experiment, the alterations are presented in their respective sections. The section discusses the individual dissolved air flotation procedures for the small-scale jar test and larger-scale batch tests and the analytical methods used to characterize the challenge water and to evaluate the results of the experiments.

3.2.1 DAF Jar Tests

Unless stated otherwise, the DAF small-scale jar test was performed on a 1-litre sample of challenge water. The procedure consisted of rapid mixing the water sample at a mean velocity gradient (G_C) of 240 s^{-1} for 60-second rapid mix period before adding the coagulant. Once the coagulant was added, the sample was mixed at the same intensity for an additional 60 s to recreate the rapid mix stage in a treatment plant. After the rapid mixing step, the motor speed was reduced to provide a $G_F = 12\ s^{-1}$ level for 900 seconds for the flocculation step. Afterwards, the motor assembly was removed, and the valve assembly was installed with the needle valve placed approximately 3 cm from the bottom of the vessel to introduce the saturated water. A three-prong clamp attached to a stand held the valve assembly in place. Before using the valve assembly, it was purged into a beaker to remove the unpressurized water and air. 100 ml of water pressurized at 480 kPa is injected to recreate a 10% recycle ratio. Once the pressurized water was injected, the system was left undisturbed for 600 s to allow the flotation to occur. Once the 600 s elapsed, water was sampled from the higher side sampling port on the jar test apparatus and analyzed.

3.2.2 LB-DAF tests

For the experiments performed with the LB-DAF, 20 litres of challenge water was transferred into the LB-DAF tank after being agitated to have consistent turbidity values. The water was mixed for two minutes at a relatively high speed ($G_C = 296\ s^{-1}$) to insure an uniform distribution. After two minutes, liquid coagulant was added, and the mixing speed was maintained for another minute. The mixing speed was then

reduced for the flocculation step; to study the impact of flocculation mixing intensity experiments were conducted using different speeds. Depending on the experiment, the flocculating stage duration ranged from 1 and 15 minutes. After flocculation, the motor was stopped, the pressurized water delivery system was purged and then inserted in the mixing vessel with the needle valve placed five centimetres from the bottom of the tank. Then, the valve was opened, and 2.2 litres (the equivalent to a 10% recycle ratio) of water from the saturator was injected into the flocculated challenge water. The injected water was supersaturated with air when released into the flocculated challenge water; thus, air bubbles precipitated into the solution forming microbubbles. The challenge water and bubble suspension was left undisturbed (i.e., without agitation) for fifteen minutes so that the floc-bubble aggregates would form, float and separate from the suspension. Samples were retrieved from the sampling port located in the front of the vessel.

3.2.3 Analytical methods for water characterization

This section covers the analytical methods used for this research. This includes the determination of pH, temperature, UV absorbance, dissolved organic carbon, specific UV absorbance, turbidity, bubble size measurements, and floc size measurements.

3.2.3.1 pH

The pH of the challenge water and the treated water was measured with a pH meter (pHbasic, Sartorius, Gottingen, Germany). The pH meter was calibrated weekly with pH 4.00, 7.00, and 10.00 buffer solutions. The samples were slowly mixed on a stir plate with a magnetic stirring bar while the pH measurement was taken.

3.2.3.2 Temperature

The water temperature was measured using a digital thermometer (Digi-Sense, Cole-Parmer, Laval, QC). The thermometer's calibration was verified weekly with iced distilled water and boiling distilled water.

3.2.3.3 Ultraviolet Absorbance at 254nm

Ultraviolet absorbance at 254nm was measured using a benchtop spectrophotometer (DR6000, Hach, Loveland, CO). The measurement was performed with a quartz cell with a 10 mm path length. Prior to the analysis, the samples were filtered through a 0.45 μm nylon membrane filter (47 mm diameter, PALL Sciences Corp, Mississauga, ON) using vacuum filtration. The UV-254 absorbance measurements were performed in triplicate.

3.2.3.4 Dissolved Organic Carbon (DOC)

The DOC concentration of the samples was measured by first vacuum filtering the samples through a 0.45 μm nylon membrane filter (47 mm diameter, PALL Sciences Corp, Mississauga, ON) and then using a UV-Persulfate oxidation-based TOC analyzer (Phoenix 8000, Tekmar-Dohrmann, Cincinnati, OH) for the analysis. The DOC analysis followed standard method 5310 C (APHA, AWWA, & WEF, 2012). The instrument was calibrated before commencing any analysis, and after every ten samples with 0, 1, 2, 4, and 8 C/L potassium phthalate solutions. Prior to the analysis the samples were filtered through a 0.45 μm nylon membrane filter (47 mm diameter, PALL Sciences Corp, Mississauga, ON) using vacuum filtration. Samples not analyzed within two hours of sampling were acidified with 0.1N HCl to a pH of 2 and stored in a refrigerator at a temperature of 4±1 degrees Celsius. The DOC measurements were performed in triplicate.

3.2.3.5 Specific UV Absorption (SUVA)

Specific UV-Absorption is the ratio between the UV_{254} absorbance per 1 cm and the DOC concentration (in mg C/L) multiplied by a factor of 100, as shown in equation 3.1.

$$SUVA = \frac{UV_{254}}{DOC} \times 100 \qquad 3.1$$

3.2.3.6 Turbidity

Turbidity was measured using a nephelometric turbidity meter (2100AN, Hach, Loveland, CO). The turbidity meter was calibrated with <0.1 NTU and 20 NTU turbidity standards and routinely checked. The turbidity measurements were performed in triplicate.

3.2.4 Bubble Size Measurements

The size of the bubbles produced by the dissolved air flotation were measured using a microscope camera (DX-1, Veho, Dayton, OH), and the images were processed with ImageJ (National Institution of Health, Bethesda, MD) and tabulated in a spreadsheet. The bubbles were produced in a 2-litre square vessel (B-ker^2, Phipps & Bird Inc., Richmond, VA) which contained 2000 ml of deionized water (Figure 3-4). The needle valve-based assembly was connected to the pressurized saturator and purged into a beaker to precondition the assembly. The needle valve-based assembly was moved to the 2-litre square vessel with the needle valve placed approximately three centimetres from the bottom, as it would be in the jar test. The needle valve assembly was held in place with a three-prong clamp secured to a stand. 0.2 litre of saturated water (the equivalent of a 10% recirculation ratio) was introduced into the vessel to produce bubbles. A wire of 131 μm was attached to the vessel's side to calibrate the images. The camera was first focused on the wire, and photos were taken to calibrate the image analysis program. Once calibrated, the entire camera assembly was slid towards the vessel to move the focus point of the camera into the water bubble matrix. None of the camera settings were modified after the initial calibration for the test period. Bubble sizes produced by the valve assembly were measured at four different saturator pressures (275, 410, 480, and 620 kPa). The bubble sizes are presented as cumulative distributions, thus they are on a base one scale, the datasets varied between 1712 units counted and 2133 units counted. For more information, see section 3.2.6 Frequency-Based Analysis. Figure 3-5 is an example photo of the images used to determine the bubble size distribution. Between 22 and 94 bubbles were measured by photo. Between 26 and 36 photos were used per pressure values.

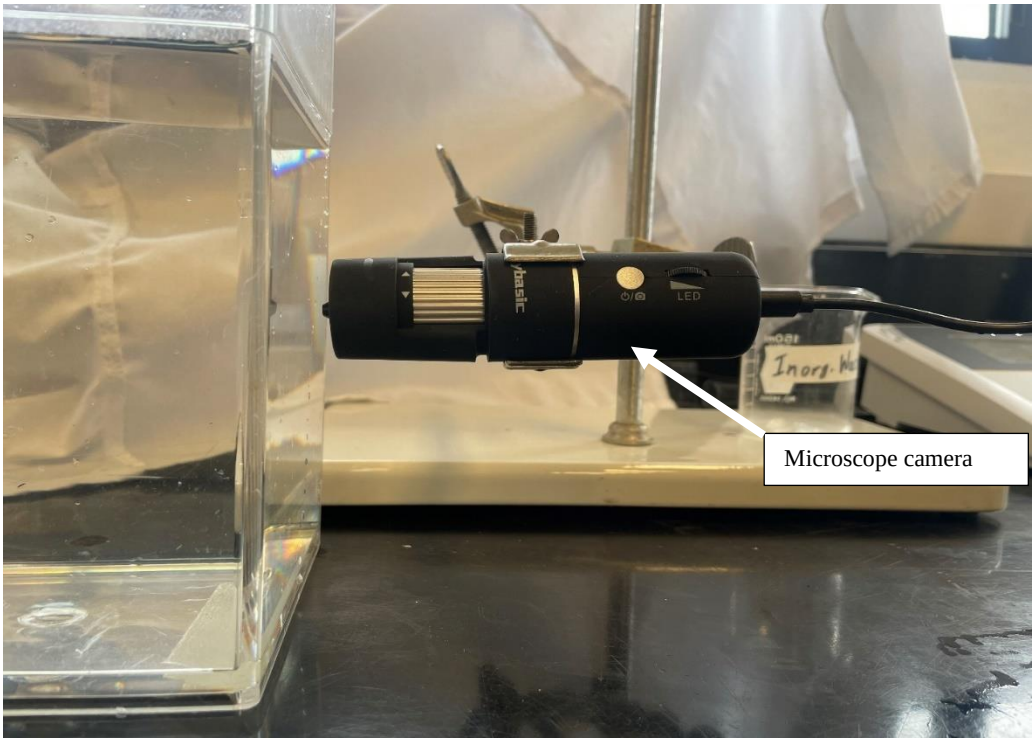

Figure 3-4: Bubble measuring microscope camera setup.

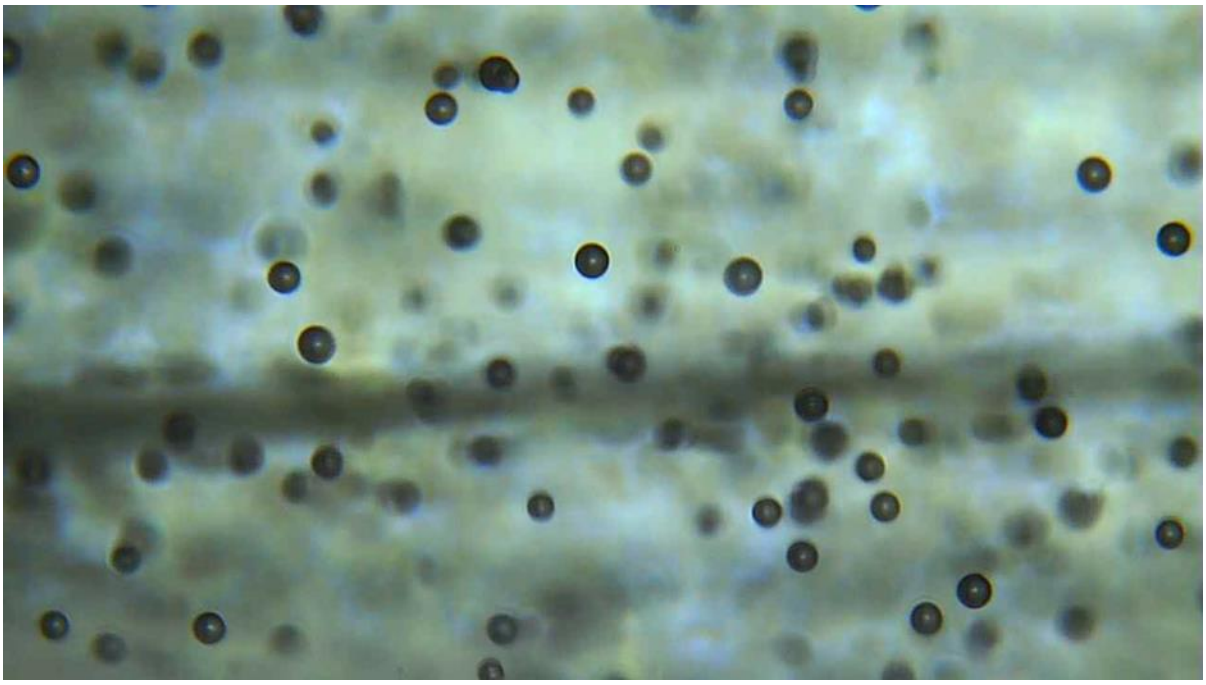

Figure 3-5: Example photo used in the bubble size measurements.

3.2.5 Floc Size Measurements

The flocs were measured using a 10-megapixel camera (A35100U, OMAX, China) attached to a microscope (model 1051, American Optical Corporation, Buffalo, NY) (Figure 3-5). The microscope camera was calibrated with a 0.01mm graduated calibration slide at a magnification of 10X for analysis. Microscopy was favored over a dynamic particle analyser due to its higher accessibility to drinking water plants and lower disturbance of the sample. Water was mixed in the small-scale 1-L jar testing equipment with coagulant in a rapid mix stage and then flocculated for 600 seconds. The pre-flotation flocculated water was sampled directly from the jar tester using the opening at the top of jar using a 3 mm I.D. glass tube. The tube was slowly introduced into the water vertically to allow the sampled column of water to rise into the tube. The time allocated for sampling was 10 seconds to prevent the settling of the floc particles. When the tube was filled, the non-submerged end of the tube was blocked with a finger to allow the extraction of the water column. The sampled water was then transferred to a microscope slide to analyze the floc sizes. Figure 3-6 is an example photo of the images used to determine the floc size distribution. Between 1 and 33 flocs were measured per photo. Between 21 and 34 photos were analysed per floc distributions

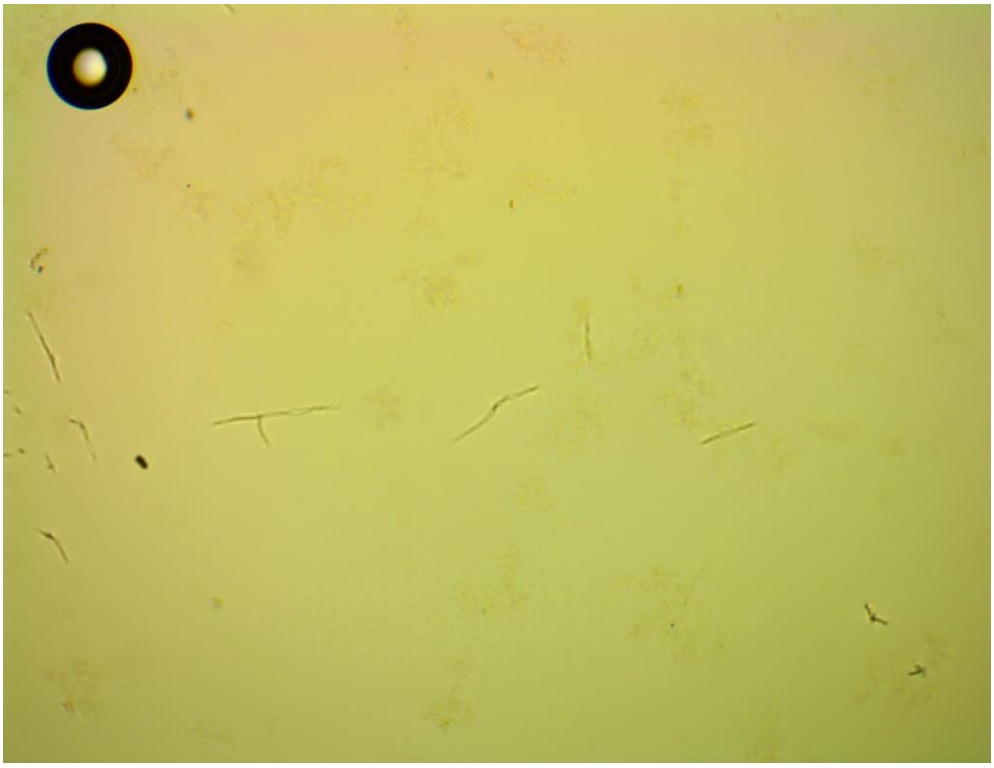

Figure 3-6: Example of photo used for floc measurement.

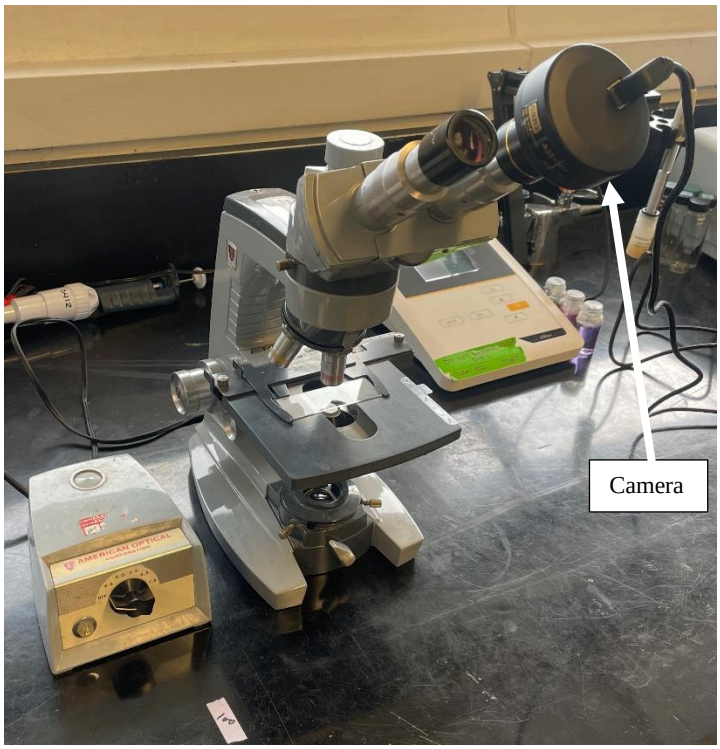

Figure 3-7: Floc measuring microscope setup.

For the post-flotation floc size analysis, the above method did not function well as it would have been necessary to puncture the floated floc layer at the water's surface. Accordingly, water samples were collected from the sampling ports located in the front portion of the small-scale jar tester and transferred using a beaker. This allowed sampling of the floated water without disturbing the float layer. The same glass tube method was used to transfer sample water from the beaker to microscope slides was used for the floated water

Multiple images were taken per slide. The microscope slide was analyzed in a sweeping horizontal motion and large vertical steps to prevent double counting of flocs. ToupView (ToupTek, Zhejiang, China) software was used to analyze the microscope photos. The software uses the images of the calibration microscope slide to determine the size of a pixel. The flocs were then dimensioned with pixels, and the size was calculated with the conversion factor. Flocs were measured before the flotation process after being flocculated at $G_F = 12\ s^{-1}$ or $G_F = 60\ s^{-1}$, and after the flotation process for every combination of flocculation

rate and saturator pressure. All the datasets are presented on a base one scale as the datasets varied between 137 units counted and 2179 units. For more information, see section 3.2.6 Frequency-Based Analysis

3.2.6 Frequency-Based Analysis

The quantitative analysis were compiled on a unitized distribution for comparison as the sample sizes varied between 1712 and 2133 for the bubble size distributions and 137 and 2179 for the floc size distributions. The unitization reduces all the frequency to values between zero and one. For the analysis, the datasets were grouped into bank sizes of equal width. The smallest bubble measured was 14 μm while the smallest floc was 8.5 μm. These may be the lower limits of these methods. To unitize the datasets, each bank was divided by the total number of units in the dataset. The cumulative distribution with the unitized values produces a distribution where the final cumulative value is one.

3.3 Experimental Plan

This section covers the experimental plan of the research. The first phase studies cold water coagulation utilizing alum as the sole coagulant without flocculation aid. The second phase studies the relationship between bubble size and floc size at the microscale. The two phases will evaluate the performance and potentially optimize the dissolved air flotation operating parameters for winter operation.

3.3.1 Phase I -Cold Water Coagulation

The Phase I experiments evaluate the feasibility of treating Ottawa River water at cold temperatures with alum without using coagulant aids. The aim is reducing the particle/turbidity load on the rapid sand filters which would be found downstream of the DAF units. The treatment processes of interest are coagulation, flocculation and DAF. A one-litre DAF jar test was used to evaluate the effect of pH, while a large batch dissolved air flotation system (LB-DAF), developed by Gonzalez-Galvis (2019), was used to assess the impact of flocculation and flocculation time.

The first part of the experiment was to determine the effective coagulant dose at baseline conditions for treatment. The standard condition is at room temperature, without pH adjustment. The second part evaluated the effect of pH adjustment on cold water conditions. The water was cooled to 2 ºC, and the treatment was performed in a walk-in fridge. Three coagulant doses were evaluated. For each coagulant dose, multiple tests with incremental addition of sodium hydroxide were performed to assess the effect of pH adjustment on cold water conditions. The third part compares the effect of flocculation mixing intensity and time to final turbidity. Water at standard room temperature conditions and cold conditions were flocculated at mixing intensities of G_F equal to 20, 37, 79, 113, and 193 s^{-1}, for 1, 3, 5, 10, and 15 min. The results comparison was performed in terms of the final (floated water) turbidity.

3.3.2 Phase II – Effect of Bubble Size on Floc Removal

The second phase of the research was to analyze the effect of bubble size on floc removal. The first part is to measure the bubble distribution formed at different pressures. The bubble size distributions were analyzed for bubbles generated when the saturator was operated at 275, 410, 480 and 610 kPa, to represent a low pressure, a slightly below typical pressure, a typical pressure and a high pressure, respectively. To evaluate the effect of bubble size on floc removal, the floc size distributions generated by flocculation at mixing speeds of 30 and 100 RPM (G_F = 12 and 60 s^{-1}, respectively) were measured before flotation. Floc size distributions after flotation were measured for all combinations of pressures and flocculation mixing intensities mentioned above. These DAF experiments were performed at room temperature with the 1-L DAF jar test apparatus. The test conditions consisted of a one-minute rapid mixing process with alum coagulant, 15-minute flocculation, the addition of saturated water (equivalent to a 10% recycle ratio) and a 10-minute flotation period. The experiments used 35 mg/L alum dose and NaOH additions to have a final pH of 6.5, the optimal conditions for room temperature coagulation.

Chapter 4 -Optimizing Dissolved Air Flotation for Cold Water Operations

Authors: R. M. Hérard, R. M. Narbaitz

The treatment of cold water to produce drinking water is unavoidable for Canadian drinking water plants. The norm for treatment using coagulation and flocculation has become using polynuclear coagulants as they are more stable with temperature variations. The main objectives of this research were to apply new low-temperature aluminum solubility knowledge to dissolved air flotation (DAF) using alum as the sole coagulant, and to evaluate the relationship between floc removal in terms of floc size against bubble size in a batch dissolved air flotation system. By increasing the operating pH to maintain close to constant pOH conditions with temperature, treatment at 2ºC was feasible. At cold temperatures the final turbidity was independent of flocculation mixing rate and flocculation time, while at room temperature it was dependent on both. Increasing the saturator pressure did not significantly decrease the mean bubble size. DAF treatment could efficiently remove flocs larger than the bubbles. The assessment of DAF efficiency based on the unitized effluent floc distribution proved inconclusive, it may be possible that the conditions resulting with the larger mean effluent floc size has a greater removal efficiency.

Keywords: alum, bubble size, cold temperature, dissolved air flotation, drinking water treatment, floc size.

4.1 Introduction

Coagulation, sedimentation, and gravity separation is one of North America's most commonly used methods for drinking water production. Their operation with inorganic coagulants has been studied since the beginning of the 20th century (Amirtharajah & Mills, 1982; Camp et al., 1940) and aluminum sulphate

(alum) has been the traditional, and most inexpensive, coagulant (Barwon, 2009; Mohamed et al., 2020; Teguh et al., 2022; Zarchi et al., 2013). However, operating with alum in cold conditions is problematic for many plants (Camp et al., 1940; Hanson & Cleasby, 1990; Morris & Knocke, 1984). Based on the Ontario municipal annual water treatment plant reports available on-line, the authors found that in Ontario only 19% of drinking water plants servicing communities with over 1,000 inhabitants that had conventional drinking water treatment used alum without flocculation aids for drinking water production (Appendix A). If treatment plants can operate with alum, there could be substantial savings. The effect of temperature on coagulation with alum was not adequately understood for many decades. Velz (1934) observed that a higher coagulant dose was required for satisfactory color removal during the Summer than in the Winter. However, this apparent contradiction of superior Winter performance can be explained. Because of their relatively high raw water pHs (6.9 to 7.8), the pH of the coagulated Winter water is within the lower part of the solubility envelope for those temperatures. And as the Winter coagulant requirement was proportional to the raw water colour, the predominant color removal mechanism appears to be charge neutralization/adsorption. During the Summer, because of the warmer temperatures the solubility envelope shifts to the left (lower pHs) and the dose used during the Winter is now outside the solubility envelope. Thus, in order to move back within the solubility envelope the coagulant dose had to be increased. This also means that during the summer sweep flocculation is much more important. Camp (1940) claimed that treatment was not affected by temperature. Morris and Knocke (1984) clearly demonstrated that turbidity removals by coagulation/flocculation/sedimentation at 1ºC were significantly worse than those at 5 and 20ºC, and the impact of temperature was more severe for low turbidity waters. They also showed that at 1ºC, increasing the alum dose could lead to restabilization, which did not occur at 20ºC for the same coagulant doses. Hanson & Cleasby (1990) observed that hydrodynamic factors, such as impeller geometry, are important at cold temperatures and that treatment with alum was more consistent when performed at constant pOH instead of pH particularly at low coagulant doses where the charge neutralization mechanism prevails.. In addition, they demonstrated that the flocs formed at 5ºC are much more fragile than those formed at 20ºC. Van Benschoten & Edzwald (1990) documented a shift in the estimated solubility envelope

when the water was coagulated with alum. Figure 4-1 presents the observation of Van Benschoten & Edzwald (1990). Pernitsky & Edzwald (2003) observed that the solubility limits with respect to pH shift over the pH range with temperature. The literature about operating with alum at cold temperatures was not elaborated as late as 2016, as observed in Bratby (2016). To date, many researchers have presented solubility envelopes, but there are no theoretical pC-pH, i.e., that based on the equilibrium constant at lower temperature, is available for cold water coagulation with alum.

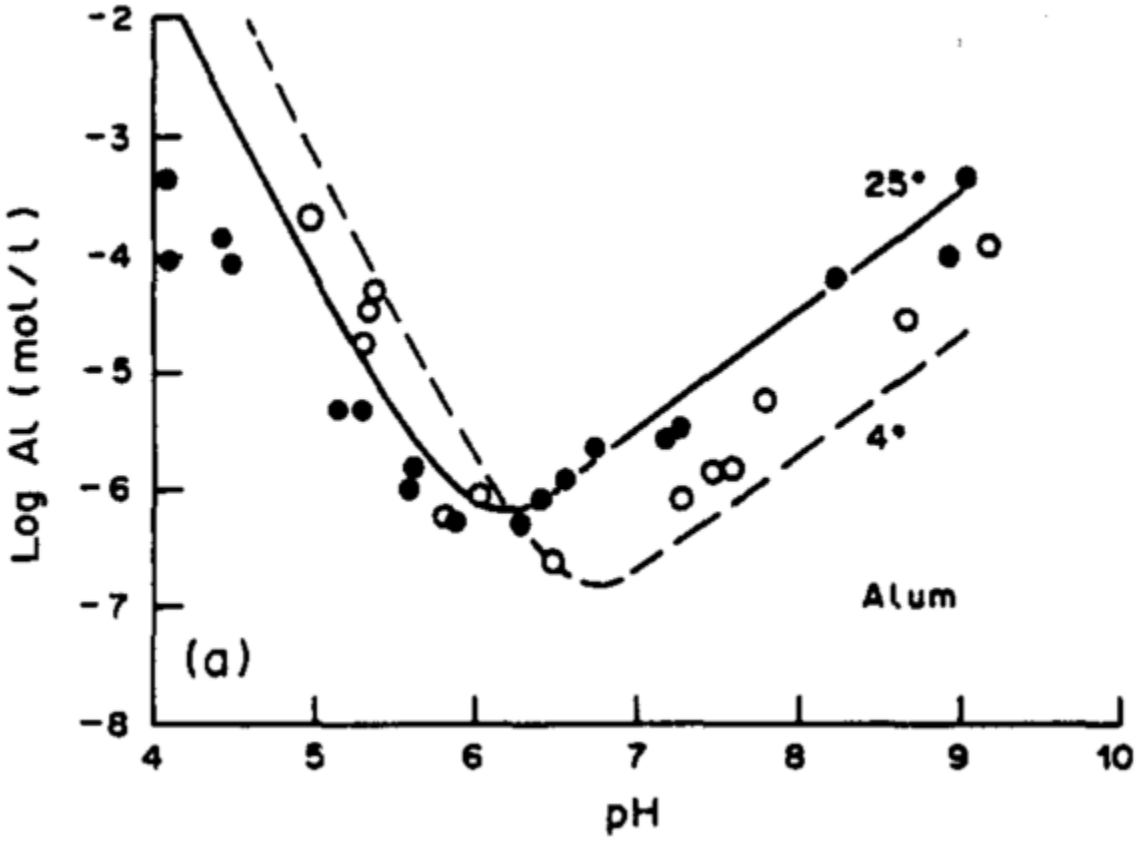

Figure 4-1: Solubility envelope at 25°C and 4°C by Van Benschoten & Edzwald (1990).

Plants operating with dissolved air flotation (DAF) are becoming more common as they can operate at several fold higher hydraulic loading rates than sedimentation plants (Crittenden et al., 2012), and they are more efficient at removing algal cells from water (Walker, 2015). DAF also has the advantage of being effective at removing smaller flocs. It has been observed that DAF treatment is efficient at treating drinking

water with shorter flocculation times. (Edzwald, 1993, 2010). The main disadvantage of dissolved air flotation is the additional cost of pumping and pressurizing water and air to high pressures to produce the required microbubbles.

To determine the impact of temperature on the particle separation one could apply a Stoke's law approach. By decreasing the temperature from 25°C to 4°C, the density increases from 997 kg/m^3 to 1000 kg/m^3 (a 0.3% increase) and the dynamic viscosity increases from 0.891 to 1.570×10^{-3} N·s/m^2 (a 76% increase) (Edzwald and Haarhoff 2012). The slight increase in water density will increase the buoyant force and also increase the drag force. But the drag force is a function of the coefficient of drag, which is inversely proportional to the Reynolds number which in turn is inversely proportional to the dynamic viscosity, thus the drag force is directly proportional to the dynamic viscosity. Thus, the temperature decrease should result in an increase in the drag force. The forces of buoyancy and drag counteract each other, and the net effect of the temperature on a settling floc is a decreased downward force. This is part of the reason why the sedimentation rate is slower in cold temperatures. For DAF the analysis is more complex because the force balance has to be applied to the floc-bubble aggregate, and introduction of the saturated water may cause the shearing of the incoming floc particles (changing their size) and their aggregation with one or more bubbles (increasing their size). So it is not clear whether the floc-bubble aggregates will necessarily be larger than the incoming flocs. Accordingly, the floc-bubble aggregate will have a different volume and density from the floc which makes the application of this type of analysis much more difficult. Malley & Edzwald (1991) demonstrated based on similar fundamentals, that DAF should be superior to sedimentation in the treatment of cold waters, and their turbidity removal bench scale studies confirmed this. We are unaware of other research of cold water temperatures on the performance of DAF. But it should be noted that Edzwald and Haarhoff (2012) state that DAF treatment of cold waters using alum alone is possible, but the pH should be increased to pH 7 or even 7.5. To our knowledge this has not been demonstrated experimentally for DAF treatment.

One variable that treatment plants can modify in DAF system is the bubble size, which is a function of the saturated water pressure, the saturated water flow rate, the type of nozzle, and the relative position in the contact and separation zones of the basin (de Rijk et al., 1994; Gorczyca & Zhang, 2007a; Haarhoff & Edzwald, 2004; Leppinen & Dalziel, 2004; Zabel, 1983). So, at the very least a plant operator can change the saturator pressure to adjust the bubble size at least to some extent. Theoretically, the optimal bubble size relative to floc size is near a one-to-one ratio, as larger flocs may break up during the rise trajectory (Han et al., 2007; Leppinen, 1999; Park et al., 2001). However, other researchers state that large flocs can be efficiently removed by smaller bubbles (Edzwald, 2010;,Gorczyca & Zhang, 2007).

This study has two main objectives. First, to study the effect of coagulation on cold water treatment with alum, as the sole coagulant without using a flocculation aid, on the DAF performance and try to relate it to the changes in the aluminum solubility diagrams with temperature. Second, to analyze the interaction between microbubbles and flocs in a DAF system at the microscopic scale to assess if the performance can be improved by altering the saturator pressure and the flocculation mixing intensity. The results of this study are expected: a) to give treatment plant operators confidence to reassess alum for cold temperature treatment as it may result in substantial savings; and b) to optimize the saturator pressures in dissolved air flotation plants to reduce the operational costs.

4.2 Materials and Methods

4.2.1 Materials

This study was conducted using Ottawa River water as it is readily available and is treated with coagulation at many treatment plants. Ottawa River water is characterized as Northern Canadian river water (Carter & Long, 1992); it has a low turbidity, low alkalinity, low hardness, relatively high colour and NOM content. Based on these water quality characteristics Ottawa River water it is more amenable to treatment by DAF than by sedimentation (Edzwald and Haarhoff, 2012).

The first portion of the study required a large quantity of water to operate the large batch dissolved air flotation test (LB-DAF), which has a 20L volume. Because of the large amount of water needed, the two different portions of the study were performed from two batches of water. One batch was collected during the Spring of 2019 from the laboratory of the Aylmer drinking water plant in Gatineau, Quebec, and was used for the cold water temperature comparison experiments. A second batch of water was collected in the winter of 2020 directly from the shores of the Ottawa River (at a nearby location) using a submersible water pump. The pump was run for 5 minutes before sampling to obtain representative samples. The different sampling location was necessitated because access to the Aylmer water treatment plant was restricted during the pandemic. The water was stored in 19-L high-density polyethylene (HDPE) buckets and 208-L HDPE barrels in a temperature-controlled room maintained at 1ºC ±1ºC.

The main consumables used were the aluminum sulphate coagulant and the chemicals used for pH adjustments. The entire research used a commercial grade liquid aluminum sulfate coagulant (ALS, Kemira, Montreal, QC). The coagulant has an aluminum concentration of 4.3±0.1% Al^{3+} with low basicity (0.1±3%) and a pH of 2.0. The pH was increased with sodium hydroxide (ACS grade, VWR Chemicals, Mississauga, ON) and reduced with hydrochloric acid (ACS grade, Fisher Chemical, Ottawa, ON).

4.2.2 Batch Dissolved Air Flotation Jar Tests

Two dissolved air flotation systems were used for the experiments: a 1-L DAF jar test apparatus and the LB-DAF system. The following procedures are the standard procedures used in this study; if they were modified for a series of tests, the modifications are specified in their respective sections.

4.2.2.1 One-litre DAF Test

The small-scale experiments used a 1-litre dissolved air flotation jar test (PFJT, Capital Controls Ltd., Didcot, Oxon, England), it was operated with a slightly different procedure than suggested by the manufacturer. The original procedure injected the pressurized water from a quarter-turn valve on the back

of the apparatus near the bottom of the vessel, it was found to result in a weak microbubble distribution. The current study uses a modified pressurized/saturated solution delivery system, it consists of a ¼ inch needle valve, which acts as a nozzle, attached at the end of a 0.635cm (¼ inch) O.D. stainless steel tube, which was introduced into the jar when the pressurized water had to be delivered. The delivery system connects to the pressurized water tank and includes a quarter-turn ball valve to control the flow. Upon the discharge of the pressurized/saturated solution through this modified delivery system into the jar test vessel it produced a uniform bubble distribution with a milky-white appearance. For the study, the saturator pressure was varied between 275 and 620 kPa. To prepare the saturator for the experiment, the saturator vessel was filled with deionized water and then pressurized using an air compressor (TAW-0308, HDX, Atlanta, GA). The saturator was then vigorously manually shaken (to provide mixing) until the pressure stabilized.

The modified test procedure consisted of adding the raw water sample into the DAF jar test vessel and mixing it intensely (mean velocity gradient (G_C) = 240 s^{-1}) for 60 s. Afterwards, liquid coagulant was added, and the jar was mixed at the same intensity for an additional 60 s. For the flocculation step the mixing intensity was reduced to either G_F=12 s^{-1} or G_F=60 s^{-1}, depending on the experiment, and it was maintained for 900 s. Afterwards, the mixing/motor assembly was removed to allow the insertion of the saturated water delivery assembly, the needle valve was placed near the bottom of the vessel and the pressurized water was injected. To recreate a 10% recycle ratio, 100 ml of water pressurized at 480 kPa were injected. After the injection of the saturated water, the system was kept undisturbed for 600 s for the flocs-bubble aggregates to form, float and separate from the water. At this point samples were collected from a sampling port in the front of the vessel.

4.2.2.2 Large Scale DAF Jar Test

The second batch jar test is a 20-L system developed by Gonzalez-Galvis & Narbaitz (2020). The system consists of a baffled acrylic vessel used for coagulation, flocculation and DAF separation, an eight-litre saturator, a variable speed motor connected to a shaft with paddles, and a needle valve based saturated

water delivery assembly similar to that used for the modified 1-L procedure. The experiments used a 10 cm by 10 cm square paddle. The procedure was as follows. First, 20L of challenge water was first transferred from a HDPE water storage bucket into the mixing vessel. The water was mixed at G_C=296 s^{-1} for one minute to obtain a uniform distribution. Liquid coagulant was added, and the water was mixed at G_C=296 s^{-1} for 60 s. This was followed by flocculation step which used a lower intensity constant mixing rate. To study the impact of flocculation mixing intensity and flocculation time, experiments were conducted using flocculation mixing rates ranging from G_F=20 s^{-1} to G_F=193 $s^{-1,}$ and flocculation times ranging from 1 to 15 min. Afterwards the mixing was stopped, the saturated water was introduced near the bottom of the tank using the needle valve-based delivery system and a 15 min period was allowed for the flotation to occur. The saturator pressure was maintained at 480 kPa and 2.2 litres (the equivalent to a 10% recycle ratio) were used in these tests. For the cold-water experiments, the tests were performed in a temperature-controlled room maintained at 1ºC ±1ºC.

4.2.3 Experimental Plan

The study is divided into two series of experiments. The first section aims to evaluate the operations at cold temperatures with alum and compare them with those at room temperature. The second section evaluates, at a microscale, the interaction between flocs and microbubbles in a dissolved air flotation system.

4.2.3.1 Warm and cold water temperature turbidity removal by DAF

The study's first phase studies DAF treatment of Ottawa River water using alum without using flocculant aids at cold temperatures and warm temperatures. In the first part, the treatment pH was increased above the recommended pH range for alum treatment but within the observed solubility limits observed by others research (Edzwald, 2020).

For the second part, the LB-DAF unit was used to study the impact of the flocculation mixing intensity and flocculation time on the turbidity removals. For comparison, this analysis was performed at

21ºC using the optimal coagulant dose identified in the first part, and this was followed by a similar analysis at 2ºC using the same coagulant dose and the optimal pH (approximately constant pOH). Five flocculation mixing intensities were analyzed, they were for G_F values between 20 s^{-1} and 193 s^{-1}. The set of analyses was performed at 2ºC and compared against the results of the 21ºC baseline. UV254 absorbance was measured for a surrogate of natural organic matter for the 2ºC experiments.

4.2.3.2 Effect of Bubble Size and Flocculation Intensity on Floc Removal

The second phase of the research was to analyze the effect of the recycled water saturator's pressure on the bubble size, the effect of the flocculation intensity (G_F) on the floc size distribution, and finally to investigate their combined effect on the floc removal. The first part measures the bubble distribution formed at various pressures ranging from 275 kPa, representing a system operating at low pressure, to as high as 610 kPa, representing operations at high pressures. To assess the effect of bubble size on floc removal, the floc size distributions were measured before flotation and after flotation for two sets of flocculation conditions, one set at G_F= 12 s^{-1} to represent a slow mixing rate and another at G_F= 60 s^{-1} to represent a faster mixing rate. The experiments were performed at room temperature with the 1L DAF jar tester. The test consisted of a one-minute rapid mixing after the alum addition, 15-minute flocculation, saturated water addition (equivalent to a 10% recycle ratio), and a 10 minutes flotation period.

4.2.4 Bubble Size Measurements Method

The bubble sizes were measured using a microscope camera (DX-1, Veho, Dayton, OH,) located approximately 1 cm from the vessel wall, and an image processing program (ImageJ, National Institution of Health, Bethesda, MD). The images were taken after the complete injection of the recycle water. Over 8000 bubbles were measure from approximately 20 to 30 images per condition. This approach was selected to demonstrate that it is a feasible alternative for plant operators at smaller treatment system to evaluate the bubble size of their system using such a relatively simple apparatus. The use of a camera for measuring bubble sizes has been used by (Gonzalez-Galvis et al., 2022; Rodrigues & Rubio, 2003; Schmideder et al.,

2022). The bubbles were produced in a square two-litre vessel (B-ker^2, Phipps & Bird Inc., Richmond, VA, USA) containing deionized water and pressurized water injected with the needle valve based pressurized water delivery apparatus. A 131 μm diameter wire was attached to the side of the vessel to calibrate the image processing software. The bubble sizes were measured at four different pressures varying from 275 kPa and 620 kPa. The bubble sizes are presented as cumulative distributions, thus they are on a base one scale, the datasets varied between 1712 units counted and 2133 units counted. The smallest bubble size measured was 14 μm and the largest was 102 μm.

4.2.5 Floc Size Measurement Method

The flocs were measured using a 10-megapixel camera (A35100U, OMAX, China) attached to a microscope (model 1051, American Optical Corporation, Buffalo, NY). The microscope camera was calibrated with a 0.01mm graduated calibration slide at a magnification of 10X. Many research studies have used DPI systems to characterize the floc size distribution (Alam et al., 2011; Alansari & Amburgey, 2020; Fitria et al., 2014; Govoreanu et al., 2009; Li et al., 2006; Verberk et al., 2007; G. R. Xu et al., 2008; Yu et al., 2006), however these systems are expensive. The microscope/camera approach used in the current study was selected because it is less expensive equipment than DPI systems, and it will allow treatment plant operators from smaller systems to evaluate their own plant operation for optimization. This method is similar to that used by Fan et al. (2020), Jarvis et al. (2005), Gonzalez-Galvis et al. (2022), Sun et al. (2016), Han et al., (2007), and Marega & Reali (2023). The flocculated pre-flotation water was sampled directly from the opening at the top of the jar tester with a 3 mm I.D. glass tube immediately after the mixer was stopped. The sampling tube collected water from the top 5 cm of the water column. The floated water was sampled from the sampling port located 75 mm from the bottom of the vessel, approximately 35% of the vessel's height. The later was necessary so as to not disturb the float. The microscope slides with water droplets were analyzed in a sweeping horizontal motion and large vertical steps to prevent double counting of flocs. ToupView (ToupTek, Zhejiang, China) software was used to analyze the microscope photos. The software uses the images of the calibration microscope slide to determine the size of a pixel. The flocs were

dimensioned with pixels, and the size was calculated with the conversion factor. The smallest floc measured was 8.5 μm. Over 3200 flocs were measure over 30 images per condition to produce the floc size distribution before flotation and, over 2400 flocs over 20 images per condition were measured to produce the size distribution after flotation. It is acknowledged that this microscope approach does not measure flocs that are as small those that can be measured by DPI systems, so it may yield a higher mean floc size, but this is a necessary compromise to have a much more affordable tool.

4.2.6 Frequency-Based Analysis

The quantitative analyses were compiled on a unitized distribution as the sample sizes varied between 1712 and 2133 for the bubble size distributions and 137 and 2179 for the floc size distributions. The unitization reduces all the frequency to values between zero and one, so that they are easier to compare. For the analysis, the datasets were grouped into bank sizes of equal width. To unitize the datasets, each bank was divided by the total number of units in the dataset.

4.2.7 Analytical Methods

The pH of the challenge water and the final water pH was measured using a pH meter (pHbasic, Sartorius, Gottingen, Germany). The water temperatures were measured using a digital K-type thermocouple (Digi-Sense, Cole-Parmer, Laval, QC). The natural organic matter concentrations were characterized by dissolved organic carbon (DOC), ultraviolet absorbance at a wavelength of 254 ηm (UV_{254}) and by the specific UV absorbance (SUVA). The UV_{254} and DOC samples were pre-filtered through a 0.45 μm nylon membrane filter (47 mm diameter, PALL Sciences Corp, Mississauga, ON) using vacuum filtration. DOC was measured using an UV-persulphate oxidation based TOC analyzer (Phoenix 8000, Tekmar-Dohrmann, Cincinnati, OH). UV_{254} was measured using a spectrophotometer (DR6000, Hach, Loveland, CO) with a 10-mm quartz cell. The specific UV absorbance was calculated by multiplying by 100 the ratio of the UV_{254} absorbance per 1 cm to the DOC concentration. The turbidity was measured with a turbidity meter (2100AN, Hach, Loveland, CO). Total hardness was determined with EDTA-based Hach

method (Hach, Loveland, CO). Alkalinity was determined by titration with hydrochloric acid and methyl orange indicator following Standard Method 2340 C (APHA/AWWA/WEF, 2012). All analytical measurements were performed in triplicate.

4.3 Results and Discussions

4.3.1 Turbidity Removal at Room and Cold Temperatures

Ottawa River water is a northern water (Carter & Long, 1992) successfully treated by coagulation by many drinking water plants in the Ottawa region. Table 4-1 presents the challenge water characteristics of the sample used for the first phase of the study. The turbidity was higher than normal, this was due to high water levels caused by the spring melt. The other characteristics are similar to the values observed by Gonzalez-Galvis & Narbaitz (2020) during the spring of 2018. Ottawa River water typically has a low turbidity, high colour, low alkalinity, low hardness and a high natural organic matter content, of which a significant fraction is hydrophobic (SUVA > 4) (Xu & Narbaitz, 2016; Zheng, 2013).

Table 4-1: Water quality characteristics of the Ottawa River water sample collected (Spring 2019) for phase one of the study.

Parameters	Spring of 2019 Ottawa River Water values
pH	6.93 ± 0.34
Turbidity (NTU)	8.87 ± 0.24
Alkalinity (mg/L as $CaCO_3$)	31.7 ± 1.10
UV-254 (cm^{-1})	0.30 ± 0.008
DOC (mg/L)	6.99 ± 0.018
SUVA ($L \cdot mg^{-1} \cdot m^{-1}$)	4.29 ± 0.11
True Color (Pt-Co)	42.5 ± 1.4
Total Hardness (mg as $CaCO_3$/L)	23.2 ± 1.7

Figure 4-2 presents the turbidity after flotation at four different coagulant doses without additional pH adjustment using Ottawa River water at 21ºC using the 1 L DAF jar tester. The coagulant doses of 30, 35 and 40 mg/L of alum (2.73, 3.18, and 3.63 mg Al^{3+}/L, respectively) resulted in successful separation, the low final turbidity (~ 0.5 NTU) represent approximately a 94% turbidity removal. As evident from the large floc mass in the jars, sweep flocculation was a significant agglomeration mechanism. Treatment with 25 mg/L of alum (2.27 mg Al^{3+}/L) resulted in significant turbidity removal but it was not as effective as that for the higher doses. At room temperatures, it is possible to have final turbidity below 0.5 NTU from Ottawa River water without additional pH adjustments in the DAF jar test apparatus. These treatment conditions are consistent with treatment at the Britannia Water Treatment plant which also add sulfuric acid to achieve their target coagulation pH of 6 to optimize NOM removal. To ensure consistent turbidity removals (i.e., not impacted by small error in the amount of coagulant added), the dose of 35 mg/L alum (5.89×10^{-5} mole/L) was selected for subsequent cold water experiments; for this dose at 21°C the pOH equaled 7.4.

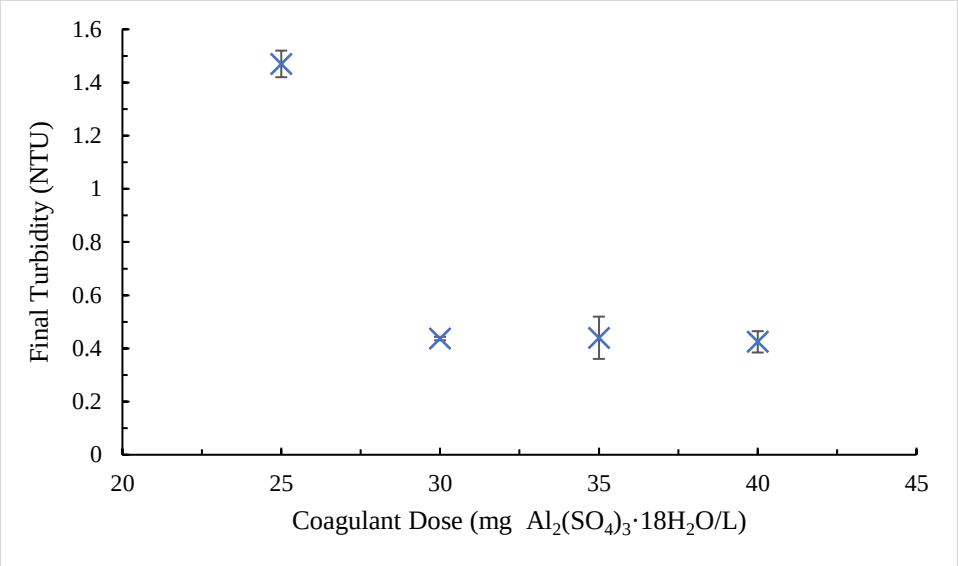

Figure 4-2: Final turbidity vs coagulant dose at 21ºC using the LB-DAF system at a flocculation intensity of G_F=12 s^{-1} for 900 s (error bars indicate one standard deviation).

Cold water (i.e., 2ºC) bench-scale DAF jar tests were performed using the same batch of Ottawa River water sample and followed the same procedures and coagulant dose (35 mg/L of alum) used to generate Figure 4-2, but the pH was increased with sodium hydroxide prior to the coagulant addition. Figure 4-3 presents the final turbidity results of these cold water tests as a function of final pH. Without adding sodium hydroxide the final pH was 6.5. Thus raising the coagulation pH can significantly decrease (i.e., improve) the DAF effluent turbidity levels. The turbidity decreased approximately linearly with the addition of sodium hydroxide until the solution's final pH reached 7.5. Additional sodium hydroxide increased the final turbidity once the optimal pH was surpassed. This pH experimentally validates the higher pH recommendation of Edzwald and Haarhoff (2012) for low temperature DAF treatment with alum alone. The final turbidity was 0.66 NTU at an optimal pH of 7.5 for water treated with 35 mg/L of alum. The final turbidity achieved at 21ºC was approximately 50% lower than the final turbidity measured at 2ºC. This is likely due to the more fragile nature of alum flocs at low temperature (Hansen & Cleasby, 1990) that does not allow the flocs to grow resulting in lower removal. The DAF plant in Aylmer, Quebec, which treats Ottawa River water, operates at a pH of 7.5 during the winter, using an advanced coagulant and a

flocculation aid but still obtains poorer performance during the winter compared to summer operations (Xu & Narbaitz, 2016).

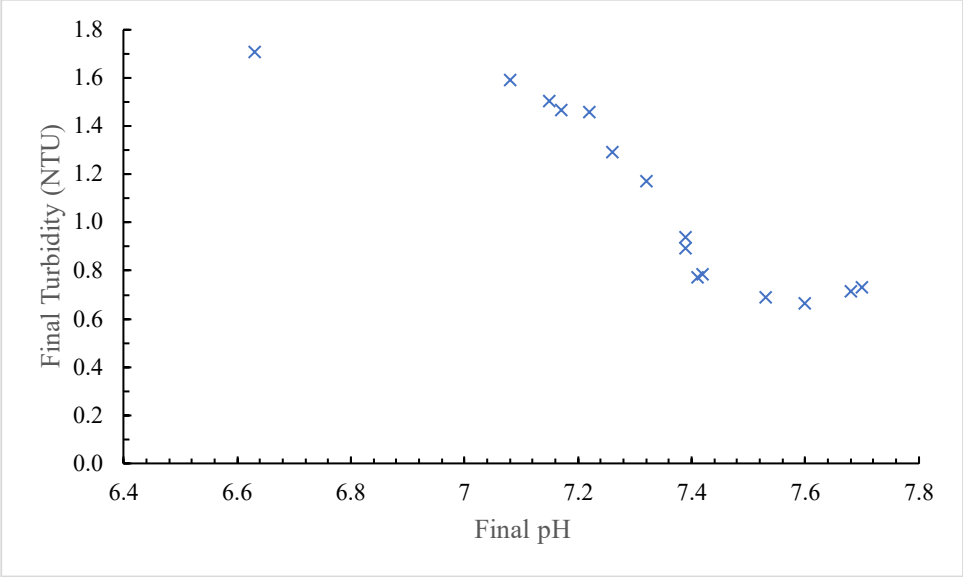

Figure 4-3: DAF floated water turbidity at 2ºC as a function of pH with 35mg/l of alum at a flocculation intensity of G_F=12 s^{-1} for 900 s.

The shift in operational pH between 21 and 2 ºC is proportional to the shift of the negative log of the water dissociation constant (pK_w) across the temperature range. Specifically, the pK_w at 21 ºC is 14.1 and increases to 14.8 at 2 ºC, a change of 0.7. The change in pH from 6.7 at 21 ºC to 7.5 at 2 ºC, maintains the solution potential of hydroxide ion (pOH) at approximately 7.4. The variation in pH between the two temperatures does not correspond directly with the theoretical change in ionization constant (0.8 vs. 0.7), this slight difference may be due to differences in solubility between the two temperatures and non-ideal characteristics of the natural water solution. However, the shift in optimal pH for 35 mg/L alum dose is consistent with aluminum solubility observations from the literature (Hanson & Cleasby, 1990; Van Benschoten & Edzwald, 1990). It should also be noted that the 35 mg/L alum (1.76×10^{-4} mole/L) dose at pH=7.5 falls well within the 4°C solubility envelope in Figure 4-1.

For 35 mg/l alum at both temperatures, the flocculation process for subsequent separation produced large flocs that are characteristic of sweep flocculation, which one would expect given the relatively high coagulant doses. In most conventional water treatment operations, sweep flocculation occurs rapidly, and the process is not dependent on rapid coagulant dispersion as the charge neutralization regime (Amirtharajah & Mills, 1982). In the sweep flocculation regime, aluminum precipitates are formed. The precipitates flocculate together and produce large flocs that are separated from water rapidly compared to flocs formed by charge neutralization (Benjamin & Lawler, 2013). When operating at cold conditions using the same coagulant dose without adjusting the pH, the final turbidity of the water increases. This indicates that the formation of aluminum precipitates occurs, but they do not flocculate into as large, rapidly settling flocs. The low final turbidity achievable at a lower temperature when operating at the higher pH indicates that the coagulation process that preconditions the particles to permit flocculation is inhibited. In the literature, it has been observed with the inefficient flocculation process at warm temperatures if the process occurs outside the optimal pH range. For example, Velz (1934) reported that a higher coagulant dose was required for satisfactory color removal during the Summer than in the Winter. However, the need for coagulant dose appears to be necessary for conditions to be within the solubility envelop, which shifts to lower pHs at higher temperatures. So for the Summer the sweep flocculation has a much more dominant role

The effect of temperature on coagulation is the shift in the optimal pH range that is beyond the typical coagulation pH. Flocculation may also be affected by temperature as the long range forces have temperature dependant parameters (Benjamin & Lawler, 2013). If the coagulation process is compromised, the interparticular forces are not supressed and the particle destabilization is not efficient resulting in low interparticle attraction forces. In the flocculation theory, all the collision efficiency factors are a function of the Hamaker constant which is a function of the interparticular forces (Han & Lawler, 1992). The inefficient coagulation thus reduces the flocculation efficiency resulting in small flocs which are difficult to remove

from suspension. The following section evaluates the effect of temperature on flocculation maintaining the coagulant dose of 35 mg/L with the same flocculating procedure.

4.4 Optimum Flocculation Operating Parameters at Room and Cold Temperatures

Floc break-ups occur when the flocs' internal forces are overcome by the shear force acting on the flocs. Figure 4-4 below compares the final turbidity of the LB-DAF treated water at 21ºC under different flocculation rates with respect to time. The experiments used 35 mg/L alum dose and NaOH additions to have a final pH of 6.7. The flocculation mixing speed was first determined based on exact location on the speed controller which resulted to odd mixing intensities.

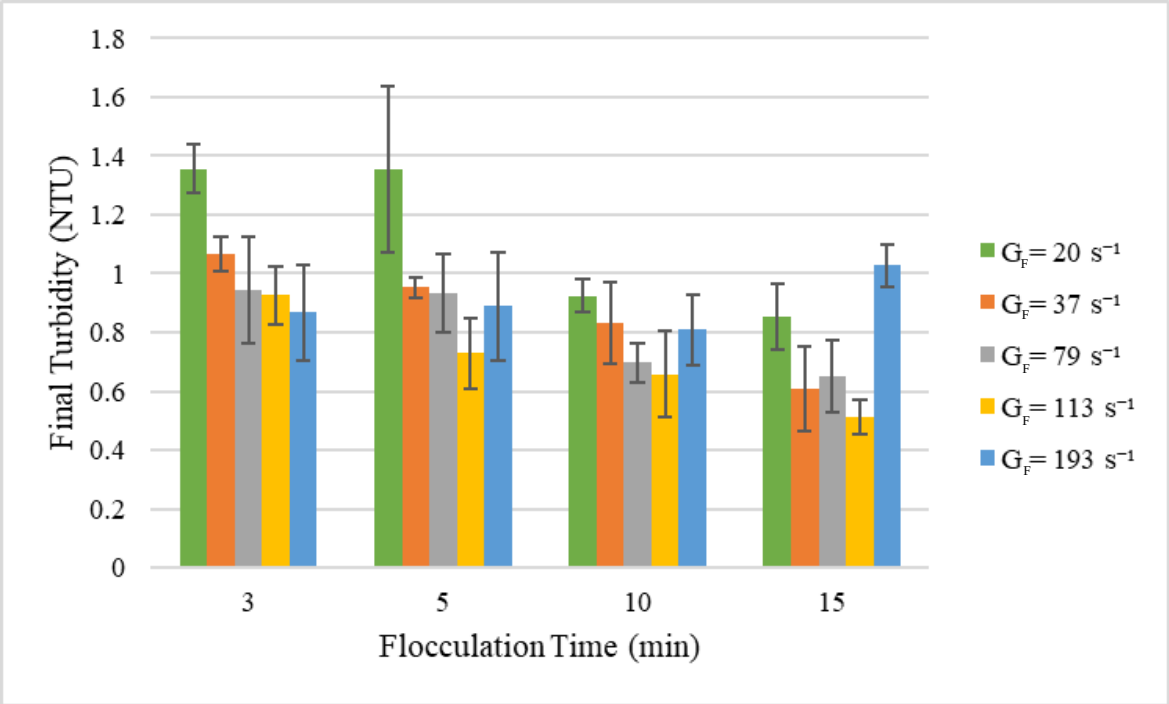

Figure 4-4: Effect of flocculation time and intensity on the LB-DAF final turbidity at 21 ºC using 35 mg/L of alum with the pH adjusted to 6.5 (error bars indicate one standard deviation).

In general, the average final turbidity decreases at a significant rate for the first three minutes and more slowly afterwards. The impact of long flocculation times was more important for the lowest-intensity mixing (i.e., G_F=20 s^{-1}). This graph appears to indicate that the flocculation G_F for values over 20 s^{-1}value does not have such a significant impact, this is consistent with the findings of Gonzalez-Galvis and Narbaitz

(2020) in their room temperature LB-DAF experiments with G_F's up to 120 s^{-1}. Increasing flocculation time is expected to lead to more floc collisions and growth in floc size, and in general increasing flocculation time appears to improve the DAF's turbidity removal. Which would suggest that increasing floc size does helps DAF perform better. Floc break-up (i.e., resulting in greater final turbidity with increasing flocculation time or mixing intensity) is not apparent at most mixing intensities, except for the samples flocculating at a G_F of 193 s^{-1}. At a 193s^{-1} flocculation rate, which is well outside the typical flocculation G_F for full-scale DAF systems (30 to 70 s^{-1}) (Amato et al., 2001), yielded higher treated water turbidities than for the other mixing intensities except for the 1 minute flocculation time. The results in Figure 4-4 are also quite similar to those of Marega (2020). The rate of flocculation is often evaluated in terms of GT, a unitless number that is the product of mean velocity gradient and the flocculation time. Figure 4-5 presents the same data in terms of the LB-DAF floated water turbidity versus GT on a logarithmic scale. The various constant G_F dataset were model using logarithmic models which shows lines in this type of graph, the correlation coefficient (R^2) are presented in Figure 4-4 in the same order as presented in the legend.

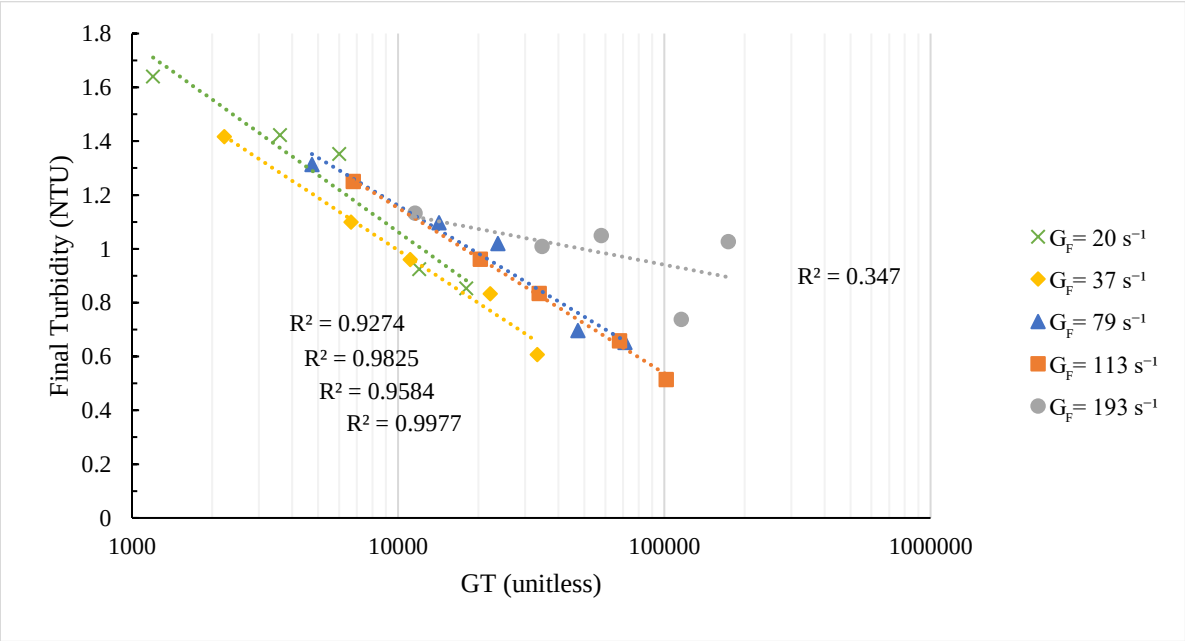

Figure 4-5: LB-DAF floated water turbidity with respect to GT 21ºC using 35 mg/L of alum adjusted to pH 6.5.

On a logarithmic scale, there is a high correlation (R^2 >0.9) between the final turbidity and GT for all mixing rates other than the highest G_F value of 193s^{-1}, which as discussed above are for conditions outside the typical operating range. The correlations indicate that increasing the mixing time or the shear rate will result in better turbidity removal up to a limit. The lack of correlation at the highest mixing intensity potentially indicates a G_F of 193s^{-1} is beyond the effective limit. The evaluation of the optimal mixing rates at warm temperatures depends on the treatment plant's limitations. If the plant operates near the system's hydraulic capacity (i.e., the shortest flocculation time), operating at a G_F of 113s^{-1} will result in the lowest final turbidity, as seen in Figure 4-5. Note from Figure 4-4 that the turbidity removal for G 37, 79, and 113 s^{-1} seems to be statistically the same; and from Figure 4-5 that the 37 s^{-1} mixing intensity had the lowest final turbidity for any values of GT. So if the plant is not operating near the hydraulic limits (i.e. has a relatively high flocculator residence time), operating at a lower shear rate of 37s^{-1} would provide the lowest final turbidity with respect to the energy input.

To evaluate the effect of cold temperature on floc break-up, the same conditions are assessed at 2ºC. The effect of mixing intensity on floc break-up at cold temperatures is presented in Figure 4-6, at the same five mixing intensity as Figure 4-4 but performed at 2 ºC. The increase in pH improves the coagulation process but the temperature related increase in water density and increased water viscosity are also a factor.

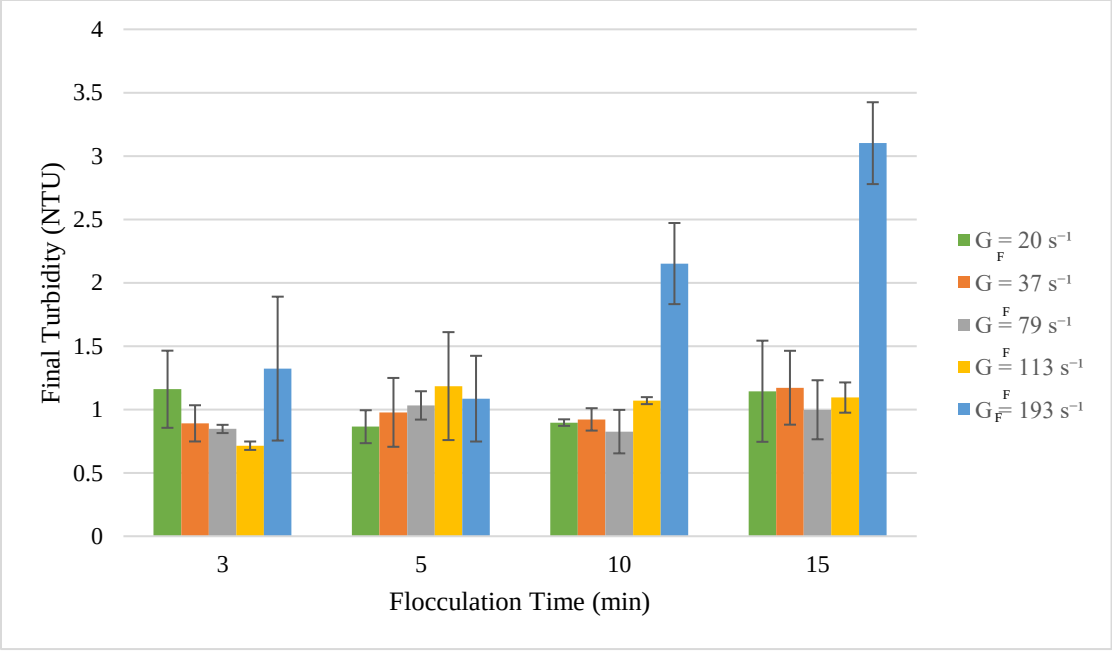

Figure 4-6: Effect of flocculation time and intensity on the LB-DAF final turbidity at 2 ºC using 35 mg/L of alum adjusted to pH 7.5 (initial turbidity = 8.9 NTU) (error bars indicate one standard deviation).

Figure 4-6 shows that final water turbidities below 1 NTU, a common target value before deep bed filtration, could be achieved at 2ºC; however, the results were not dependent on flocculation time and mixing intensity as it was observed at room temperature. The exception was the highest flocculation mixing rate (193 s^{-1}), for which the final turbidity increased proportionally to the flocculation time. The two next highest flocculation mixing rates, G_F equal to 113 s^{-1} and 79s^{-1} produced final water turbidities below one NTU at the lowest time tested (i.e., three minutes) but produced higher final turbidity at all other points other than the 79s^{-1} data point at ten minutes. The two lowest flocculation mixing rates produced final water turbidities equal to or less than 1 NTU with longer flocculation times. Conducting a linear regression of the final turbidity vs. time, the 95% confidence limit of the slopes for G_F=20, 37, 79, and 113 s^{-1} includes zero, accordingly the final turbidity was independent of time for the four lowest mixing rates.

Figure 4-7 compares the final water turbidity to the unitless constant GT on a logarithmic scale. The trendlines represent logarithmic regressions of the individual datasets. The squares of the correlation

coefficient (R^2) are in the same order as presented in the legend. The flocs formed at lower temperatures are significantly more fragile than flocs formed at higher temperatures (Hanson & Cleasby, 1990). At the highest mixing rate, a significant correlation exists between final turbidity and increased GT. The correlation does not indicate that increased GT values cause floc break-up; but presumably floc break-up is likely the reason for the G_F = 193 s^{-1}. It should be repeated, that this level of flocculation intensity is far greater than it is normally used in practice. Evaluating the 20 s^{-1}, 37 s^{-1}, 79 s^{-1} and 113 s^{-1} correlations using a linear regressions, the 95% confidence interval of the slope includes zero indicating no correlation between final turbidity and GT.

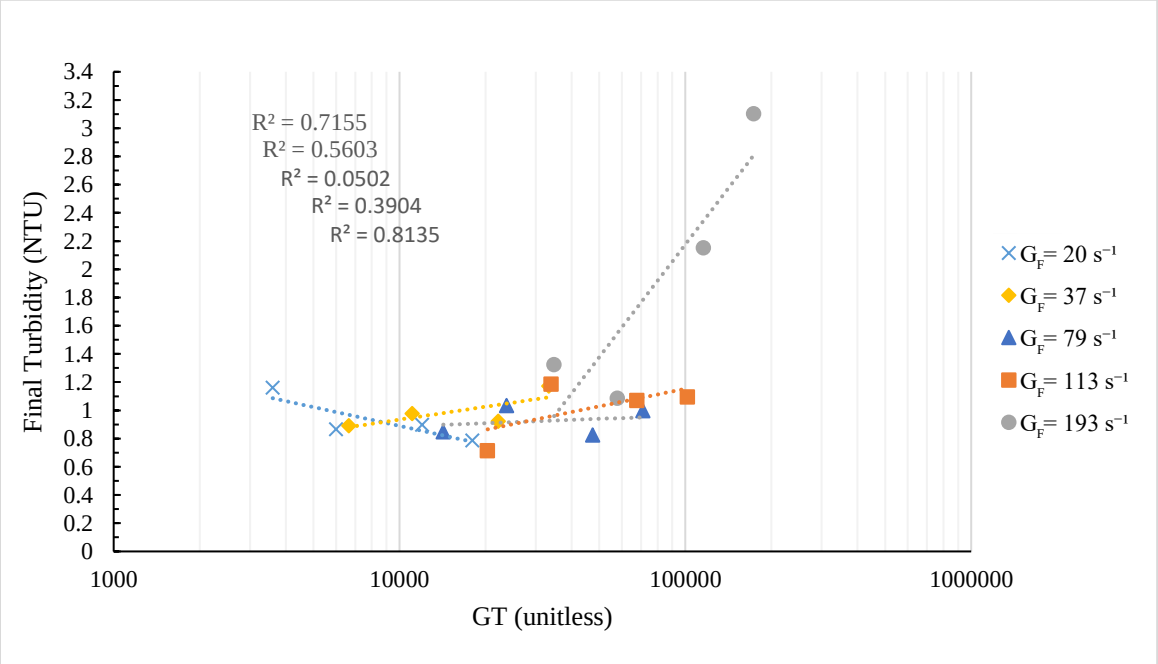

Figure 4-7: LB-DAF floated water turbidity with respect to GT 2ºC using 35 mg/L of alum adjusted to pH 7.5.

Figure 4-8 demonstrates the significant UV-254 removals achieved for cold water treatment. Turbidity removal is an important parameter for drinking water treatment, but organic removal is also important as the reaction of organic compounds with chemical disinfectants results in the formation of disinfection by-products (Dejaeger et al., 2022) and may complex and increase the solubility of metal ions

(Sillanpää, 2015). UV_{254} absorbance removal is an indirect measurement of DOC removal for Ottawa River water, as observed by Gonzalez-Galvis & Narbaitz (2020). UV_{254} absorbance is a more directly measuring of the molecular double bonds more commonly associated with the hydrophobic fraction of NOM, which is effectively removed by systems using coagulation and flocculation. UV_{254} absorbance is measured with a HACH DR6000 spectrophotometer. The UV-254 removal is high and consistent over the entire range of flocculation time. Although it is not represented here, the flocculation mixing intensity (i.e., G_F) did not affect the UV-254 removal. The UV-254 removal for cold treatment of Ottawa River water is nearly identical to previous studies treating Ottawa River water from the same season of previous years but tested at room temperatures under conventional conditions. (Gonzalez Galvis, 2019) Others have shown that principal variable controlling NOM removal is the coagulant dose (Crittenden et al., 2012; Malley & Edzwald, 1991), and the above analysis was for a single coagulant dose so constant UV_{254} removals were expected.

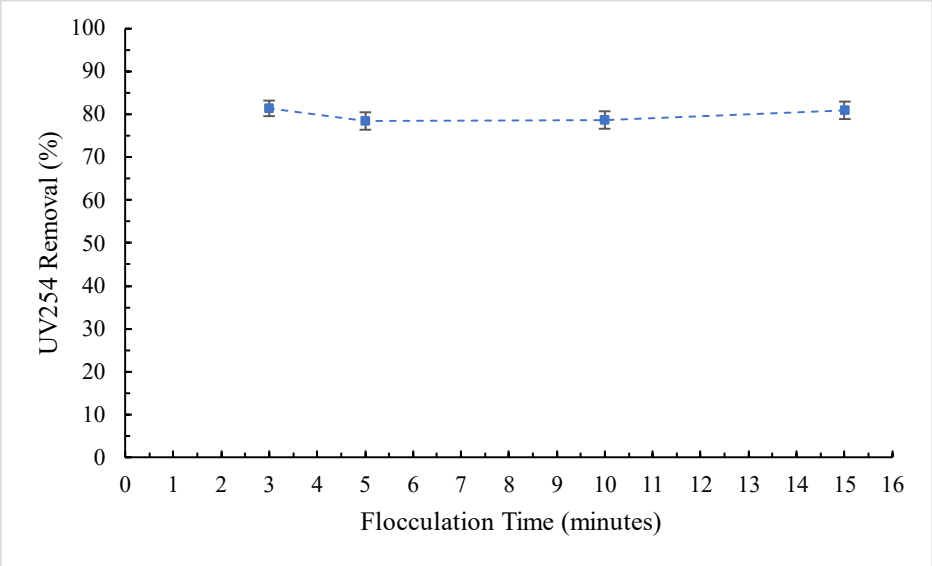

Figure 4-8: UV-254 removal for cold water treatment, treatment at 2ºC, pH of 7.5, 35 mg/L of alum and mixing intensity of G = 37 s^{-1} (error bars indicate one standard deviation).

Treatment of drinking water at cold temperatures using alum as a coagulant is more challenging than at room temperature, but it can be effective if the treatment system is optimized. This includes

increased operational pH and reduced flocculation mixing rate relative to operations at warmer temperatures. The results indicate that optimizing the treatment process for turbidity is feasible, but some limitations can prevent the optimization at cold temperatures. At a fixed temperature, disinfection by-product precursors are removed more efficiently at a lower pH (Crittenden et al., 2012). As the UV-254 are considered a good indicators of DBP precursors(Edzwald et al., 1985; Hua et al., 2015) , Figure 4-7 shows that even at 2ºC using a coagulation pH of 7.5 DAF should be very effectively removing UV-254 and thus minimizing DBP formation. Depending on the particular water characteristics, the formation of disinfection by-products may not be a concern under cold conditions as the kinetic rate of these reaction decrease with decreasing temperature.

An additional constraint that may affect the operation of conventional drinking water plants in Canada is the proposed regulation that drinking water plants must target a non-health-related operational guideline of residual aluminum below 0.05 mg/L (Health Canada, 2019). Based on the alum pC-pH diagrams, this regulation limits the pH range at which water treatment can occur, as only a limited pH range produces results with aluminum solubility below 0.05 mg/l. Alum has the advantage that the solubility diagram transitions towards higher pH values as temperature decreases when measured in distilled water. Other commonly used aluminum coagulants also have pH ranges that maintain a residual aluminium concentration below 0.05 mg/l, but they do so over a narrower pH range compared to alum (Pernitsky & Edzwald, 2003). The more limited pH range of the advanced coagulants may cause difficulties while treating water sources with greater fluctuating water quality, such as small rivers or waters influenced by external variations, such as navigation locks or reservoir discharges. This may not be a concern for some plants since the alum solubility decreases with temperature (Van Benschoten & Edzwald, 1990).

The less-than-ideal pH range could produce smaller flocs entering the gravity separation process as they are not in the optimal sweep flocculation range as identified by Amirtharajah & Mills (1982). For the sedimentation process, separation could be achieved by having longer sedimentation times to remove the smaller particles. Dissolved air flotation is likely less sensitive to smaller floc sizes as the flocs are

removed when they aggregate with bubbles and rise to the water surface where they are removed. The following section compares the effect of DAF saturator operating pressure on the floc size entering the dissolved air flotation process.

4.5 Floc Size vs DAF Bubble Size

This study's second phase evaluates the interaction between the bubbles formed within a dissolved air flotation system and the flocs formed with alum and Ottawa River water. Table 4-2 presents the water characteristics of the Ottawa River water used for the study collected during the winter of 2020. Most parameters are similar to the spring sampling campaign (Table 4-1), the turbidity is much lower but more consistent earlier winter measurements (Xu & Narbaitz, 2016; Gonzalez-Galvis, 2019). The overall water characteristics are similar to those of the water collected by Gonzalez Galvis (2019) during the winter of 2018.

Table 4-2: Water quality characteristics of the Ottawa River sample collected for phase two of the study.

Parameters	Winter 2020 Ottawa River Values
pH	6.81 ± 0.24
Turbidity (NTU)	2.98 ± 0.30
Alkalinity (mg/L as $CaCO_3$)	39.5 ± 1.15
UV-254 (cm^{-1})	0.27 ± 0.008
DOC (mg/L)	5.95 ± 0.018
SUVA ($L \cdot mg^{-1} \cdot m^{-1}$)	4.58 ± 0.15
True Color (Pt-Co)	43.2 ± 1.3
Total Hardness (mg/L as $CaCO_3$)	36.8 ± 1.8

Figure 4-9 represents the bubbles' cumulative distribution for four DAF saturator operational pressures tested. Each of the cumulative distributions was obtained from the analysis of 20 to 30 images. The average bubble size decreases as the saturator pressure increases. Smaller bubbles are formed as the pressure decrease across the injection nozzle is greater. Only for the lowest operating pressure the bubble size distribution seems significantly different.

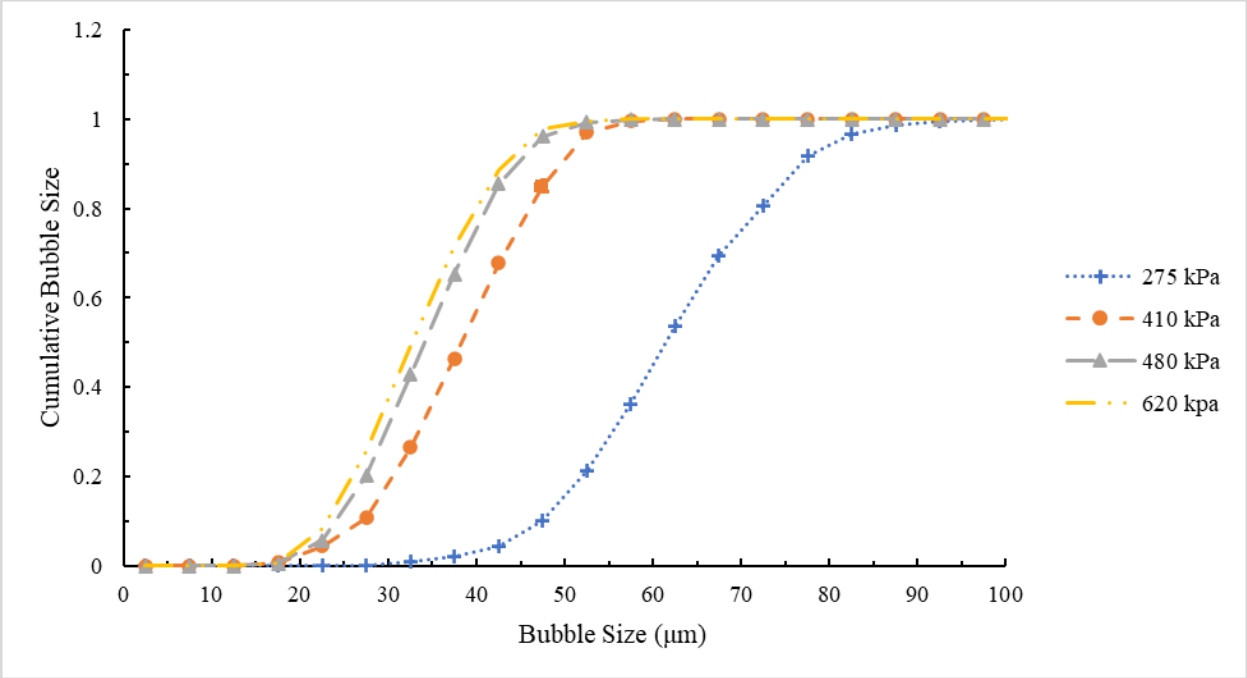

Figure 4-9: Cumulative bubble size in DAF system at room temperature.

The mean bubble size and standard deviation in the function of pressure are presented in Table 4-3. As the pressure increases, the mean bubble size decreases. The mean bubble size difference between 480 kPa and 620 kPa decrease with increasing saturator pressure, as expected, however the difference is only 0.6 µm. At high pressures (>410kPa), based on the overlapping confidence limits the reduction in the bubble size caused by an increase in pressure is statistically insignificant, as observed by (Zhang et al., 2015; Gonzalez-Galvis, 2019). It was encouraging that these confidence limits were significantly tighter than those of Gonzalez-Galvis (2019), this is likely due to the measuring technique is more reproducible and/or the bubble delivery system in this study operated more reliably.

Table 4-3: Bubble size with respect to saturator pressure.

Pressure (kPa)	Mean Bubble Size (μm)	Bubble Size Standard deviation (μm)
275	65.8	± 11.7
410	40.7	± 8.3
480	36.3	± 7.4
610	35.7	± 7.3

The bubble size measurements in the current study fall within the range of reported in the literature. Zabel (1983) had mean bubble size between 40 μm and 90 μm at 485 kPa; de Rijk et al. (1994) had mean bubble sizes varying between 37 μm and 72 μm at a pressure of 500 kPa; and Haarhoff & Edzwald (2004) had mean bubble sizes of 82 μm, 62 μm and 32 μm at 200 kPa, 500 kPa and 600 kPa, respectively. All three performed their experiment in continuous flow systems where bubble size measurements varies with flowrate. Gonzalez-Galvis & Narbaitz (2020) measured mean bubble sizes of 66.5 μm, 54.4 μm, and 47.7 μm at 482 kPa, 551 kPa, and 620 kPa, respectively, in a batch system. They used a apparatuses similar to (Zhang et al., 2015) that pulled the water through a narrow tube under vacuum to a viewing window to measure the bubble size. Marega & Reali (2023) used an unintrusive method of measuring flocs and obtained a mean bubble size of 40 ±13 μm for a saturator pressure of 500 kPa, which is within the confidence limits of the measurements of the current study. It should be acknowledged that the slightly lower mean values in the current study may be affected by the measurement method used and/or the effectiveness of the particular nozzle device (i.e., needle valve) in the saturated water delivery system. The main implication of the statistically the same mean bubble size with increasing pressure (within the normal range) seems to be that changing the saturator pressure should not significantly improve the performance of the DAF.

The floc size distribution before contact with the bubbles was studied to systematically evaluate the effect of pressure on the floc removal. A slow mixing rate of G_F = 12 s^{-1} and a higher mixing rate of G_F = 60 s^{-1} were used. The cumulative distribution of the floc sizes is presented in Figure 4-10. Only a small portion of the coagulated Ottawa River water at G_F= 60 s^{-1} produced flocs in the 25 to 50 µm size range which some claim are necessary for effective separation by DAF (Edzwald and Haarhoff, 2004; Edzwald, 2010; Gorczyca and Zhang, 2007). However, others claim that DAF is effective for the removal of much larger floc sizes (Marega & Reali, 2023). It seems that before the G_F increases to a level where there significant floc breakage due to shear, apparently there is minimum level of mixing (G_F >12 s -1) that is required to enhance particle growth.

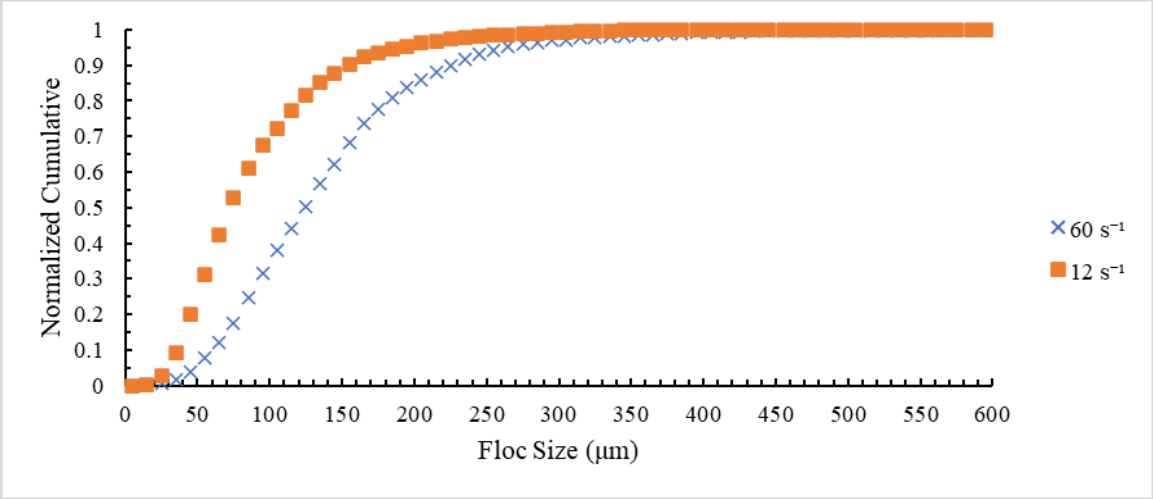

Figure 4-10: Cumulative floc size after flocculation at room temperature. 35 mg/l of alum, pH =6.5.

The mean floc size at a G_F of 12 s^{-1} was 77 µm with a standard deviation of ±53.3 µm, and the mean floc size at 60 s^{-1} was 129 µm and a standard deviation of ±78 µm. The average floc size for water flocculated at 12 s^{-1} is significantly smaller than particles mixed at an intensity of 60 s^{-1}. 70% of flocs mixed at 12 s^{-1} is smaller than 100 µm, while only 35% are smaller than 100 µm at 60 s^{-1}. The current method

produced floc size distributions similar to those reported by Gorczyca & Zhang (2007) and Gonzalez-Galvis et al., (2022), but smaller in size than that measured by Marega & Reali (2023).

Figure 4-11 is the floc size of the floated water produced by the flotation process for water flocculated at G_F = 12 s^{-1}. The graph compares the cumulative floc size of the effluent at the four tested pressures with the pre flotation floc size distribution. For the four floated waters the normalized curves follow the same general shape with a minor difference between the DAF with a saturator pressure of 275 kPa and when the saturator pressure is 610 kPa. Thus, the saturator pressure has a relatively small impact on the floc size distribution of the floated water. The saturator pressure may not have a significant impact because the mean bubble sizes produced using the different saturator pressures are in fact quite similar. As the data has been normalized (to compensate for the different number of particles) the comparison of the particle distributions of the flocculated and floated waters is not straight forward. However, Figure 4-11 clearly shows that the particle sizes in the floated waters are much smaller than those in the flocculated water, and this indicates that the larger flocs are being removed by the flotation

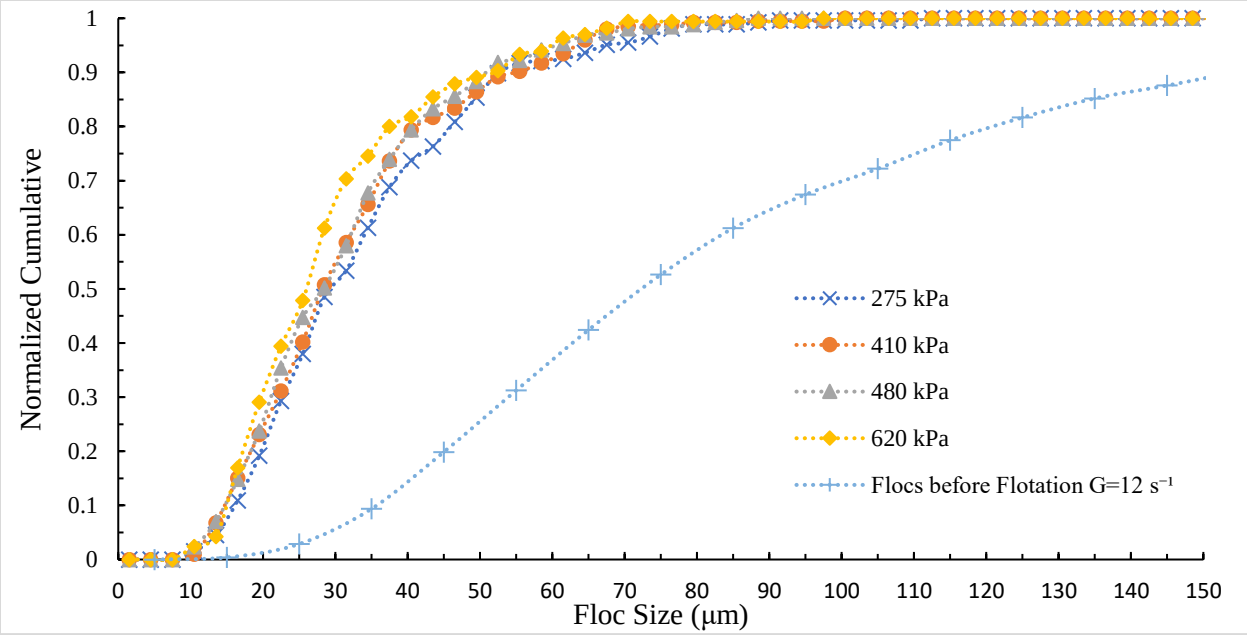

Figure 4-11: Cumulative floc size of the floated water produced with 35 mg/L alum dose, flocculation at G = 12 s^{-1} and DAF flotation.

Figure 4-12 shows the analogous cumulative graph for floc size for the water flocculated at 60 s^{-1} before flotation and after flotation at the four studied pressures. For the G_F = 60 s^{-1} tests the mean floated water floc sizes were 45.4 , 44.3, 40.1 and 31.4 µm at 275, 410, 480 and 620 kPa, respectively. It should be noted that a significant reduction in post-flotation mean particle size was observed for water flocculated at a mixing intensity of 60 s^{-1} and a flotation pressure of 620 kPa while the mean bubble size only slightly decreased. It was also observed that significantly less flocs were present after flotation when measuring the floc size with the microscope. With the larger flocs formed at 60 s^{-1} compared to 12 s^{-}, the effect of the saturator pressure is more significant. The increase in pressure results in a decrease in floc size within the floated water, however the mean floc size after flotation using G_F = 60 s^{-1} is larger than that flocculated at 12 s^{-1}. This is potentially caused by the fact that the mean floc size before flotation was 77 µm for flocs flocculated at 12 s^{-1} while the flocs formed at a G_F of 60 s^{-1} had a mean floc size of 129 µm. Because the unitized version of these graphs, having the smaller floc/particles sizes in the floated water may not yield the better treatment. Although we do not have turbidity data for these same flocculation G_F values, the data for the closest G_F values seems to indicate this. The floated water particle size for G_F=12 s^{-1} was smaller

than that for G_F= 60 s^{-1}, Figure 4-3 shows the run for G= (the closest to G_F=12 s^{-1}) had a higher floated water turbidity than runs with G_F=37 and 79 s^{-1} (the closest to G_F=60 s^{-1}). It is possible that a greater portion of the solids are removed in the water flocculated at 60 s^{-1} since the majority of the flocs were larger.

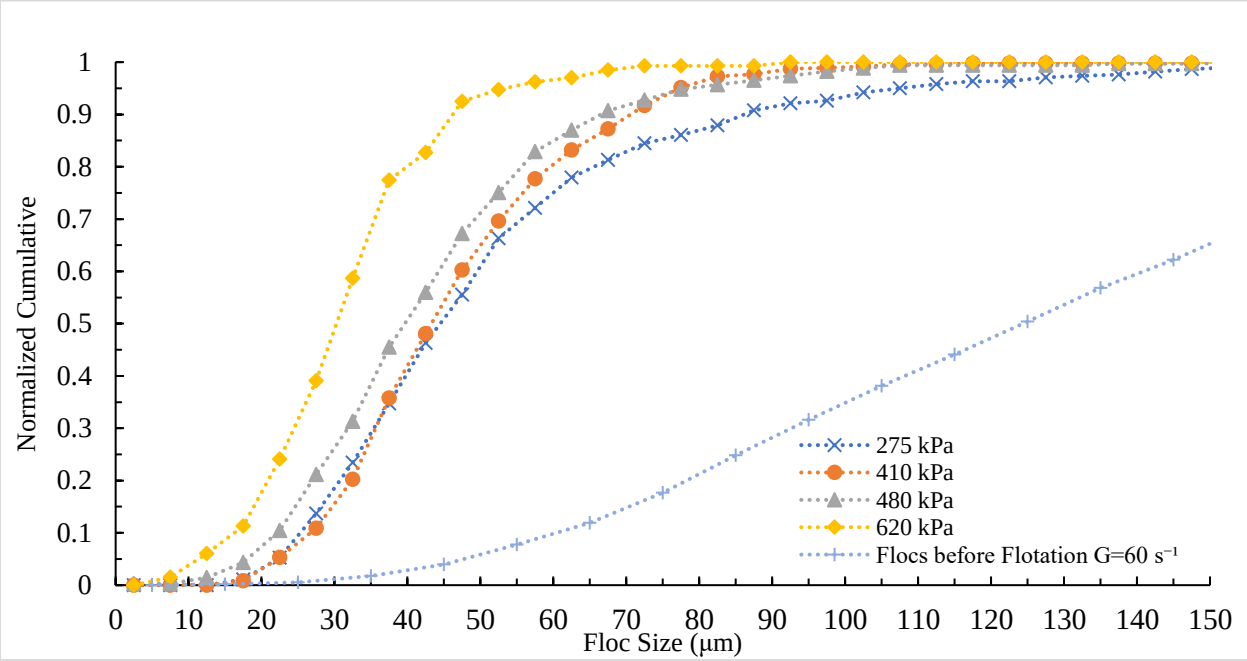

Figure 4-12: Cumulative floc size of the floated water produced with 35mg/L alum dose, flocculation at G_F = 60 s^{-1} and DAF flotation.

Many authors claim for optimal DAF operation the bubble size and the bubble size should be approximately the same ((Edzwald, 2010; Park et al., 2001)), however in this study DAF worked well with much larger flocs (77 and 129 um) than bubbles (36 um). These results are consistent with the findings of later is consistent with the work of Fukushi et al., 1995; Han et al., 2007; Leppinen, 1999; Marega & Reali, 2023. It should be noted that the shear induced by the pressurised water injection can result in floc breakage and thus the actual floc size (agglomerating with the bubbles) distribution is unlikely to be same as that of that feed flocs that would be separated without the breakage. In addition, there may be additional floc

agglomeration in the separation process resulting in inaccurate floc representation and a direct floc size comparison cannot be performed.

4.6 Conclusions

Removing turbidity from drinking water in cold conditions is feasible with aluminum sulphate. The operating pH must increase towards more alkaline conditions to achieve suitable operation, this experimentally confirms the recommendation of Edzwald & Haarhoff (2012). This is probably caused by a shift in aluminum solubility with temperature and effective areas within the solubility envelope. The optimal pOH for effective turbidity removal by DAF using 35 mg alum/L was essentially the same at 2 and 21°C, this is consistent with the work of Hansen & Cleasby (1990) and Van Benschoten & Edzwald (1990). Due to other constraints, such as residual aluminum concentrations < 0.05 mg/L, and maintaining high removals of disinfection by-product precursors, operating at an optimal pH for turbidity removal may not be feasible. Increasing the saturator pressure did not significantly decrease the mean bubble size. DAF treatment could efficiently remove flocs larger than the bubble. The effect of flocculation mixing intensity on the floated floc size distribution and floc removal was inconclusive, it may be possible that the conditions resulting with the larger mean final floc size has a greater removal efficiency since it began with a smaller fraction of small flocs entering the flotation stage.

4.7 References

Adler, P. M. (1981). Heterocoagulation in Shear Flow. *Journal of Colloidal Interface Science*, *83*(1), 106–115. https://doi.org/https://doi.org/10.1016/0021-9797(81)90015-1

Alam, N., Ozdemir, O., Hampton, M. A., & Nguyen, A. V. (2011). Dewatering of Coal Plant Tailings: Flocculation Followed by Filtration. *Fuel*, *90*(1), 26–35. https://doi.org/10.1016/j.fuel.2010.08.006

Alansari, A., & Amburgey, J. (2020). Critical Elements of Flocculation in Drinking Water Treatment. *AWWA Water Science*, *2*(6). https://doi.org/10.1002/aws2.1213

Amato, T., Edzwald, J. K., Tobiason, J. E., Dahlquist, J., & Hedberg, T. (2001). An Integrated Approach to Dissolved Air Flotation. *Water Science and Technology*, *43*(8), 19–26. https://doi.org/10.2166/wst.2001.0455

Amirtharajah, A., & Mills, K. M. (1982). Rapid-Mix Design for Mechanisms of Alum Coagulation. *Journal of the American Water Works Association*, *74*(4), 210–216. https://doi.org/https://doi.org/10.1002/j.1551-8833.1982.tb04890.x

APHA/AWWA/WEF. (2012). *Standard Methods for the Examination of Water and Wastewater* (22nd ed.). American Public Health Association American Water Works Association & Water Environment Federation.

Barwon, D. S. (2009). Cost Saving Coagulation Comparison at Lorne Water Treatment Plant. *72nd Annual Victorian Water Industry Engineers and Operators Conference*.

Benjamin, M. M., & Lawler, D. F. (2013). *Water Quality Engineering : Physical/Chemical Treatment Processes*. John Wiley and Sons.

Bratby, J. (2016). *Coagulation and Flocculation in Water and Wastewater Treatment* (3rd ed.). IWA Publishing.

Camp, T. R., Root, D. A., & Bhoota, B. V. (1940). Effects of Temperature on Rate of Floc Formation. *Journal (American Water Works Association)*, *32*(11), 1913–1927. https://doi.org/https://doi.org/10.1002/j.1551-8833.1940.tb19608.x

Carter, K., & Long, B. W. (1992). Canada's Cooperative Approach to Drinking Water Regulation. *Journal of American Water Works Association*, *84*(4), 120–128.

Chu, W. H., Gao, N. Y., Templeton, M. R., & Yin, D. Q. (2011). Comparison of Inclined Plate Sedimentation and Dissolved Air Flotation for the Minimisation of Subsequent Nitrogenous Disinfection By-Product Formation. *Chemosphere*, *83*(5), 647–651. https://doi.org/10.1016/j.chemosphere.2011.02.033

Cliff, R., Grace, J. R., & Webber, M. E. (1978). *Bubbles, Drops, and Particles*. Dover Publications, INC.

Crittenden, J. C., Trussell, R. R., Hand, D. W., Howe, K. J., & Tchobanoglous, G. (2012). *MWH's Water Treatment : Principles and Design*. John Wiley & Sons.

Crossley, I. A., & Valade, M. T. (2006). A Review of the Technological Developments of Dissolved Air Flotation. *Journal of Water Supply: Research and Technology - AQUA*, *55*(7–8), 479–491. https://doi.org/10.2166/aqua.2006.057

Cui, H., Huang, X., Yu, Z., Chen, P., & Cao, X. (2020). Application Progress of Enhanced Coagulation in Water Treatment. *RSC Advances*, *10*(34), 20231–20244. https://doi.org/10.1039/d0ra02979c

de Rijk, S. E., Jaap H.J.M., van der, G., & den Blanken, J. G. (1994). Bubble Size in Flotation Thickening. *Water Research*, *28*(2), 465–473. https://doi.org/10.1016/0043-1354(94)90284-4

Dejaeger, K., Criquet, J., Vanoppen, M., Vignal, C., Billon, G., & Cornelissen, E. R. (2022). Identification of Disinfection By-Product Precursors by Natural Organic Matter Fractionation: a Review. *Environmental Chemistry Letters*, *20*(6), 3861–3882. https://doi.org/10.1007/s10311-022-01478-x

Donaldson, E. C., & Alam, W. (2008). Surface Forces. In *Wettability* (pp. 57–119). Gulf Publishing Company. https://doi.org/10.1016/b978-1-933762-29-6.50008-9

Edzwald, J. K. (1993). Algae, Bubbles, Coagulants, and Dissolved Air Flotation. *Water Science and Technology*, *27*(10), 67–81. https://iwaponline.com/wst/article-pdf/27/10/67/117962/67.pdf

Edzwald, J. K. (2010). Dissolved Air Flotation and Me. In *Water Research* (Vol. 44, Issue 7, pp. 2077–2106). https://doi.org/10.1016/j.watres.2009.12.040

Edzwald, J. K. (2020). Aluminum in Drinking Water: Occurrence, Effects, and Control. *Journal American Water Works Association*, 34–41. https://doi.org/https://doi.org/10.1002/awwa.1499

Edzwald, J. K., Becker, W. C., & Wattier, K. L. (1985). Surrogate parameters for monitoring organic matter and THM precursors. *Journal / American Water Works Association*, *77*(4), 122–131. https://doi.org/10.1002/j.1551-8833.1985.tb05521.x

Edzwald, J. K., & Haarhoff, J. (2011). *Dissolved Air Flotation for Water Clarification*. McGraw Hill.

Fan, Y., Ma, X., Dong, X., Feng, Z., & Dong, Y. (2020). Characterisation of Floc Size, Effective Density and Sedimentation Under Various Flocculation Mechanisms. *Water Science and Technology*, *82*(7), 1261–1271. https://doi.org/10.2166/wst.2020.385

Feng, X., Baojie, Z., & Chery, L. (2008). Effects of Low Temperature on Aluminum(III) Hydrolysis: Theoretical and Experimental Studies. *Journal of Environmental Sciences*, *20*(8), 907–914. https://doi.org/10.1016/S1001-0742(08)62185-3

Fitria, D., Scholz, M., Swift, G. M., & Hutchinson, S. M. (2014). Impact of Sludge Floc Size and Water Composition on Dewaterability. *Chemical Engineering and Technology*, *37*(3), 471–477. https://doi.org/10.1002/ceat.201300378

Friedlander, S. K. (1977). *Smoke, Dust, and Haze Fundamentals of Aerosol Dynamics*. Oxford University Press.

Fukushi, K., Tambo, N., & Matsui, Y. (1995). A Kinetic Model for Dissolved Air Flotation in Water and Wastewater Treatment. *Water Science and Technology*, *31*(3–4), 37–47. https://doi.org/https://doi.org/10.1016/0273-1223(95)00202-X

Go, R. J. C., Yang, H. L., Kan, C. C., Ong, D. C., Garcia-Segura, S., & de Luna, M. D. G. (2021). Natural Organic Matter Removal from Raw Surface Water: Benchmarking Performance of Chemical Coagulants Through Excitation-Emission Fluorescence Matrix Spectroscopy Analysis. *Water*, *13*(2). https://doi.org/10.3390/w13020146

Gonzalez Gavis, J. P. (2019). *Development of Large Batch Bench-Scale Dissolved Air Flotation System for Drinking Water Treatment Tests*. Universtity of Ottawa.

Gonzalez-Galvis, J. P., & Narbaitz, R. M. (2020). Large Batch bench-Scale Dissolved Air Flotation System (LB-DAF) for Drinking Water Treatability Tests. *Environmental Science: Water Research and Technology*, *6*(4), 1004–1017. https://doi.org/10.1039/c9ew00935c

Gorczyca, B., & Zhang, G. (2007a). Floc Size Distributions in Dissolved Air Flotation of Winnipeg Tap Water. *Environmental Technology*, *28*, 243–254. https://doi.org/10.1080/09593332808618786

Gorczyca, B., & Zhang, G. (2007b). Floc size distributions in dissolved air flotation of Winnipeg tap water. *Environmental Technology*, *28*(3), 243–254. https://doi.org/10.1080/09593332808618786

Govoreanu, R., Saveyn, H., Van Der Meeren, P., Nopens, I., & Vanrolleghem, P. A. (2009). A Methodological Approach for Direct Quantification of the Activated Sludge Floc Size Distribution by Using Different Techniques. *Water Science and Technology*, *60*(7), 1857–1867. https://doi.org/10.2166/wst.2009.535

Gregory, R., Zabel. Thomas, & Edzwald, J. K. (1999). Sedimentation and Flotation. In *Water Quality and Treatment - A Handbook of Community Water Supplies* (Fifth, pp. 7.1-7.87). McGraw-Hill.

Haarhoff, J., & Edzwald, J. K. (2004). Dissolved Air Flotation Modelling: Insights and Shortcomings. *Journal of Water Supply*, *53*(3), 127–150. https://iwaponline.com/aqua/article-pdf/53/3/127/402453/127.pdf

Han, M., Kim, T. Il, & Kim, J. (2007). Effects of Floc and Bubble Size on the Efficiency of the Dissolved Air Flotation (DAF) Process. *Water Science and Technology*, *56*(10), 109–115. https://doi.org/10.2166/wst.2007.779

Han, M., & Lawler, D. F. (1992). The (Relative) Insignificance of G in Flocculation. *Journal of American Water Works Association*, *84*(10), 79–91. https://doi.org/https://doi.org/10.1002/j.1551-8833.1992.tb05869.x

Hanna, G. P. J., & Rubin, A. J. (1970). Effect of Sulfate and Other Ions in Coagulation With Aluminum(III). *Journal of American Water Works Association*, *62*(5), 315–321. https://doi.org/10.1002/j.1551-8833.1970.tb03912.x

Hanson, A. T., & Cleasby, J. L. (1990). The Effects of Temperature on Turbulent Flocculation: Fluid Dynamics and Chemistry. *Journal of American Water Works Association*, *82*(11), 56–73. https://doi.org/https://doi.org/10.1002/j.1551-8833.1990.tb07053.x

Hayden, P. L., & Rubin, A. J. (1974). Systematic Investigation of the Hydrolysis and Precipitation of Aluminum(III). In A. J. Rubin (Ed.), *Aqueous Environmental Chemistry of Metals* (pp. 317–381). Ann Arbor Science Publishers.

Health Canada. (2019). *Aluminum in Drinking Water*.

Hua, G., Reckhow, D. A., & Abusallout, I. (2015). Correlation between SUVA and DBP formation during chlorination and chloramination of NOM fractions from different sources. *Chemosphere*, *130*, 82–89. https://doi.org/10.1016/j.chemosphere.2015.03.039

Jarvis, P., Jefferson, B., & Parsons, S. A. (2005). Measuring Floc Structural Characteristics. In *Reviews in Environmental Science and Biotechnology* (Vol. 4, Issues 1–2, pp. 1–18). https://doi.org/10.1007/s11157-005-7092-1

Jetoo, S., Grover, V. I., & Krantzberg, G. (2015). The Toledo Drinking Water Advisory: Suggested Application of the Water Safety Planning Approach. *Sustainability (Switzerland)*, *7*(8), 9787–9808. https://doi.org/10.3390/su7089787

Johnson, P. N., & Amirtharajah, A. (1983). Ferric Chloride and Alum as Single and Dual Coagulants. *Journal of American Water Works Association*, *75*(5), 232–239. https://doi.org/https://doi.org/10.1002/j.1551-8833.1983.tb05122.x

Kiuru, H. J. (2001). Development of Dissolved Air Flotation Technology from the First Generation to the Newest (third) One (DAF in Turbulent Flow Conditions). *Water Science and Technology*, *43*(8), 1–7. https://doi.org/https://doi.org/10.2166/wst.2001.0450

Kuriqi, A., Pinheiro, A. N., Sordo-Ward, A., Bejarano, M. D., & Garrote, L. (2021). Ecological Impacts of Run-of-River Hydropower Plants—Current Status and Future Prospects on the Brink of Energy Transition. *Renewable and Sustainable Energy Reviews*, *142*, 1–17. https://doi.org/10.1016/j.rser.2021.110833

Lane, E. W. (1955). The Importance of Fluvial Morphology in Hydraulic Engineering. *American Society of Civil Engineers Journal*, *81*(July).

Leppinen, D. M. (1999). Trajectory Analysis and Collision Efficiency During Microbubble Flotation. *Journal of Colloid and Interface Science*, *212*(2), 431–442. https://doi.org/10.1006/jcis.1998.6075

Leppinen, D. M., & Dalziel, S. B. (2004). Bubble Size Distribution in Dissolved Air Flotation Tanks. *Journal of Water Supply*, *53*(8), 531–543. https://iwaponline.com/aqua/article-pdf/53/8/531/402551/531.pdf

Li, T., Zhu, Z., Wang, D., Yao, C., & Tang, H. (2006). Characterization of Floc Size, Strength and Structure Under Various Coagulation Mechanisms. *Powder Technology*, *168*(2), 104–110. https://doi.org/10.1016/j.powtec.2006.07.003

Lin, Q., Dong, F., Miao, Y., Li, C., & Fei, W. (2020). Removal of Disinfection By-Products and Their Precursors During Drinking Water Treatment Processes. *Water Environment Research*, *92*(5), 698–705. https://doi.org/10.1002/wer.1263

Liu, R., Guo, T., Ma, M., Yan, M., Qi, J., Hu, C., Liu, G., Liu, H., Qu, J., & van der Meer, W. (2019). Preferential Binding Between Intracellular Organic Matters and Al13 Polymer to Enhance Coagulation Performance. *Journal of Environmental Sciences (China)*, *76*, 1–11. https://doi.org/10.1016/j.jes.2018.05.011

Lundh, M., Jönsson, L., & Dahlquist, J. (2002). The Influence of Contact Zone Configuration on the Flow Structure in a Dissolved Air Flotation Pilot Plant. *Water Research*, *36*(6), 1585–1595. https://doi.org/10.1016/S0043-1354(01)00357-8

Malley, J. P., & Edzwald, J. K. (1991). Comparison of DAF With Conventional Treatment. *Journal American Water Work Association*, *83*(9), 56–61. https://doi.org/https://doi.org/10.1002/j.1551-8833.1991.tb07214.x

Marega, G., & Reali, M. (2023). Characterization of Flocs and Bubbles Size Distribution in The Dissolved Air Flotation Process Using Non-Intrusive Image Analysis. *American Water Works Association ACE23*.

Matijevic, E. (1973). Colloid Stability and Complex Chemistry. *Journal of Colloidal and Interface Science*, *43*(2), 217–245. https://doi.org/https://doi.org/10.1016/0021-9797(73)90371-8

Matijević, E., & Stryker, L. J. (1966). Coagulation and Reversal of Charge of Lyophobic Colloids by Hydrolyzed Metal Ions. III. Aluminum Sulfate. *Journal of Colloid and Interface Science*, *22*(1), 68–77. https://doi.org/10.1016/0021-9797(66)90068-3

McCooke, N. J., & West, J. R. (1978). The Coagulation of a Kaolinite Suspension with Aluminium Sulphate. *Journal of Water Resources*, *12*, 793–798. https://doi.org/10.1016/0043-1354(78)90029-5

Metcalfe, G., Speetjens, M. F. M., Lester, D. R., & Clercx, H. J. H. (2012). Beyond passive: Chaotic Transport in Stirred Fluids. In *Advances in Applied Mechanics* (Vol. 45, pp. 109–188). Academic Press Inc. https://doi.org/10.1016/B978-0-12-380876-9.00004-5

Mohamed, A. Y. A., Siggins, A., Healy, M. G., Ó hUallacháin, D., Fenton, O., & Tuohy, P. (2020). Appraisal and Ranking of Poly-Aluminium Chloride, Ferric Chloride and Alum for the Treatment of Dairy Soiled Water. *Journal of Environmental Management*, *267*. https://doi.org/10.1016/j.jenvman.2020.110567

Morris, J. K., & Knocke, W. R. (1984). Temperature Effects on the Use of Metal-Ion Coagulants for Water Treatment. *Journal of American Water Works Association*, *76*(3), 74–79. https://doi.org/https://doi.org/10.1002/j.1551-8833.1984.tb05302.x

Mustereț, C. P., Morosanu, I., Ciobanu, R., Plavan, O., Gherghel, A., Al-Refai, M., Roman, I., & Teodosiu, C. (2021). Assessment of Coagulation–Flocculation Process Efficiency for the Natural Organic Matter Removal in Drinking Water Treatment. *Water* , *13*(21). https://doi.org/10.3390/w13213073

Pablo, G. G. J., Maria, J. L. A., & Felipe, M. U. A. (2022). Low-Cost Methodology for the Characterization of Floc Size in Low Turbidity and Low Alkalinity Waters Using Image Analysis. *Water Practice and Technology*, *17*(4), 887–900. https://doi.org/10.2166/wpt.2022.026

Packham, R. F. (1962). The Coagulation Process. I. Effect of pH and the Nature of the Turbidity. *Journal of Applied Chemistry*, *12*, 556–564. https://doi.org/https://doi.org/10.1002/jctb.5010121207

Park, Y., Han, M., Kwak, D., & Pack, C. (2001). Effect of Particle and Bubble Size on the Removal Efficiency in DAF. *Asian-Pacific Regional Conference*.

Pernitsky, D. J., & Edzwald, J. K. (2003). Solubility of polyaluminium coagulants. *Journal of Water Supply : Research and Technology*, *52*(6), 395–406. https://doi.org/https://doi.org/10.2166/aqua.2003.0036

Rance Bare, W. F., Jones, N. B., & Middlebrooks, E. J. (1975). Algae Removal Using Dissolved Air Flotation. *Journal of Water Pollution Control Federation*, *47*(1), 153–169. https://www.jstor.org/stable/25038604

Rodrigues, R. T., & Rubio, J. (2003). New Basis for Measuring the Size Distribution of Bubbles. *Minerals Engineering*, *16*(8), 757–765. https://doi.org/10.1016/S0892-6875(03)00181-X

Rubin, A. J., & Kovac, T. W. (1974). Effect of Aluminum(III) Hydrolysis on Alum Coagulation. In *Chemistry of Water Supply, Treatment, and Distribution* (pp. 159–179). Ann Arbor Science.

Schmideder, S., Thurin, L., Kaur, G., & Briesen, H. (2022). Inline Imaging Reveals Evolution of the Size Distribution and the Concentration of Microbubbles in Dissolved Air Flotation. *Water Research*, *224*(119027), 1–12. https://doi.org/10.1016/j.watres.2022.119027

Sillanpää, M. (2015). Natural Organic Matter in Water : Characterization and Treatment Methods. In *Natural Organic Matter in Water*. Butterworth-Heinemann. https://doi.org/10.1016/B978-0-12-824274-2.00003-X

Smoluchowski, • M V. (1917). Versuch Einer Mathematischen Theorie der Koagulationskinetik Kolloider Lösnngen. *Losungen. Z. Physik Chem.*, *92*, 129–168.

Spielman, L. A. (1970). Viscous Interactions in Brownian Coagulation. *Journal of Colloid and Interaction Science*, *33*(4), 562–571. https://doi.org/10.1016/0021-9797(70)90008-1

Stumm, W., Morgan, J. J., & Black, A. P. (1962). Chemical Aspects of Coagulation. *Journal of American Water Works Association* , *54*(8), 971–994.

Sun, S., Weber-Shirk, M., & Lion, L. W. (2016). Characterization of Flocs and Floc Size Distributions Using Image Analysis. *Environmental Engineering Science*, *33*(1), 25–34. https://doi.org/10.1089/ees.2015.0311

Tafvizi, H., & Husain, T. (2022). Enhanced Coagulation for Removal of Natural Organic Matter and Disinfection Byproducts: Multivariate Optimization. *Environmental Engineering Science*, *39*(2), 155–167. https://doi.org/10.1089/ees.2020.0372

Tambo, N., & Watanabe, Y. (1978). Physical Characteristics of Flocs--I. The Floc Density Function and Aluminium Floc. *Water Research*, *13*, 409–419. https://doi.org/https://doi.org/10.1016/0043-1354(79)90033-2

Teguh, D., Agustina, T. E., Ridho, M. H., Febriyanti, N., & Ermaya, D. (2022). The Effectiveness and Cost Optimization of Coagulant Aluminum Chlorohydrate (ACH), Aluminum Sulfate (AS) and Poly Aluminium Chloride (PAC) in Coagulation Process at The PT. Pupuk Sriwijaya (PT.Pusri) Utility Unit. *Indonesian Journal of Environmental Management and Sustainability*, *6*, 189–195. https://doi.org/10.26554/ijems.2022.6.1.189-195

Tian, C., Wu, Y., Wei, M., & Feng, C. (2018). A Novel Understanding of Residual Nano-Al13 Formation and Degradation During Coagulation and Flocculation: a Proof Based on ESI-TOF-MS. *Environmental Science: Nano*, *5*(11), 2712–2721. https://doi.org/10.1039/c8en00921j

Valade, M. T., Becker, W. C., & Edzwald, J. K. (2009). Treatment Selection Guidelines for Particle and NOM Removal. *Journal of Water Supply: Research and Technology - AQUA*, *58*(6), 424–432. https://doi.org/10.2166/aqua.2009.201

Valioulis, I. A., & John, E. (1984). Collision Efficiencies of Diffusing Spherical Particles: Hydrodynamic, van er Waals and Electrostatic Forces. *Advances in Colloid and Interface Sciences*, *20*, 1–20.

Van Benschoten, J. E., & Edzwald, J. K. (1990). Chemical Aspects of Coagulation Using Aluminum Salts I. Hydrolytic Reaction of Alum and Polyaluminum Chloride. *Water Research*, *24*(12), 1519–1526. https://doi.org/https://doi.org/10.1016/0043-1354(90)90087-M

Velz, C. J. (1934). Influence of Temperature on Coagulation. *Journal of Civil Engineering*, *4*(345).

Verberk, J. Q. J. C., O'Halloran, K. J., Hamilton, L. A., Vreeburg, J. H. G., & Van Dijk, J. C. (2007). Measuring Particles in Drinking Water Transportation Systems with Particle Counters. *Journal*

of Water Supply: Research and Technology - AQUA, *56*(5), 345–355. https://doi.org/10.2166/aqua.2007.069

Walker, H. W. (2015). *Harmful Algae Bloom in Drinking Water - Removal of Cyanobacterial Cells and Toxins* (A. J. Forsgren, Ed.). CRC Press.

Wang, L. K. (2021). Operation and Performance of the AquaDAF ® Process System for Water Purification. *Environmental Flotation Engineering*, 301–341. https://doi.org/10.17613/7xwx-xr75

Wang, P., Jiao, R., Liu, L., Xiao, F., An, G., & Wang, D. (2019). Optimized Coagulation Pathway of Al13: Effect of In-Situ Aggregation of Al13. *Chemosphere*, *230*, 76–83. https://doi.org/10.1016/j.chemosphere.2019.05.053

Xu, B., & Narbaitz, R. M. (2016). Improved Membrane Pretreatment of High Hydrophobic Natural Organic Matter (NOM) Waters by Floatation. *Journal of Membrane Science*, *518*, 120–130. https://doi.org/10.1016/j.memsci.2016.02.056

Xu, G. R., Fitzpatrick, C. S. B., & Gregory, J. (2008). Floc Formation, Size Distribution, and its Transformation Detected by Online Laser Particle Counter. *Separation Science and Technology*, *43*(7), 1725–1736. https://doi.org/10.1080/01496390801973706

Xu, W., Gao, B., Yue, Q., & Wang, Q. (2011). Effect of Preformed and Non-Preformed Al13 Species on Evolution of Floc Size, Strength and Fractal Nature of Humic Acid Flocs in Coagulation Process. *Separation and Purification Technology*, *78*(1), 83–90. https://doi.org/10.1016/j.seppur.2011.01.025

Yu, J., Wang, D., Ge, X., Yan, M., & Yang, M. (2006). Flocculation of Kaolin Particles by Two Typical Polyelectrolytes: A Comparative Study on the Kinetics and Floc Structures. *Colloids*

and Surfaces A: Physicochemical and Engineering Aspects, *290*(1–3), 288–294. https://doi.org/10.1016/j.colsurfa.2006.05.040

Zabel, T. (1983). Flotation in Water Treatment. In *The Scientific Basis of Flotation* (pp. 349–377). https://doi.org/10.1007/978-94-009-6926-1

Zarchi, I., Friedler, E., & Rebhun, M. (2013). Polyaluminium Chloride as an Alternative to Alum for the Direct Filtration of Drinking Water. *Environmental Technology*, *34*(9), 1199–1209. https://doi.org/10.1080/09593330.2012.743594

Zhang, W. H., Zhang, J., Zhao, B., & Zhu, P. (2015). Microbubble Size Distribution Measurement in a DAF System. *Industrial and Engineering Chemistry Research*, *54*, 5179–5183. https://doi.org/10.1021/acs.iecr.5b00109

Zheng, D. (2013). *Effects of Coagulation on the Removal of Natural Organic Matter, Genotoxicity, and Precursors to Halogenated Furanones*. University of Toronto.

Chapter 5 -Conclusions

5.1 Overview

This thesis investigated the performance of DAF for the treatment of a low turbidity, low alkalinity, relatively high NOM river water using alum as the sole coagulant. The optimum coagulant dose resulted in conditions were sweep flocculation was significant. This dissertation studied the effect of water temperature on turbidity removals and the interaction between flocs and bubbles of a DAF system at a microscopic scale. Knowledge of these two research topics will allow plant operators and managers to economically optimize drinking water treatment operating with dissolved air flotation.

5.2 Treatment with Alum at Cold Temperatures

According to the results, treatment at cold temperatures using the same coagulant dose may be feasible if the process pH is adjusted so that the pOH is the same as that for warm water conditions. With such a pH adjustment, the coagulation process can be effective and forms large flocs even at cold temperatures. For the low turbidity, low alkalinity, high NOM concentration river water studied, at low temperatures the DAF turbidity removals appears to be independent of the flocculation mixing intensity and flocculation time, while at room temperature the turbidity removal are impacted by both the flocculation mixing intensity and flocculation time.

5.3 Floc and Bubble Size Interaction for DAF

Increasing the saturator pressure did not significantly decrease the mean bubble size. The average floc size was significantly larger than the average bubble size, and this combination was effective at removing the majority of the flocs as the post flotation particle sizes were much smaller than the incoming flocs. This indicates that flocs attach to bubbles that are significantly smaller in size. The effect of

flocculation intensity on the particle removal based on the size of the DAF effluent particles was inconclusive. It may be possible that the conditions resulting with the larger mean final floc size has a greater removal efficiency since it began with a smaller fraction of small flocs entering the flotation stage.

5.5 Recommendations for Future Work

Based on the finding of this research into coagulation and flocculation at cold temperatures and bubble floc interaction, the following are recommendations for future work:

1. Cold water operations for drinking water treatment with alum for turbidity removal is feasible without flocculation aids, but research into DAF removal of other important parameters is necessary. These include disinfection by-product precursors and disinfection by-product formation potential. The reaction rate for by-product formation may be reduced at colder temperatures, but DBP formation is still a concern in some situations, such as with large distribution systems or residences on trucked water distribution systems that hold their water in heated residences are still of concern. In addition, other parameters such as metal solubility, residual aluminum concentrations, colour removal and taste and odour removal should be investigated.
2. Investigate the effect of rapid mixing on cold water flocculation. For sweep flocculation, the rapid dispersion of coagulant is not necessary (Amirtharajah & Mills, 1982), but excessive rapid mixing may result in irreversible floc breakage.
3. Investigate the interaction between bubble size and floc size in cold temperatures and their impact on floated water particle size and turbidity
4. Investigate the interaction between bubble size and floc size in a continuous DAF system, as the continuous system have a more elaborate flow pattern (Lundh et al., 2002).
5. The interaction between bubble size and floc size should be studied with waters of different characteristics from the water in the current study, that is a water with low turbidity and had

relatively high organic concentrations consisting of primarily hydrophobic organics (SUVA = 4.58).

Chapter 6 -References

Adler, P. M. (1981). Heterocoagulation in Shear Flow. *Journal of Colloidal Interface Science*, *83*(1), 106–115. https://doi.org/https://doi.org/10.1016/0021-9797(81)90015-1

Alam, N., Ozdemir, O., Hampton, M. A., & Nguyen, A. V. (2011). Dewatering of Coal Plant Tailings: Flocculation Followed by Filtration. *Fuel*, *90*(1), 26–35. https://doi.org/10.1016/j.fuel.2010.08.006

Alansari, A., & Amburgey, J. (2020). Critical Elements of Flocculation in Drinking Water Treatment. *AWWA Water Science*, *2*(6), 1-15. https://doi.org/10.1002/aws2.1213

Amato, T., Edzwald, J. K., Tobiason, J. E., Dahlquist, J., & Hedberg, T. (2001). An Integrated Approach to Dissolved Air Flotation. *Water Science and Technology*, *43*(8), 19–26. https://doi.org/10.2166/wst.2001.0455

Amirtharajah, A., & Mills, K. M. (1982). Rapid-Mix Design for Mechanisms of Alum Coagulation. *Journal of the American Water Works Association*, *74*(4), 210–216. https://doi.org/https://doi.org/10.1002/j.1551-8833.1982.tb04890.x

APHA/AWWA/WEF. (2012). *Standard Methods for the Examination of Water and Wastewater* 22nd ed.. In E.W. Rice, R.B. Baird, A.D. Eaton, L.S. Clescerl (Eds.), American Public Health Association American Water Works Association & Water Environment Federation, Washington, DC.

Barwon, D. S. (2009). Cost Saving Coagulation Comparison at Lorne Water Treatment Plant. *72nd Annual Victorian Water Industry Engineers and Operators Conference*. Water Industry Operators Association of Australia, Shepparton, Australia http://www.wioa.org.au/conference_papers/09_vic/documents/SeanDoyleposter.pdf

Benjamin, M. M., & Lawler, D. F. (2013). *Water Quality Engineering : Physical/Chemical Treatment Processes*. John Wiley and Sons, Hoboken, NJ.

Bratby, J. (2016). *Coagulation and Flocculation in Water and Wastewater Treatment* 3ed. IWA Publishing, London, *15*(0), 9781780407500. https://doi.org/10.2166/9781780407500

Camp, T. R., Root, D. A., & Bhoota, B. V. (1940). Effects of Temperature on Rate of Floc Formation. *Journal American Water Works Association*, *32*(11), 1913–1927. https://doi.org/10.1002/j.1551-8833.1940.tb19608.x

Carter, K., & Long, B. W. (1992). Canada's Cooperative Approach to Drinking Water Regulation. *Journal of American Water Works Association*, *84*(4), 120–128. https://www.jstor.org/stable/41294275

Chu, W. H., Gao, N. Y., Templeton, M. R., & Yin, D. Q. (2011). Comparison of Inclined Plate Sedimentation and Dissolved Air Flotation for the Minimisation of Subsequent Nitrogenous Disinfection By-Product Formation. *Chemosphere*, *83*(5), 647–651. https://doi.org/10.1016/j.chemosphere.2011.02.033

Cliff, R., Grace, J. R., & Webber, M. E. (1978). *Bubbles, Drops, and Particles*. Dover Publications, INC. Mineola, NY.

Crittenden, J. C., Trussell, R. R., Hand, D. W., Howe, K. J., & Tchobanoglous, G. (2012). *MWH's Water Treatment : Principles and Design*. Third ed., John Wiley & Sons, Hoboken, NJ.

Crossley, I. A., & Valade, M. T. (2006). A Review of the Technological Developments of Dissolved Air Flotation. *Aqua*, *55*(7–8), 479–491. https://doi.org/10.2166/aqua.2006.057

Cui, H., Huang, X., Yu, Z., Chen, P., & Cao, X. (2020). Application Progress of Enhanced Coagulation in Water Treatment. *RSC Advances*, *10*(34), 20231–20244. https://doi.org/10.1039/d0ra02979c

de Rijk, S. E., Jaap H.J.M., van der, G., & den Blanken, J. G. (1994). Bubble Size in Flotation Thickening. *Water Research*, *28*(2), 465–473. https://doi.org/10.1016/0043-1354(94)90284-4

Dejaeger, K., Criquet, J., Vanoppen, M., Vignal, C., Billon, G., & Cornelissen, E. R. (2022). Identification of Disinfection By-Product Precursors by Natural Organic Matter Fractionation: A Review. *Environmental Chemistry Letters*, *20*(6), 3861–3882. https://doi.org/10.1007/s10311-022-01478-x

Donaldson, E. C., & Alam, W. (2008). Surface Forces. In *Wettability* (pp. 57–119). Gulf Publishing Company. Houston, TX. https://doi.org/10.1016/b978-1-933762-29-6.50008-9

Edzwald, J. K. (1993). Algae, Bubbles, Coagulants, and Dissolved Air Flotation. *Water Science and Technology*, *27*(10), 67–81. https://doi.org/10.2166/wst.1993.0207

Edzwald, J. K. (2010). Dissolved Air Flotation and Me. *Water Research*, *44*(7), 2077–2106. https://doi.org/10.1016/j.watres.2009.12.040

Edzwald, J. K. (2020). Aluminum in Drinking Water: Occurrence, Effects, and Control. *Journal American Water Works Association, 112*(5), 34–41. https://doi.org/10.1002/awwa.1499

Edzwald, J. K., Becker, W. C., & Wattier, K. L. (1985). Surrogate parameters for monitoring organic matter and THM precursors. *Journal American Water Works Association*, *77*(4), 122–132. https://doi.org/10.1002/j.1551-8833.1985.tb05521.x

Edzwald, J. K., & Haarhoff, J. (2012). *Dissolved Air Flotation for Water Clarification*. McGraw Hill Professional, Toronto, ON.

Fan, Y., Ma, X., Dong, X., Feng, Z., & Dong, Y. (2020). Characterisation of Floc Size, Effective Density and Sedimentation Under Various Flocculation Mechanisms. *Water Science and Technology*, 82(7), 1261–1271. https://doi.org/10.2166/wst.2020.385

Feng, X., Baojie, Z., & Chery, L. (2008). Effects of Low Temperature on Aluminum(III) Hydrolysis: Theoretical and Experimental Studies. *Journal of Environmental Sciences*, *20*(8), 907–914. https://doi.org/10.1016/S1001-0742(08)62185-3

Fitria, D., Scholz, M., Swift, G. M., & Hutchinson, S. M. (2014). Impact of Sludge Floc Size and Water Composition on Dewaterability. *Chemical Engineering and Technology*, 37(3), 471–477. https://doi.org/10.1002/ceat.201300378

Friedlander, S. K. (1977). *Smoke, Dust, and Haze Fundamentals of Aerosol Dynamics*. Oxford University Press, Oxford, UK.

Fukushi, K., Tambo, N., & Matsui, Y. (1995). A Kinetic Model for Dissolved Air Flotation in Water and Wastewater Treatment. *Water Science and Technology*, 31(3–4), 37–47. https://doi.org/10.1016/0273-1223(95)00202-X

Go, R. J. C., Yang, H. L., Kan, C. C., Ong, D. C., Garcia-Segura, S., & de Luna, M. D. G. (2021). Natural Organic Matter Removal from Raw Surface Water: Benchmarking Performance of Chemical Coagulants Through Excitation-Emission Fluorescence Matrix Spectroscopy Analysis. *Water*, *13*(2),146. https://doi.org/10.3390/w13020146

Gonzalez Gavis, J. P. (2019). *Development of Large Batch Bench-Scale Dissolved Air Flotation System for Drinking Water Treatment Tests*. Ph.D. thesis, Dept. of Civil Engineering, University of Ottawa, Ottawa, ON.

Gonzalez-Galvis, J. P., & Narbaitz, R. M. (2020). Large Batch bench-Scale Dissolved Air Flotation System (LB-DAF) for Drinking Water Treatability Tests. *Environmental Science: Water Research and Technology*, 6(4), 1004–1017. https://doi.org/10.1039/c9ew00935c

Gonzalez-Galvis, J. P., Londoño, Á. M. J., & Felipe, M. U. A (2022). Low-Cost Methodology for the Characterization of Floc Size in Low Turbidity and Low Alkalinity Waters Using Image Analysis. *Water Practice and Technology*, 17(4), 887–900. https://doi.org/10.2166/ wpt.2022.026

Gorczyca, B., & Zhang, G. (2007). Floc Size Distributions in Dissolved Air Flotation of Winnipeg Tap Water. *Environmental Technology*, 28, 243–254. https://doi.org/10.1080/09593332808618786

Govoreanu, R., Saveyn, H., Van Der Meeren, P., Nopens, I., & Vanrolleghem, P. A. (2009). A Methodological Approach for Direct Quantification of the Activated Sludge Floc Size Distribution by Using Different Techniques. *Water Science and Technology*, 60(7), 1857–1867. https://doi.org/10.2166/wst.2009.535

Gregory, R., Zabel. T., & Edzwald, J. K. (1999). Sedimentation and Flotation. Chapter 7 In *Water Quality and Treatment - A Handbook of Community Water Supplies*, Fifth ed., *In R.D. Letterman (Ed.)*, pp. 7.1-7.87. McGraw-Hill, Toronto, ON.

Haarhoff, J., & Edzwald, J. K. (2004). Dissolved Air Flotation Modelling: Insights and Shortcomings. *Journal of Water Supply*, 53(3), 127–150. https://doi.org/10.2166/aqua.2004.0012

Han, M., & Lawler, D. F. (1992). The (Relative) Insignificance of G in Flocculation. *Journal of American Water Works Association*, 84(10), 79–91. https://doi.org/10.1002/j.1551-8833.1992.tb05869.x

Han, M. J., Kim, T., & Kim, J. (2007). Effects of floc and bubble size on the efficiency of the dissolved air flotation (DAF) process. *Water Science and Technology*, *56*(10), 109–115. https://doi.org/10.2166/wst.2007.779

Hanna, G. P. J., & Rubin, A. J. (1970). Effect of Sulfate and Other Ions in Coagulation With Aluminum(III). *Journal of American Water Works Association*, 62(5), 315–321. https://doi.org/10.1002/j.1551-8833.1970.tb03912.x

Hanson, A. T., & Cleasby, J. L. (1990). The Effects of Temperature on Turbulent Flocculation: Fluid Dynamics and Chemistry. *Journal of American Water Works Association*, 82(11), 56–73. https://doi.org/10.1002/j.1551-8833.1990.tb07053.x

Hayden, P. L., & Rubin, A. J. (1974). Systematic Investigation of the Hydrolysis and Precipitation of Aluminum(III). In A. J. Rubin (Ed.), *Aqueous Environmental Chemistry of Metals* (pp. 317–381). Ann Arbor Science Publishers, Ann Arbor, MI.

Health Canada. (2019). *Aluminum in Drinking Water*. Health Canada, Ottawa, ON.

https://www.canada.ca/en/health-canada/programs/consultation-aluminum-drinking-water/document.html

Hua, G., Reckhow, D. A., & Abusallout, I. (2015). Correlation between SUVA and DBP formation during chlorination and chloramination of NOM fractions from different sources. *Chemosphere*, *130*, 82–89. https://doi.org/10.1016/j.chemosphere.2015.03.039

Jarvis, P., Jefferson, B., & Parsons, S. A. (2005). Measuring Floc Structural Characteristics. *Reviews in Environmental Science and Bio/Technology*, 4(1–2), 1–18. https://doi.org/10.1007/s11157-005-7092-1

Jasim, S. Y., Ndiongue, S., Johnson, B., Schweitzer, L., & Borikar, D. (2008). The effect of ozone on cold water coagulation. *Ozone: Science and Engineering*, 30(1), 27–33. https://doi.org/10.1080/01919510701753366

Jetoo, S., Grover, V. I., & Krantzberg, G. (2015). The Toledo Drinking Water Advisory: Suggested Application of the Water Safety Planning Approach. *Sustainability*, 7(8), 9787–9808. https://doi.org/10.3390/su7089787

Johnson, P. N., & Amirtharajah, A. (1983). Ferric Chloride and Alum as Single and Dual Coagulants. *Journal of American Water Works Association*, 75(5), 232–239. https://doi.org/10.1002/j.1551-8833.1983.tb05122.x

Kiuru, H. J. (2001). Development of Dissolved Air Flotation Technology from the First Generation to the Newest (third) One (DAF in Turbulent Flow Conditions). *Water Science and Technology*, 43(8), 1–7. https://doi.org/10.2166/wst.2001.0450

Kuriqi, A., Pinheiro, A. N., Sordo-Ward, A., Bejarano, M. D., & Garrote, L. (2021). Ecological Impacts of Run-of-River Hydropower Plants—Current Status and Future Prospects on the Brink of Energy Transition. *Renewable and Sustainable Energy Reviews*, 142, 1–17. https://doi.org/10.1016/j.rser.2021.110833

Lane, E. W. (1955). The Importance of Fluvial Morphology in Hydraulic Engineering. *American Society of Civil Engineers Journal*, *81*(745), 1-13.

Leppinen, D. (1999). Trajectory Analysis and Collision Efficiency during Microbubble Flotation. *Journal of Colloid and Interface Science*, *212*(2), 431–442. https://doi.org/10.1006/jcis.1998.6075

Leppinen, D. M., & Dalziel, S. B. (2004). Bubble Size Distribution in Dissolved Air Flotation Tanks. *Aqua*, 53(8), 531–543. https://doi.org/10.2166/aqua.2004.0042

Li, T., Zhu, Z., Wang, D., Yao, C., & Tang, H. (2006). Characterization of Floc Size, Strength and Structure Under Various Coagulation Mechanisms. *Powder Technology*, 168(2), 104–110. https://doi.org/10.1016/j.powtec.2006.07.003

Lin, Q., Dong, F., Miao, Y., Li, C., & Fei, W. (2019). Removal of Disinfection By-Products and Their Precursors During Drinking Water Treatment Processes. *Water Environment Research*, 92(5), 698–705. https://doi.org/10.1002/wer.1263

Liu, R., Guo, T., Ma, M., Yan, M., Qi, J., Hu, C., Liu, G., Liu, H., Qu, J., & van der Meer, W. (2019). Preferential Binding Between Intracellular Organic Matters and Al13 Polymer to Enhance Coagulation Performance. *Journal of Environmental Sciences*, 76, 1–11. https://doi.org/10.1016/j.jes.2018.05.011

Lundh, M., Jönsson, L., & Dahlquist, J. (2002). The Influence of Contact Zone Configuration on the Flow Structure in a Dissolved Air Flotation Pilot Plant. *Water Research*, 36(6), 1585–1595. https://doi.org/10.1016/S0043-1354(01)00357-8

Malley, J. P., & Edzwald, J. K. (1991). Comparison of DAF With Conventional Treatment. *Journal American Water Work Association*, 83(9), 56–61. https://doi.org/10.1002/j.1551-8833.1991.tb07214.x

Marega, G. (2020) Influência das características da partículas floculadas e de microbolhas de ar no proceso de flotação por ar dissolvido. MASc Thesis, Dept. of Hydraulics and Sanitary Engineering, Univ of Sao Paulo, Sao Carlos, BR.

Marega, G., & Reali, M. (2023). Characterization of Flocs and Bubbles Size Distribution in The Dissolved Air Flotation Process Using Non-Intrusive Image Analysis. *Proceedings of the American Water Works Association ACE23 conference*, American Water Works Association, Denver, CO.

Matijevic, E. (1973). Colloid Stability and Complex Chemistry. *Journal of Colloidal and Interface Science*, *43*(2), 217–245. https://doi.org/10.1016/0021-9797(73)90371-8

Matijević, E., & Stryker, L. J. (1966). Coagulation and Reversal of Charge of Lyophobic Colloids by Hydrolyzed Metal Ions. III. Aluminum Sulfate. *Journal of Colloid and Interface Science*, 22(1), 68–77. https://doi.org/10.1016/0021-9797(66)90068-3

McCooke, N. J., & West, J. R. (1978). The Coagulation of a Kaolinite Suspension with Aluminium Sulphate. *Water Research*, 12(10), 793–798. https://doi.org/10.1016/0043-1354(78)90029-5

Metcalfe, G., Speetjens, M. F. M., Lester, D. R., & Clercx, H. J. H. (2012). Beyond passive: Chaotic Transport in Stirred Fluids. In *Advances in Applied Mechanics*, 45, 109–188) https://doi.org/10.1016/B978-0-12-380876-9.00004-5

Mohamed, A. Y. A., Siggins, A., Healy, M. G., Ó hUallacháin, D., Fenton, O., & Tuohy, P. (2020). Appraisal and Ranking of Poly-Aluminium Chloride, Ferric Chloride and Alum for the Treatment of Dairy Soiled Water. *Journal of Environmental Management*, 267(1) 1-9. https://doi.org/10.1016/j.jenvman.2020.110567

Morris, J. K., & Knocke, W. R. (1984). Temperature Effects on the Use of Metal-Ion Coagulants for Water Treatment. *Journal of American Water Works Association*, 76(3), 74–79. https://doi.org/10.1002/j.1551-8833.1984.tb05302.x

Mustereț, C. P., Morosanu, I., Ciobanu, R., Plavan, O., Gherghel, A., Al-Refai, M., Roman, I., & Teodosiu, C. (2021). Assessment of Coagulation–Flocculation Process Efficiency for the Natural Organic Matter Removal in Drinking Water Treatment. *Water*, *13*(21). https://doi.org/10.3390/w13213073

Packham, R. F. (1962). The Coagulation Process. I. Effect of pH and the Nature of the Turbidity. *Journal of Applied Chemistry*, 12(12), 556–564. https://doi.org/10.1002/jctb.5010121207

Park, Y., Han, M., Kwak, D., & Pack, C. (2001). Effect of Particle and Bubble Size on the Removal Efficiency in DAF. *Asian-Pacific Regional Conference*. Asian-Pacific, Singapore https://doi.org/10.2166/wst.2007.

Pernitsky, D. J., & Edzwald, J. K. (2003). Solubility of Polyaluminium Coagulants. *Aqua*, 52(6), 395–406. https://doi.org/10.2166/aqua.2003.0036

Rance Bare, W. F., Jones, N. B., & Middlebrooks, E. J. (1975). Algae Removal Using Dissolved Air Flotation. *Journal of Water Pollution Control Federation*, 47(1), 153–169. https://www.jstor.org/stable/25038604

Rodrigues, R. T., & Rubio, J. (2003). New basis for measuring the size distribution of bubbles. *Minerals Engineering*, *16*(8), 757–765. https://doi.org/10.1016/s0892-6875(03)00181-x

Rubin, A. J., & Kovac, T. W. (1974). Effect of Aluminum(III) Hydrolysis on Alum Coagulation. In *Chemistry of Water Supply, Treatment, and Distribution* (pp. 159–179). A.J. Rubin (Ed) Ann Arbor Science, Ann Arbor, MI.

Schmideder, S., Thurin, L., Kaur, G., & Briesen, H. (2022). Inline imaging reveals evolution of the size distribution and the concentration of microbubbles in dissolved air flotation. *Water Research*, *224*, 119027. https://doi.org/10.1016/j.watres.2022.119027

Sillanpää, M. (2015). Natural Organic Matter in Water : Characterization of NOM In *Natural Organic Matter in Water*. Butterworth-Heinemann, Waltham, MA. https://doi.org/10.1016/B978-0-12-801503-2.00002-1

Smoluchowski, M V. (1917). Versuch Einer Mathematischen Theorie der Koagulationskinetik Kolloider Lösnngen. *Losungen. Z. Physik Chem.*, *92*, 129–168.

Spielman, L. A. (1970). Viscous Interactions in Brownian Coagulation. *Journal of Colloid and Interaction Science*, 33(4), 562–571. https://doi.org/10.1016/0021-9797(70)90008-1

Stumm, W., Morgan, J. J., & Black, A. P. (1962). Chemical Aspects of Coagulation. *Journal of American Water Works Association*, 54(8), 971–994. https://doi.org/10.1002/j.1551-8833.1962.tb00922.x

Stumm, W., & O'Melia, C. R. (1968). Stoichiometry of Coagulation. *Journal American Water Works Association*, *60*(5), 514–539. https://doi.org/10.1002/j.1551-8833.1968.tb03579.x

Sun, S., Weber-Shirk, M., & Lion, L. W. (2016). Characterization of Flocs and Floc Size Distributions Using Image Analysis. *Environmental Engineering Science*, 33(1), 25–34. https://doi.org/10.1089/ees.2015.0311

Tafvizi, H., & Husain, T. (2022). Enhanced Coagulation for Removal of Natural Organic Matter and Disinfection Byproducts: Multivariate Optimization. *Environmental Engineering Science*, 39(2), 155–167. https://doi.org/10.1089/ees.2020.0372

Tambo, N., & Watanabe, Y. (1978). Physical Characteristics of Flocs--I. The Floc Density Function and Aluminium Floc. *Water Research*, 13(5), 409–419. /https://doi.org/10.1016/0043-1354(79)90033-2

Teguh, D., Agustina, T. E., Ridho, M. H., Febriyanti, N., & Ermaya, D. (2022). The Effectiveness and Cost Optimization of Coagulant Aluminum Chlorohydrate (ACH), Aluminum Sulfate (AS) and Poly Aluminium Chloride (PAC) in Coagulation Process at The PT. Pupuk Sriwijaya (PT.Pusri) Utility Unit. *Indonesian Journal of Environmental Management and Sustainability*, 6(1), 189–195. https://doi.org/10.26554/ijems.2022.6.1.189-195

Tian, C., Wu, Y., Wei, M., & Feng, C. (2018). A Novel Understanding of Residual Nano-Al13 Formation and Degradation During Coagulation and Flocculation: a Proof Based on ESI-TOF-MS. *Environmental Science: Nano*, 5(11), 2712–2721. https://doi.org/10.1039/c8en00921j

Valade, M. T., Becker, W. C., & Edzwald, J. K. (2009). Treatment Selection Guidelines for Particle and NOM Removal. *Journal of Water Supply: Research and Technology – Aqua*, 58(6), 424–432. https://doi.org/10.2166/aqua.2009.201

Valioulis, I. A., & John, E. (1984). Collision Efficiencies of Diffusing Spherical Particles: Hydrodynamic, van er Waals and Electrostatic Forces. *Advances in Colloid and Interface Science*, 20(1), 1–20. https://doi.org/10.1016/0001-8686(84)80001-9

Van Benschoten, J. E., & Edzwald, J. K. (1990). Chemical Aspects of Coagulation Using Aluminum Salts I. Hydrolytic Reaction of Alum and Polyaluminum Chloride. *Water Research*, 24(12), 1519–1526. https://doi.org/10.1016/0043-1354(90)90087-M

Velz, C. J. (1934). Influence of Temperature on Coagulation. *Journal of Civil Engineering*, *4*(345).

Verberk, J. Q. J. C., O'Halloran, K. J., Hamilton, L. A., Vreeburg, J. H. G., & Van Dijk, J. C. (2007). Measuring Particles in Drinking Water Transportation Systems with Particle Counters. *Aqua*, 56(5), 345–355. https://doi.org/10.2166/aqua.2007.069

Walker, H. W. (2015). *Harmful Algae Bloom in Drinking Water - Removal of Cyanobacterial Cells and Toxins*, CRC Press, Boca Raton, FL.

Wang, L. K. (2021). *Operation and Performance of the AquaDAF ® Process System for Water Purification. In Handbook of Environmental Engineering* (pp. 301–341). Springer International Publishing, New York, NY. https://doi.org/10.1007/978-3-030-54642-7_8

Wang, P., Jiao, R., Liu, L., Xiao, F., An, G., & Wang, D. (2019). Optimized Coagulation Pathway of Al13: Effect of In-Situ Aggregation of Al13. *Chemosphere*, 230, 76–83. https://doi.org/10.1016/j.chemosphere.2019.05.053

Xu, B., & Narbaitz, R. M. (2016). Improved Membrane Pretreatment of High Hydrophobic Natural Organic Matter (NOM) Waters by Floatation. *Journal of Membrane Science*, 518, 120–130. https://doi.org/10.1016/j.memsci.2016.02.056

Xu, G. R., Fitzpatrick, C. S. B., & Gregory, J. (2008). Floc Formation, Size Distribution, and its Transformation Detected by Online Laser Particle Counter. *Separation Science and Technology*, *43*(7), 1725–1736. https://doi.org/10.1080/01496390801973706

Xu, W., Gao, B., Yue, Q., & Wang, Q. (2011). Effect of Preformed and Non-Preformed Al13 Species on Evolution of Floc Size, Strength and Fractal Nature of Humic Acid Flocs in Coagulation Process. *Separation and Purification Technology*, 78(1), 83–90. https://doi.org/10.1016/j.seppur.2011.01.025

Yu, J., Wang, D., Ge, X., Yan, M., & Yang, M. (2006). Flocculation of Kaolin Particles by Two Typical Polyelectrolytes: A Comparative Study on the Kinetics and Floc Structures. *Colloids and Surfaces A: Physicochemical and Engineering Aspects*, 290(1–3), 288–294. https://doi.org/10.1016/j.colsurfa.2006.05.040

Zabel, T. (1983). Flotation in Water Treatment. In *The Scientific Basis of Flotation* (pp. 349–377). G. Barbery (Ed) ,Springer International Publishing, New York, NY https://doi.org/10.1007/978-94-009-6926-1

Zarchi, I., Friedler, E., & Rebhun, M. (2013). Polyaluminium Chloride as an Alternative to Alum for the Direct Filtration of Drinking Water. *Environmental Technology*, 34(9), 1199–1209. https://doi.org/10.1080/09593330.2012.743594

Zhang, W. H., Zhang, J., Zhao, B., & Zhu, P. (2015). Microbubble Size Distribution Measurement in a DAF System. *Industrial and Engineering Chemistry Research*, 54, 5179–5183. https://doi.org/10.1021/acs.iecr.5b00109

Zheng, D. (2013). *Effects of Coagulation on the Removal of Natural Organic Matter, Genotoxicity, and Precursors to Halogenated Furanones*. M.A.Sc. thesis, Dept of Civil Engineering, University of Toronto, Toronto, ON.

Appendix A Summary of coagulants used by treatment plants.

The following information was obtained from municipal drinking water reports for municipalities servicing over 1,000 people and are using coagulant without membrane filtration.

Water treatment plants coagulant used in area							
City	**Coagulant**	**Coagulation aid**	**Technology**	**Only Alum**	**Alum with polymer**	**Advance Coagulant**	**Advanced Coagulants with Polymer**
Ottawa	Alum	Activated Silicate	Sedimentation		1		
Hawkesbury	Alum Summer and Aluminum Hydroxide during the Winter	Activated Silicate	Pulsator				1
Rockland	Aluminum Chloride Hydroxide Sulphate PAX-XL6	Magnafloc LT27AG	Actiflo				1
Arnprior	PAC	Polymer	Actiflo				1
Renfrew	PAS8	Polymer BASF	Actiflo				1
Cobden	PAS8	Superfloc 492PWG	Sedimentation with Settling Tubes				1
Carleton Place	PAS8	Polymer BASF	Actiflo				1
Petawawa	PAS8	Superfloc A-100	Sedimentation				1
Deep River	PAX-XL6	Magnafloc LT27AG	Actiflo				1
Sturgeon Falls	Polualuminum Chloride	Polymer	Sedimentation				1
Verner	PACl	Polymer	Sedimentation				1
Sudbury	Alum	Polymer	Sedimentation		1		
Vermilion Sudbury	Alum	Polyfloc CP1160	Pulsatube		1		
Alexandria	Coagulant	Polymer	Sedimentation		1		
Perth	PAX-XL6		Sedimentation			1	
Desoronto	Polyaluminum Chloride Blend	Anionic Polymer	DAF				1
Huntsville	SternPac PAC		Sedimentation			1	
Bracebridge	Alum		Sedimentation	1			
Gravenhurst	Polyaluminum Chloride Blend	Cationic polymer	Direct Filtration After Coag/Flocc				1
Orillia	Polyaluminium Chloride	Polymer	Direct Filtration After Coag/Flocc				1
Brantford	Polyaluminium Chloride	Flopam AN 934 PWG	Actiflo				1
Owen Sound	PAX-XL6 Colder Months (<10C)		Direct Filtration After Coag/Flocc			1	

	PAX-XL-1900 Warmer						
Barry's Bay	Alum		Direct Filtration After Coag/Flocc	1			
Chapleau	Alum	Polymer	Sedimentation		1		
Eganville	Hydroxylated Aluminum Sulphate	Polyelectrolyte	Sedimentation				1
Jarvis	poly-aluminum chloride	Polymer	Actiflo				1
Beaverton	Alum		Direct Filtration After Coag/Flocc	1			
Bowmanville	Polyaluminum Chloride		Direct Filtration After Coag/Flocc			1	
Newcastle	Polyaluminum Chloride		Direct Filtration After Coag/Flocc			1	
Oshawa	Alum		Sedimentation	1			
Kitchener	Polyaluminum Chloride		Sedimentation			1	
Red Lake	Alum	Polymer	Sedimentation		1		
Stevensville	Alum		Sedimentation	1			
longlac	Alum	Nalco 8181 Polymer	Sedimentation		1		
Stoney Point	Alum		Sedimentation	1			
Moosonee	Polyaluminum Chloride	Polymer	Upflow Clarifier				1
Geraldton	Alum	Polymer	Sedimentation		1		
Lake Huron Primary System	Alum	Polymer (LT20 & LT25)	Sedimentation		1		
Wheatley	Alum	Polymer	Clarifier		1		
Frankford	Polyaluminum Chloride Blend		Sedimentation			1	
Haileybury	Alum	Polymer	Sedimentation		1		
Campbellford	Polyaluminum Chloride	Polymer Magnafloc LT27A	Sedimentation				1
Hearst	Alum	Polymer	Sedimentation		1		
Bobcaygeon	SternPac PAC		Sedimentation			1	
Espanola	Polyaluminum Chloride	Magnafloc LT27AG	Reavtivitor Clarifier				1
Prescott	Alum		Direct Filtration After Coag/Flocc	1			
Meaford	PAX-XL1900		Direct Filtration After Coag/Flocc			1	
Dryden	Alum	Nalclear 8181	Sedimenrtation		1		
Gananoque	Alum		Direct Filtration After Coag/Flocc	1			
Dunnville	Alum		Sedimentation	1			
Kirkland Lake	Alum	Flopam FO4240PWG	Pulsator		1		
Fort Frances	Alum	Polymer	Clarifier		1		
Goderich	SternPac PAC		Sedimentation			1	
Napanee	Alum		Sedimentation	1			

Kincardine	modified alum	Magnafloc LT27AG	Actiflo				1
Smiths Falls	PAX-XL6	Magnafloc LT22s	DAF				1
Hamilton	Polyaluminum Chloride		Sedimentation			1	
Kenora	Alum	BASF LY-22S	Clarifier		1		
Elliot Lake	Polyaluminum Chloride		Direct Filtration After Coag/Flocc			1	
Amherstburg	Alum	Polymer	Upflow Clarifier		1		
Cobourg	Alum	Flowpam An934PWG	Sedimentation		1		
Brockville	Polyaluminum Chloride		Direct Filtration After Coag/Flocc			1	
Lindsay	Polyaluminum Chloride	Polymer	Actiflo				1
Timmins	Alum	Polymer	Actiflo		1		
St. Thomas	Alum	Polymer	Sedimentation		1		
Cornwall	Polyaluminum Chloride		Sedimentation			1	
Sault Ste. Marie	Alum			1			
Belleville	Alum		DAF	1			
Peterborough	Alum		Sedimentation	1			
Kingston	Polyaluminum Chloride		Sedimentation			1	
Windsor	Polyaluminum Chloride	Cationic Polymer	Sedimentation				1
Toronto	Alum			1			
Quantity of cities using coagulant				14	20	15	23

Appendix 2 Cold Water Research Data

Appendix 2.1 Data for Figure 4-2: Final Turbidity vs Coagulant Dose at 21ºC using DAF

Alum Dose	Temperatu	Average Fi	Standard Dev
25	21	1.47	0.05
30	21	0.437	0.006806859
35	21	0.44	0.079480815
40	21	0.424667	0.040203648

Appendix 2.2 Data for Figure 4-3: DAF floated water turbidity at 2ºC as a function of pH with 35mg/l of alum.

pH	Average Final
6.63	1.706666667
7.08	1.59
7.17	1.503333333
7.25	1.466666667
7.19	1.456666667
7.28	1.29
7.32	1.173333333
7.39	0.938333333
7.39	0.895
7.42	0.783666667
7.41	0.772666667
7.55	0.688333333
7.58	0.664
7.68	0.714333333
7.5	0.733666667

Appendix 2.3 Data for Figure 4-4: Effect of flocculation time and intensity on the LB-DAF final turbidity at 21 ºC using 35 mg/L of alum with the pH adjusted to 6.5.

G = 20 s^{-1}		
Time (s)	Turbidity (NTU)	Standard Dev
15	0.853166667	0.112973301
10	0.924777778	0.054977874
5	1.353333333	0.284018779
3	1.356666667	0.084063468

G = 37 s^{-1}		
Time (s)	Turbidity (NTU)	Standard Dev
15	0.607833333	0.143714184
10	0.833	0.139678202
5	0.952333333	0.035668847
3	1.065333333	0.059081864

G = 79 s^{-1}		
Time (s)	Turbidity (NTU)	Standard Dev
15	0.652833333	0.122264331
10	0.696833333	0.068285919
5	0.933833333	0.131641052
3	0.945833333	0.180510849

G = 113 s^{-1}		
Time (s)	Turbidity (NTU)	Standard Dev
15	0.514166667	0.059192623
10	0.658	0.145281795
5	0.728166667	0.121470024
3	0.926333333	0.097522647

G = 193 s^{-1}		
Time (s)	Turbidity (NTU)	Standard Dev
15	1.026833333	0.073240472
10	0.809	0.120326223
5	0.889666667	0.183260107
3	0.867166667	0.163789397

Appendix 2.4 Data for Figure 4 5: LB-DAF floated water turbidity with respect to GT 21ºC using 35 mg/L of alum adjusted to pH 6.5.

Time	G	GT	
15	79	71100	0.652833333
10	79	47400	0.696833333
5	79	23700	1.02
3	79	14220	1.096666667
1	79	4740	1.313333333
15	113	101700	0.514166667
10	113	67800	0.658
5	113	33900	0.835
3	113	20340	0.961333333
1	113	6780	1.25
15	193	173700	1.026833333
10	193	115800	0.738333333
5	193	57900	1.05
3	193	34740	1.009
1	193	11580	1.133333333
15	37	33300	0.607833333
10	37	22200	0.833
5	37	11100	0.960333333
3	37	6660	1.1
1	37	2220	1.416666667
15	20	18000	0.853166667
10	20	12000	0.924777778
5	20	6000	1.353333333
3	20	3600	1.423333333
1	20	1200	1.64

Appendix 2.5 Data for Figure 4 6: Effect of flocculation time and intensity on the LB-DAF final turbidity at 2 ºC using 35 mg/L of alum adjusted to pH 7.5 (initial turbidity = 8.9 NTU)

G = 20 s^{-1}		
Time (s)	Turbidity (NTU)	Standard Dev
3	1.16	0.304368198
5	0.864333333	0.129974869
10	0.896666667	0.025718994
15	1.144166667	0.399048577

G = 37 s^{-1}		
Time (s)	Turbidity (NTU)	Standard Dev
3	0.890666667	0.142844904
5	0.977333333	0.271652474
10	0.922	0.088315344
15	1.171833333	0.291403786

G = 79 s^{-1}		
Time (s)	Turbidity (NTU)	Standard Dev
3	0.846666667	0.032469473
5	1.032166667	0.111893551
10	0.8255	0.171565439
15	0.997833333	0.233045418

G = 113 s^{-1}		
Time (s)	Turbidity (NTU)	Standard Dev
3	0.714333333	0.033218469
5	1.184666667	0.425878699
10	1.07	0.027568098
15	1.094333333	0.119401284

G = 193 s^{-1}		
Time (s)	Turbidity (NTU)	Standard Dev
3	1.322666667	0.567698394
5	1.0855	0.338141834
10	2.151666667	0.320088529
15	3.101666667	0.323073779

Appendix 2.6 Data for Figure 4-7: LB-DAF floated water turbidity with respect to GT 2oC using 35 mg/L of alum adjusted to pH 7.5.

Time	G	GT	A final
15	79	71100	0.997833333
10	79	47400	0.8255
5	79	23700	1.032166667
3	79	14220	0.846666667
1	79	4740	0.779666667
15	113	101700	1.094333333
10	113	67800	1.07
5	113	33900	1.184666667
3	113	20340	0.714333333
1	113	6780	1.032666667
15	193	173700	3.101666667
10	193	115800	2.151666667
5	193	57900	1.0855
3	193	34740	1.322666667
15	37	33300	1.171833333
10	37	22200	0.922
5	37	11100	0.977333333
3	37	6660	0.890666667
1	37	2220	1.196666667
15	20	18000	0.785
10	20	12000	0.896666667
5	20	6000	0.864333333
3	20	3600	1.16

Appendix 2.7 Data for Figure 4-8: UV-254 Removal for Cold Water Treatment, Treatment at 2ºC, pH of 7.5, 35 mg/L of Alum and Mixing Intensity of 37 s-1.

UV Removal		
G	Flocculatio	uv removal
79	15	0.802326
79	10	0.799419
79	5	0.757267
79	3	0.8125
113	15	0.829942
113	10	0.758721
113	5	0.813953
113	3	0.832849
193	15	0.834302
193	10	0.774709
193	5	0.795058
37	15	0.787791
37	10	0.789244
37	5	0.781977
20	15	0.795058
20	10	0.809593
20	5	0.776163
20	3	0.799419

Appendix 3 Floc Size vs DAF Bubble Size Data

Appendix 3.1 Data for Figure 4-8: Cumulative bubble size in DAF system at room temperature

Bubble size 275 kPa		
	Frequency	Cumulative
0<=x<5	0	0
5<=x<10	0	0
10<=x<15	0	0
15<=x<20	0	0
20<=x<25	0	0
25<=x<30	1	0.0005
30<=x<35	16	0.0084
35<=x<40	23	0.0199
40<=x<45	46	0.0427
45<=x<50	119	0.1018
50<=x<55	225	0.2135
55<=x<60	302	0.3635
60<=x<65	353	0.5387
65<=x<70	316	0.6956
70<=x<75	229	0.8093
75<=x<80	220	0.9186
80<=x<85	102	0.9692
85<=x<90	40	0.9891
90<=x<95	17	0.9975
95<=x<100	5	1
x>=100	5	1

Bubble size 410 kPa		
	Frequency	Cumulative
0<=x<5	0	0
5<=x<10	0	0
10<=x<15	0	0.0070
15<=x<20	12	0.0444
20<=x<25	64	0.1081
25<=x<30	109	0.2646
30<=x<35	268	0.4638
35<=x<40	341	0.6776
40<=x<45	366	0.8499
45<=x<50	295	0.9696
50<=x<55	205	0.9959
55<=x<60	45	0.9994
60<=x<65	6	1
65<=x<70	1	1
70<=x<75	0	1
75<=x<80	0	1
80<=x<85	0	1
85<=x<90	0	1
90<=x<95	0	1
95<=x<100	0	1

Continue Appendix 3.1 Data for Figure 4-8: Cumulative bubble size in DAF system at room temperature

Bubble size 480 kPa		
	Frequency	Cumulative
0<=x<5	0	0
5<=x<10	0	0
10<=x<15	0	0
15<=x<20	14	0.0066
20<=x<25	108	0.0577
25<=x<30	304	0.2016
30<=x<35	479	0.4283
35<=x<40	475	0.6531
40<=x<45	427	0.8552
45<=x<50	225	0.9617
50<=x<55	67	0.9934
55<=x<60	10	0.9981
60<=x<65	4	1
65<=x<70	0	1
70<=x<75	0	1
75<=x<80	0	1
80<=x<85	0	1
85<=x<90	0	1
90<=x<95	0	1
95<=x<100	0	1
x>=100	0	1

Bubble size 620 kPa		
	Frequency	Cumulative
0<=x<5	0	0
5<=x<10	0	0
10<=x<15	1	0.0005
15<=x<20	12	0.0063
20<=x<25	162	0.0847
25<=x<30	353	0.2554
30<=x<35	490	0.4925
35<=x<40	458	0.7141
40<=x<45	358	0.8873
45<=x<50	188	0.9782
50<=x<55	33	0.9942
55<=x<60	11	0.9995
60<=x<65	1	1
65<=x<70	0	1
70<=x<75	0	1
75<=x<80	0	1
80<=x<85	0	1
85<=x<90	0	1
90<=x<95	0	1
95<=x<100	0	1
x>=100	0	1

Appendix 3.2 Data for Figure 4-9: Cumulative floc size after flocculation at room temperature. 35 mg/l of alum, pH =6.5

Before DAF 12 s^{-1}		
	Frequency	Cumulative
0<=x<10	0	0
10<=x<20	4	0.0038
20<=x<30	26	0.0287
30<=x<40	68	0.0936
40<=x<50	110	0.1987
50<=x<60	119	0.3123
60<=x<70	117	0.4241
70<=x<80	107	0.5263
80<=x<90	90	0.6122
90<=x<100	65	0.6743
100<=x<11	50	0.7221
110<=x<12	55	0.7746
120<=x<13	44	0.8166
130<=x<14	37	0.8520
140<=x<15	25	0.8758
150<=x<16	27	0.9016
160<=x<17	22	0.9226
170<=x<18	13	0.9351
180<=x<19	12	0.9465
190<=x<20	8	0.9542
200<=x<21	10	0.9637
210<=x<22	5	0.9685
220<=x<23	7	0.9752

Continue Before DAF 12 s^{-1}		
	Frequency	Cumulative
230<=x<24	4	0.9790
240<=x<25	4	0.9828
250<=x<26	1	0.9838
260<=x<27	2	0.9857
270<=x<28	2	0.9876
280<=x<29	3	0.9904
290<=x<30	2	0.9924
300<=x<31	2	0.9943
310<=x<32	1	0.9952
320<=x<33	1	0.9962
330<=x<34	1	0.9971
340<=x<35	1	0.9981
350<=x<36	1	0.9990
360<=x<37	0	0.9990
370<=x<38	0	0.9990
380<=x<39	0	0.9990
390<=x<40	0	0.9990
400<=x<41	0	0.9990
410<=x<42	0	0.9990
420<=x<43	0	0.9990
430<=x<44	0	0.9990
440<=x<45	1	1

Continue Appendix 3.2 Data for Figure 4-9: Cumulative floc size after flocculation at room temperature. 35 mg/l of alum, pH =6.5

Before DAF 60 s^{-1}		
	Frequency	Cumulative
0<=x<10	0	0
10<=x<20	4	0.0018
20<=x<30	8	0.0055
30<=x<40	26	0.0174
40<=x<50	48	0.0395
50<=x<60	83	0.0776
60<=x<70	91	0.1194
70<=x<80	125	0.1768
80<=x<90	156	0.2484
90<=x<100	148	0.3163
100<=x<11	141	0.3811
110<=x<12	130	0.4408
120<=x<13	137	0.5037
130<=x<14	141	0.5684
140<=x<15	117	0.6221
150<=x<16	133	0.6832
160<=x<17	120	0.7383
170<=x<18	80	0.7750
180<=x<19	77	0.8104
190<=x<20	63	0.8393
200<=x<21	47	0.8609
210<=x<22	43	0.8806
220<=x<23	39	0.8985
230<=x<24	38	0.9160
240<=x<25	31	0.9302
250<=x<26	28	0.9431
260<=x<27	23	0.9536
270<=x<28	15	0.9605
280<=x<29	6	0.9633
290<=x<30	16	0.9706
300<=x<31	4	0.9725
310<=x<32	9	0.9766

Continue Before DAF 60 s^{-1}		
	Frequency	Cumulative
320<=x<33	3	0.9780
330<=x<34	6	0.9807
340<=x<35	4	0.9826
350<=x<36	3	0.9839
360<=x<37	6	0.9867
370<=x<38	3	0.9881
380<=x<39	5	0.9904
390<=x<40	2	0.9913
400<=x<41	2	0.9922
410<=x<42	3	0.9936
420<=x<43	1	0.9940
430<=x<44	1	0.9945
440<=x<45	1	0.9949
450<=x<46	2	0.9959
460<=x<47	0	0.9959
470<=x<48	0	0.9959
480<=x<49	1	0.9963
490<=x<50	0	0.9963
500<=x<51	0	0.9963
510<=x<52	0	0.9963
520<=x<53	0	0.9963
530<=x<54	0	0.9963
540<=x<55	1	0.9968
550<=x<56	2	0.9977
560<=x<57	1	0.9982
570<=x<58	0	0.9982
580<=x<59	0	0.9982
590<=x<60	0	0.9982
600<=x<61	2	0.9991
610<=x<62	0	0.9991
620<=x<63	0	0.9991

Continue Before DAF 60 s^{-1}		
	Frequency	Cumulative
630<=x<64	0	0.9991
640<=x<65	0	0.9991
650<=x<66	0	0.9991
660<=x<67	0	0.9991
670<=x<68	0	0.9991
680<=x<69	0	0.9991
690<=x<70	0	0.9991
700<=x<71	0	0.9991
710<=x<72	0	0.9991
720<=x<73	0	0.9991
730<=x<74	0	0.9991
740<=x<75	0	0.9991
750<=x<76	0	0.9991
760<=x<77	0	0.9991
770<=x<78	0	0.9991
780<=x<79	1	0.9995
790<=x<80	0	0.9995
800<=x<81	0	0.9995
810<=x<82	0	0.9995
820<=x<83	0	0.9995
830<=x<84	0	0.9995
840<=x<85	0	0.9995
850<=x<86	0	0.9995
860<=x<87	1	1.0000

Appendix 3.3 Data for Figure 4-10 : Cumulative floc size of the floated water produced with 35 mg/L alum dose, flocculation at G = 12 s-1 and DAF flotation

After DAF 12 s^{-1}, 275 kPa		
	Frequency	Cumulative
0<=x<3	0	0
3<=x<6	0	0
6<=x<9	0	0
9<=x<12	4	0.0150
12<=x<15	8	0.0451
15<=x<18	17	0.1090
18<=x<21	22	0.1917
21<=x<24	27	0.2932
24<=x<27	23	0.3797
27<=x<30	28	0.4850
30<=x<33	13	0.5338
33<=x<36	21	0.6128
36<=x<39	20	0.6880
39<=x<42	13	0.7368
42<=x<45	7	0.7632
45<=x<48	12	0.8083
48<=x<51	12	0.8534
51<=x<54	12	0.8985
54<=x<57	5	0.9173
57<=x<60	1	0.9211
60<=x<63	1	0.9248
63<=x<66	3	0.9361
66<=x<69	4	0.9511
69<=x<72	1	0.9549
72<=x<75	3	0.9662
75<=x<78	4	0.9812
78<=x<81	2	0.9887
81<=x<84	0	0.9887
84<=x<87	0	0.9887
87<=x<90	1	0.9925
90<=x<93	1	0.9962
93<=x<96	0	0.9962
96<=x<99	0	0.9962
99<=x<102	0	0.9962
102<=x<10	0	0.9962
105<=x<10	0	0.9962
108<=x<11	0	0.9962
111<=x<11	1	1

After DAF 12 s^{-1}, 410 kPa		
	Frequency	Cumulative
0<=x<3	0	0
3<=x<6	0	0
6<=x<9	0	0
9<=x<12	4	0.0101
12<=x<15	23	0.0678
15<=x<18	33	0.1508
18<=x<21	32	0.2312
21<=x<24	32	0.3116
24<=x<27	36	0.4020
27<=x<30	42	0.5075
30<=x<33	31	0.5854
33<=x<36	28	0.6558
36<=x<39	32	0.7362
39<=x<42	23	0.7940
42<=x<45	9	0.8166
45<=x<48	7	0.8342
48<=x<51	12	0.8643
51<=x<54	11	0.8920
54<=x<57	4	0.9020
57<=x<60	6	0.9171
60<=x<63	7	0.9347
63<=x<66	10	0.9598
66<=x<69	8	0.9799
69<=x<72	2	0.9849
72<=x<75	1	0.9874
75<=x<78	0	0.9874
78<=x<81	2	0.9925
81<=x<84	0	0.9925
84<=x<87	0	0.9925
87<=x<90	1	0.9950
90<=x<93	0	0.9950
93<=x<96	0	0.9950
96<=x<99	0	0.9950
99<=x<102	2	1

After DAF 12 s^{-1}, 480 kPa		
	Frequency	Cumulative
0<=x<3	0	0
3<=x<6	0	0
6<=x<9	0	0
9<=x<12	6	0.0233
12<=x<15	12	0.0700
15<=x<18	20	0.1479
18<=x<21	23	0.2374
21<=x<24	30	0.3541
24<=x<27	24	0.4475
27<=x<30	14	0.5019
30<=x<33	20	0.5798
33<=x<36	25	0.6770
36<=x<39	16	0.7393
39<=x<42	14	0.7938
42<=x<45	10	0.8327
45<=x<48	6	0.8560
48<=x<51	7	0.8833
51<=x<54	9	0.9183
54<=x<57	1	0.9222
57<=x<60	5	0.9416
60<=x<63	3	0.9533
63<=x<66	4	0.9689
66<=x<69	1	0.9728
69<=x<72	2	0.9805
72<=x<75	1	0.9844
75<=x<78	0	0.9844
78<=x<81	1	0.9883
81<=x<84	1	0.9922
84<=x<87	1	0.9961
87<=x<90	1	1

Continue Appendix 3.3 Data for Figure 4-10 : Cumulative floc size of the floated water produced with 35 mg/L alum dose, flocculation at G = 12 s-1 and DAF flotation

After DAF 12 s^{-1}, 620 kPa		
	Frequency	Cumulative
0<=x<3	0	0
3<=x<6	0	0
6<=x<9	0	0
9<=x<12	4	0.0242
12<=x<15	3	0.0424
15<=x<18	21	0.1697
18<=x<21	20	0.2909
21<=x<24	17	0.3939
24<=x<27	14	0.4788
27<=x<30	22	0.6121
30<=x<33	15	0.7030
33<=x<36	7	0.7455
36<=x<39	9	0.8000
39<=x<42	3	0.8182
42<=x<45	6	0.8545
45<=x<48	4	0.8788
48<=x<51	2	0.8909
51<=x<54	2	0.9030
54<=x<57	5	0.9333
57<=x<60	1	0.9394
60<=x<63	4	0.9636
63<=x<66	1	0.9697
66<=x<69	2	0.9818
69<=x<72	2	0.9939
72<=x<75	0	0.9939
75<=x<78	0	0.9939
78<=x<81	0	0.9939
81<=x<84	0	0.9939
84<=x<87	0	0.9939
87<=x<90	0	0.9939
90<=x<93	0	0.9939
93<=x<96	0	0.9939
96<=x<99	1	1

Appendix 3.4 Data for Figure 4-11: Cumulative floc size of the floated water produced with 35mg/L alum dose, flocculation at G = 60 s-1 and DAF flotation.

After DAF 60 s^{-1}, 275 kPa		
	Frequency	Cumulative
0<=x<3	0	0
3<=x<6	0	0
6<=x<9	0	0
9<=x<12	0	0
12<=x<15	0	0
15<=x<18	3	0.0079
18<=x<21	3	0.0158
21<=x<24	9	0.0395
24<=x<27	17	0.0842
27<=x<30	20	0.1368
30<=x<33	21	0.1921
33<=x<36	30	0.2711
36<=x<39	19	0.3211
39<=x<42	23	0.3816
42<=x<45	31	0.4632
45<=x<48	22	0.5211
48<=x<51	30	0.6000
51<=x<54	17	0.6447
54<=x<57	15	0.6842
57<=x<60	14	0.7211
60<=x<63	15	0.7605
63<=x<66	10	0.7868
66<=x<69	9	0.8105
69<=x<72	6	0.8263
72<=x<75	7	0.8447
75<=x<78	5	0.8579
78<=x<81	1	0.8605
81<=x<84	7	0.8789
84<=x<87	4	0.8895
87<=x<90	7	0.9079
90<=x<93	2	0.9132
93<=x<96	4	0.9237
96<=x<99	1	0.9263
99<=x<102	5	0.9395
102<=x<10	1	0.9421
105<=x<10	1	0.9447
108<=x<11	2	0.9500
111<=x<11	3	0.9579
114<=x<11	1	0.9605
117<=x<12	1	0.9632
120<=x<12	0	0.9632
123<=x<12	0	0.9632

Continue After DAF 60 s^{-1}, 275 kPa		
	Frequency	Cumulative
126<=x<12	2	0.9684
129<=x<13	1	0.9711
132<=x<13	1	0.9737
135<=x<13	1	0.9763
138<=x<14	1	0.9789
141<=x<14	1	0.9816
144<=x<14	2	0.9868
147<=x<15	0	0.9868
150<=x<15	1	0.9895
153<=x<15	0	0.9895
156<=x<15	0	0.9895
159<=x<16	1	0.9921
162<=x<16	0	0.9921
165<=x<16	0	0.9921
168<=x<17	0	0.9921
171<=x<17	0	0.9921
174<=x<17	0	0.9921
177<=x<18	0	0.9921
180<=x<18	0	0.9921
183<=x<18	0	0.9921
186<=x<18	0	0.9921
189<=x<19	1	0.9947
192<=x<19	0	0.9947
195<=x<19	0	0.9947
198<=x<20	0	0.9947
201<=x<20	0	0.9947
204<=x<20	0	0.9947
207<=x<21	0	0.9947
210<=x<21	0	0.9947
213<=x<21	0	0.9947
216<=x<21	0	0.9947
219<=x<22	0	0.9947
222<=x<22	0	0.9947
225<=x<22	0	0.9947
228<=x<23	0	0.9947
231<=x<23	0	0.9947
234<=x<23	0	0.9947
237<=x<24	0	0.9947
240<=x<24	0	0.9947
243<=x<24	0	0.9947
246<=x<24	0	0.9947
249<=x<25	2	1

After DAF 60 s^{-1}, 410 kPa		
	Frequency	Cumulative
0<=x<3	0	0
3<=x<6	0	0
6<=x<9	0	0
9<=x<12	0	0
12<=x<15	0	0
15<=x<18	1	0.0021
18<=x<21	8	0.0191
21<=x<24	13	0.0468
24<=x<27	12	0.0723
27<=x<30	17	0.1085
30<=x<33	22	0.1553
33<=x<36	33	0.2255
36<=x<39	44	0.3191
39<=x<42	38	0.4000
42<=x<45	38	0.4809
45<=x<48	34	0.5532
48<=x<51	35	0.6277
51<=x<54	24	0.6787
54<=x<57	23	0.7277
57<=x<60	23	0.7766
60<=x<63	17	0.8128
63<=x<66	11	0.8362
66<=x<69	14	0.8660

Continue Appendix 3.4 Data for Figure 4-11: Cumulative floc size of the floated water produced with 35mg/L alum dose, flocculation at G = 60 s-1 and DAF flotation.

Continue After DAF 60 s^{-1}, 410 kPa		
	Frequency	Cumulative
69<=x<72	14	0.8957
72<=x<75	10	0.9170
75<=x<78	6	0.9298
78<=x<81	13	0.9574
81<=x<84	3	0.9638
84<=x<87	6	0.9766
87<=x<90	0	0.9766
90<=x<93	3	0.9830
93<=x<96	2	0.9872
96<=x<99	1	0.9894
99<=x<102	0	0.9894
102<=x<10	1	0.9915
105<=x<10	1	0.9936
108<=x<11	1	0.9957
111<=x<11	0	0.9957
114<=x<11	0	0.9957
117<=x<12	1	0.9979
120<=x<12	0	0.9979
123<=x<12	0	0.9979
126<=x<12	0	0.9979
129<=x<13	0	0.9979
132<=x<13	0	0.9979

After DAF 60 s^{-1}, 480 kPa		
	Frequency	Cumulative
0<=x<3	0	0
3<=x<6	0	0
6<=x<9	0	0
9<=x<12	2	0.0058
12<=x<15	2	0.0116
15<=x<18	7	0.0320
18<=x<21	7	0.0523
21<=x<24	12	0.0872
24<=x<27	16	0.1337
27<=x<30	26	0.2093
30<=x<33	20	0.2674
33<=x<36	27	0.3459
36<=x<39	27	0.4244
39<=x<42	29	0.5087
42<=x<45	17	0.5581
45<=x<48	21	0.6192
48<=x<51	24	0.6890
51<=x<54	14	0.7297
54<=x<57	21	0.7907
57<=x<60	13	0.8285
60<=x<63	5	0.8430
63<=x<66	13	0.8808
66<=x<69	8	0.9041

Continue After DAF 60 s^{-1}, 480 kPa		
	Frequency	Cumulative
69<=x<72	5	0.9186
72<=x<75	3	0.9273
75<=x<78	6	0.9448
78<=x<81	2	0.9506
81<=x<84	2	0.9564
84<=x<87	0	0.9564
87<=x<90	3	0.9651
90<=x<93	2	0.9709
93<=x<96	1	0.9738
96<=x<99	3	0.9826
99<=x<102	0	0.9826
102<=x<10	2	0.9884
105<=x<10	2	0.9942
108<=x<11	0	0.9942
111<=x<11	0	0.9942
114<=x<11	0	0.9942
117<=x<12	0	0.9942
120<=x<12	0	0.9942
123<=x<12	0	0.9942
126<=x<12	0	0.9942
129<=x<13	0	0.9942
132<=x<13	0	0.9942
135<=x<13	1	0.9971

Continue Appendix 3.4 Data for Figure 4-11: Cumulative floc size of the floated water produced with 35mg/L alum dose, flocculation at G = 60 s-1 and DAF flotation.

After DAF 60 s^{-1}, 625 kPa		
	Frequency	Cumulative
0<=x<3	0	0
3<=x<6	0	0
6<=x<9	1	0.0075
9<=x<12	2	0.0226
12<=x<15	5	0.0602
15<=x<18	3	0.0827
18<=x<21	6	0.1278
21<=x<24	11	0.2105
24<=x<27	11	0.2932
27<=x<30	13	0.3910
30<=x<33	15	0.5038
33<=x<36	13	0.6015
36<=x<39	17	0.7293
39<=x<42	7	0.7820
42<=x<45	6	0.8271
45<=x<48	9	0.8947
48<=x<51	6	0.9398
51<=x<54	1	0.9474
54<=x<57	1	0.9549
57<=x<60	1	0.9624
60<=x<63	1	0.9699
63<=x<66	1	0.9774
66<=x<69	1	0.9850
69<=x<72	0	0.9850
72<=x<75	1	0.9925
75<=x<78	0	0.9925
78<=x<81	0	0.9925
81<=x<84	0	0.9925
84<=x<87	0	0.9925
87<=x<90	0	0.9925
90<=x<93	1	1